Geological Quarterly, 2025, 69, 60
DOI: https://doi.org/10.7306/gq.1833

Tonian and Permian magmatic episodes in the Zavkhan Terrane (Western Mongolia); evidence from the Khasagt Mountains

Stanisław Z. MIKULSKI[1], Antoni WÓJCIK[1], Rafał SIKORA[1] and Ewa KRZEMIŃSKA[1, *]

[1] Polish Geological Institute – National Research Institute, Rakowiecka 4, 00-975 Warszawa, Poland; ORCID: 0000-0002-9941-5630 [S.Z.M.], 0000-0002-06-2-5837 [A.W.], 0000-0001-9007-2910 [R.S.], 0000-0002-6832-8104 [E.K.]

Mikulski, SZ., Wójcik, A., Sikora, R, Krzemińska, E., 2025. Tonian and Permian magmatic episodes in the Zavkhan Terrane (Western Mongolia); evidence from the Khasagt Mountains. Geological Quarterly, 69, 60; https://doi.org/10.7306/gq.1833

We provide the first account of whole-rock geochemistry and U-Pb SHRIMP geochronology applied to the igneous rocks exposed in the Khasagt Mountains at the margin of the Zavkhan Terrane in Western Mongolia (Central Asian Orogenic Belt). The results show that the area experienced magmatic episodes in the Tonian Period of the Neoproterozoic: at 815–800 Ma recorded by the emplacement of granite, Q-monzonite and alkali gabbro, followed by a subsequent pulse of latibasalt lavas and subvolcanic dykes at 787–769 Ma. Subsequently, in the northern part of the Khasagt region, zircons from alkaline granites and volcanic rocks revealed an early Permian igneous episode at 276–268 Ma. Both late Tonian and early Permian events have been recorded in several terranes of the Mongolian Collage, facilitating more detailed correlation. Our study of the Khasagt Mountains highlights the significance of using multiple geochemical discriminators. These intrusive suites provide evidence of bimodal magmatism, with an alkaline signature (i.e. Nb/Yb >4), in both late Tonian and early Permian time, and also indicate other geochemical features such as high Th/U ratios in zircons, typical of an extension regime. These new investigations of the Khasagt igneous rocks have showed links to giant rift systems and global processes. The Tonian episode was related to an early stage of Rodinia rifting, and the Permian episode to the Central Asian intra-continental rift system.

Key words: SHRIMP U-Pb geochronology, geochemistry, rift magmatism, terrane margin, Mongolian collage, Central Asian Orogenic Belt.

INTRODUCTION

In the last few decades, several geochronological studies have been carried out in Mongolia. The most effective were those associated with geochemical characterisation, crucial to the genetic interpretation of dated igneous processes, especially in such a complex area as the Central Asian Orogenic Belt (CAOB; e.g., Mossakovsky et al., 1993; Khain et al., 2003; Jahn, 2004; Windley et al., 2007). This Asian region is also known as the Altaids (e.g., Suess, 1901, 1908; Şengör et al., 1993, 2022; Wilhem et al., 2012). The CAOB structure, the length of which is estimated at 5,000 km, represents a long-lived Neoproterozoic–Mesozoic accretionary orogen (*sensu* Cawood et al., 2009). It remains one of the largest orogenic belts on Earth (e.g., Xiao et al., 2003; Windley et al., 2007; Schulmann and Paterson, 2011; Kröner, 2017), extending from east of the Ural Mountains in the west (Fig. 1A) to far eastern Siberia, constituting a basic geological unit in the tectonic structure of a number of countries (southern Russia, Mongolia, Kazakhstan and northern China). Like many other accretionary orogenic belts, the CAOB consists of a diverse array of microcontinents, arc terranes, accretionary wedges, fragments of oceanic volcanic islands (seamounts) and possibly, basaltic plateaus, and oceanic crust (ophiolites; e.g., Safonova et al., 2011), each contributing to its rich geological history Their tectonic assembly and evolution (between ~1000–250 Ma) has been a focus of numerous studies (Şengör et al., 1993; Dergunov, 2001; Badarch et al., 2002; Windley et al., 2007; Yakubchuk, 2008; Xiao et al., 2009, 2015; Kröner, 2015; Kröner et al., 2017; Schulmann et al., 2023). The CAOB terranes that include also remnants of early Precambrian continental crust (Badarch et al., 2002) reflect complex evolution from the latest Mesoproterozoic (e.g., Khain et al., 2002; Turkina, 2002) to the early Mesozoic (e.g., Xiao et al., 2009; Ganbat et al., 2021). Based on differences in the timing of accretion and the overall structure of the terranes, two structures named as the Kazakh and Mongolian collages have been defined (e.g., Xiao et al., 2018; Guy et al., 2021). The Mongolian collage of terranes includes large areas of central Mongolia (Fig. 1).

One of the cratonic fragments, mantled with Neoproterozoic and early Paleozoic successions embedded in the Mongolian Collage (Fig.1B), is the Zavkhan Terrane (or Dzabkhan according to Mossakovsky et al., 1994). Its origin, tectonic history and genetic links to the neighbouring blocks, e.g. the Tuva-Mongolia, Baidrag terranes, are still uncertain (Kozakov et al., 2012, 2014; Kilian et al., 2016; Bold et al., 2016a; Naemura et al., 2020; Kovach et al., 2021; Soejono et al., 2023).

* Corresponding author, e-mail: ewa.krzeminska@pgi.gov.pl

Received: July 7, 2025; accepted: December 14, 2025; first published online: December 31, 2025

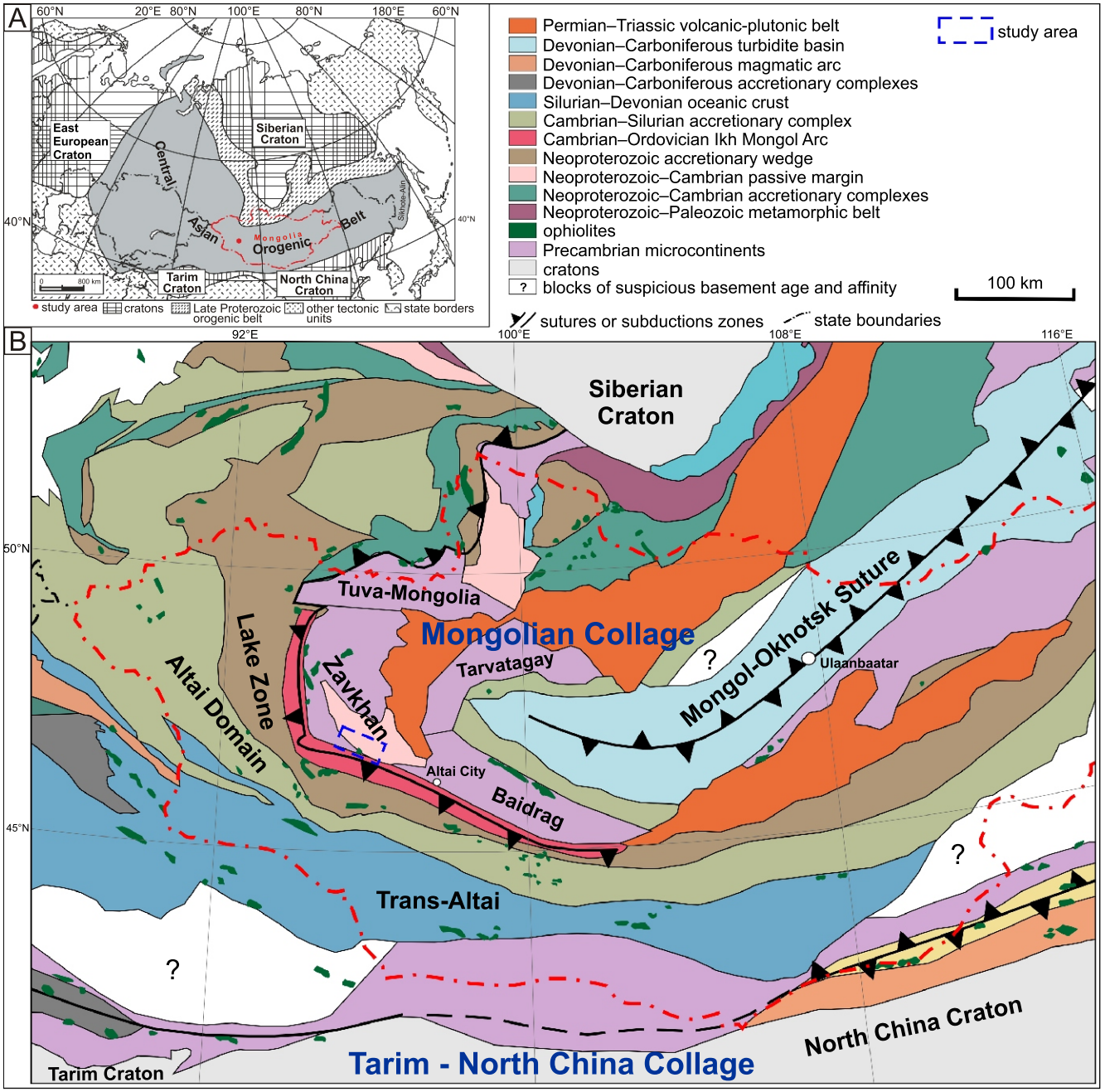


Fig. 1. Simplified maps of the Central Asian Orogenic Belt (CAOB) and study area

A – the position of the CAOB on a schematic tectonic map of Central and Eastern Asia (after Han et al., 2010, modified); **B** – zonation of the Mongolian Collage system within the CAOB showing position of the Zavkhan terrane and adjacent blocks (after Soejono et al., 2025; Peřesty et al., 2025, modified)

Updating the understanding of the structure, tectonic position and evolution of these blocks and numerous smaller units within CAOB can be helped by the provision of new geochronological data. The timing of key crustal growth episodes is of fundamental importance to constraining geotectonic models. Thus, precise defining the temporal range and characteristics of the associated magmatic activity helps place constraints both on the types of tectonic boundaries and on the motion of plates relative to one another.

The Khasagt Mountains (Fig. 2) provide a unique opportunity to examine the lithological diversity, and unravel the complex record, of episodes of magmatic activity within it, remnants of which are observed at outcrop (Fig. 3). In this contribution, we describe the SHRIMP U-Pb zircon and titanite geochronology of seventeen igneous samples, combined with whole-rock geochemistry, from the Khasagt Mountains area. These investigations of magmatic rocks provide constraints into the late Proterozoic to late Paleozoic evolution of the Zavkhan terrane, adding new data that can be included in further regional correlation and help update the geological map of this region.

REGIONAL AND LOCAL GEOLOGY

The study area, the Khasagt Mountains, located in the Zavkhan Terrane in the axial part of CAOB, belongs to the western part of the Mongolia Collage (Fig. 1). The evolution of this part of the CAOB has long been discussed (e.g., Badarch et al.,

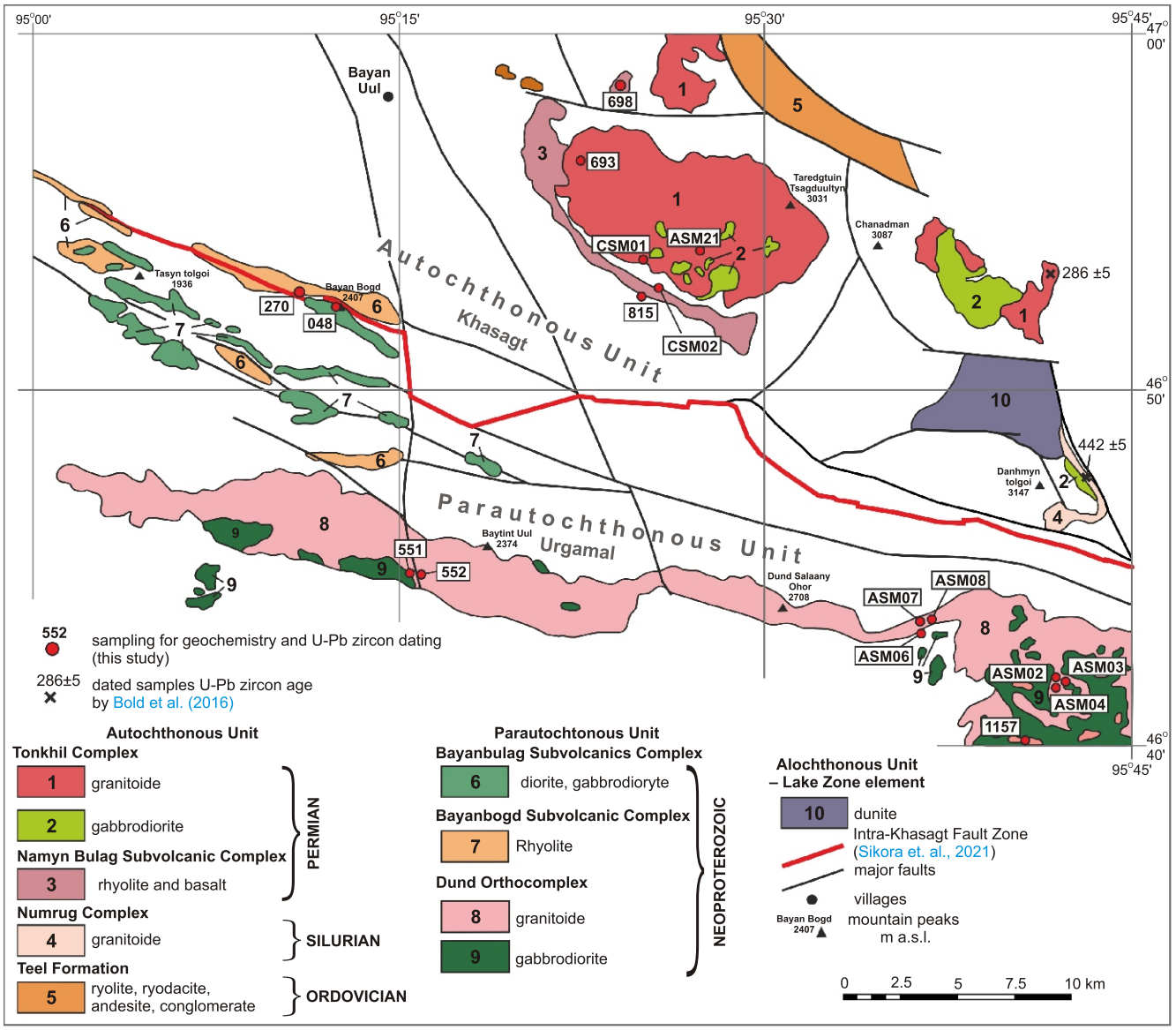


Fig. 2. A schematic geological map of crystalline rocks of the Khasagt area (Énhbayar et al., 2005, modified)

The locations of samples collected are indicated. Intra-Khasagt Fault Zone after Sikora et al. (2021)

2002; Calais et al., 2003). The CAOB comprises several east-west trending lithostratigraphic domains interpreted as an assemblage of accreted terranes or tectonic zones. The geological structure is known to be a combination of microcontinents and mobile belts (e.g., Kovach et al., 2013). Nevertheless, attempts to match lithostratigraphic domains to surface fault patterns (using geochronology, structural constraints, supported by aerial potential field measurements) have revealed some disagreements regarding the positions of suspected terranes (e.g., Badarch et al., 2002; Kröner et al., 2010; Guy et al., 2014). Their early stage of evolution is still difficult to decipher, because the northern CAOB may have evolved as a distinct accretionary collage outside of the Gondwana supercontinent, from the Ediacaran to the beginning of the Paleozoic Era (e.g., Şengör et al., 1993; Jiang et al., 2017; Zhao et al., 2018; Li et al., 2019; Long et al., 2019; Cawood et al., 2021; Broussolle et al., 2024). The origin of the CAOB can be traced back to the breakup of the Rodinia supercontinent (Cocks and Torsvik, 2005, 2007; Windley et al., 2007; Rojas-Agramonte et al., 2011). Rift-related dyke swarms with isotopic ages of 974–900 Myr (Dobretsev et al., 2003) indicate the beginning of these processes in the early Neoproterozoic. However, in the north-central CAOB the formation of island arc and active continental margin complexes at ~1.1–1.0 Ga was associated with the final stage of Rodinia assembly, which initiated subduction in the Mirovian Ocean and led to the development of accretionary orogens around supercontinent margins (e.g., Kovach et al., 2021). Tectono-magmatic activity in the CAOB is considered to have started ~1020 Ma (Khain et al., 2002) and to have continued until the latest Permian (Xiao et al., 2003) or Jurassic (Van der Voo et al., 2015).

Within the CAOB assemblage, the Zavkhan cratonic terrane (or block or microcontinent), situated in western Mongolia (Fig. 1B), is one of the prominent microcontinents belonging to the axial zone of the Mongolian Collage (i.e. the blocks located in Mongolia and Far East China). Palaeomagnetic and palaeofloral data indicate that Precambrian microcontinents had mostly amalgamated by the end of the Ordovician (e.g.,

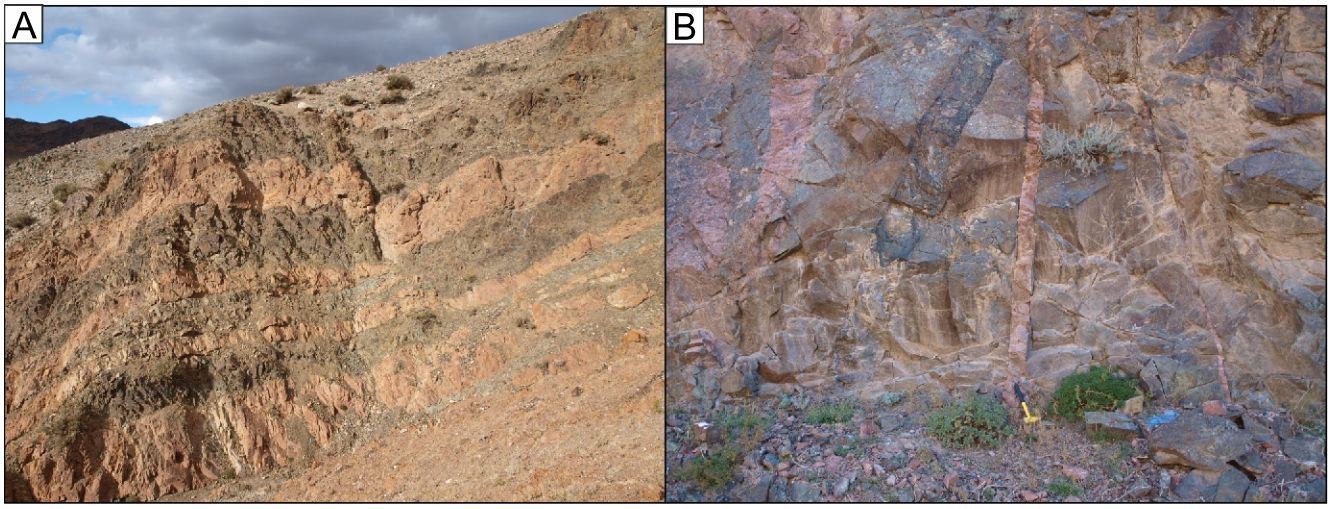


Fig. 3. Field photographs of rock-types dominant in the Khasagt Mountains area of exploration: exposures of the Dund Ortho Complex with typical bimodal magmatic rocks and contacts between red granitoids and mafic dykes

Windley et al., 2007). They form a stabilized block, bordered on its southern side by the Main Mongolian Lineament, which according to Windley et al. (2007) and Lehmann et al. (2010) mark a major late Ordovician plate boundary.

Several geological maps of this area (Fig.1B) indicate (Parfenov et al., 2002; Badarch et al., 2002; Enkhbayar et al., 2005; Bold et al., 2016a) at least three fault-bounded units from east to west: the Zavkhan–Baydrag blocks (terranes), the Lake Zone (arc) and the Hovd Zone (Jian et al., 2014). In previous publications, the Zavkhan Block has been called either a cratonic terrane (Badarch et al., 2002) or microcontinent (e.g., Lehmann et al., 2010; Wilhem et al., 2012). Its northern boundary is constituted by the E–W-trending strike-slip Bulnai Fault.

According to the latest data, the Cambrian–Ordovician Ikh-Mongol Arc System developed around the terrane from the west and south, also surrounding the neighbouring (to the east) Baidrag Terrane (Janoušek et al., 2018). In this perspective, the Precambrian microcontinents in western Mongolia, together with the Lake Zone, define the western extent of the Mongolian Orocline. In the southwestern part of the Zavkhan Terrane, including the Khasagt Mountains, two units are distinguished: Bold et al. (2016a) recognised a division of the autochthonous (Khasagt) terrane in the north-east from the para-autochthonous (Urgamal) terrane in the south-west (Enkhbayar et al., 2005; Bold et al., 2016a).

In the study area (Fig. 2) both of these units occur. They are saparated by a major tectonic zone linked to the Bayanbogd Hoyor, Onder Ulaan, and Huron Showhyn faults (Enkhbayar et al., 2005; Sikora, 2015). The presence of faulting in this zone was previously suggested by Bold et al. (2016b). Due to the regional significance of this structure, the term Intra-Khasagt Fault Zone (IKFZ) was used (Sikora et al., 2021). The IKFZ separates two sampling sub-areas, clearly referring to the parautochthonous versus autochthonous divisions. This zone separates the parauatochthonous Urgamal Zone with metamorphosed rocks from the very weakly metamorphosed and unmetamorphosed rocks of the autochthonous Khasagt Zone.

The geochronological and Nd isotopic whole-rock data suggest that the Zavkhan Microcontinent is characterized by extensive early Neoproterozoic crustal growth with reworking of early Precambrian crust (Kozakov et al., 2011, 2013, 2014; Kovach et al., 2013; Kröner et al., 2017; Yarmolyuk and Degtyarev, 2019). The Precambrian gneissic basement is as old as 1868 ±3 Myr (Burashnikov, 1990) or 1968 ±13 Myr (Bold et al., 2016b). The recently published geological, geochronological and isotopic data demonstrate (Yarmolyuk et al., 2008; Kozakov et al., 2014; Kovach et al., 2019, 2021; Soejono et al., 2023) that the Zavkhan Terrane represents a composite terrane consisting of ~860–800 Myr active continental margin or Japan-type arc complexes in the north accompanied by reworked (at ~800–720 Ma) early Precambrian continental crust in the south. They are separated by a Mélange Zone composed of an ~960–930 Myr island arc complex and an early (?) Precambrian high-grade complex.

Kozakov et al. (2021) summarized the available geochronological, and isotopic data of the northern Zavkhan Terrane and distinguished several zones and blocks that differ in structure and rock association. The metamorphic complexes have been described in more detail by Kovach et al. (2021), Peřestý et al. (2025) and Soejono et al. (2025).

The parautochthonous region of the Zavkhan Terrane is composed of amphibolite to granulite facies paragneisses and orthogneisses and greenschist facies metasedimentary and volcanic rock sequences. Its oldest part remains the Khavchig complex gneiss, which was dated at 1967 ±13 Myr with inherited cores as old as 2469 ±27 Myr (Bold et al., 2016b). After a magmatic hiatus of more than 1 billion years, the Zavkhan terrane was intruded by trondhjemites of the Kharuul Massif and gabbro dykes of the Mélange Zone at about 960–930 Ma in an oceanic island arc setting (Kovach et al., 2021) and by a 839 ±11 Myr granite (Bold et al., 2016a), which is present as gneiss of the Buduun Formation. The Buduun Formation and Khavchig complex were intruded at 811.36 ±0.24 Ma by gabbro, gabbro-diorite, and diorite arc-related intrusions of the Dund orthocomplex (Bold et al., 2016a; Ruzhentsev and Burashnikov, 1996). The Dund Orthocomplex is overlain by ~811–787 Myr arc-volcanic and volcaniclastic rocks of the Yargait and Zavkhan formations.

Rhyolites of the Zavkhan Formation have previously been reported between ~802 and 787 Ma (Bold et al., 2016a). Their zircon chemical compositions are consistent with an arc origin (Yang et al., 2012). North of the Zavkhan River, the Zavkhan Formation is intruded by 770.31 ±0.23 Myr alkaline granites, which have been interpreted to be rift-related based on whole-rock geochemistry (Yarmolyuk et al., 2008).

This rifting alkaline magmatism started at 770.31 ±0.23 Ma, was followed by deposition of the Khasagt Formation (Bold et al., 2016b) in narrow rift grabens from 770 to 717 Ma and pas-

sive margin sedimentation of the Tsagaan-Olom Group between 717 and 580 Ma. In the Zavkhan terrane, Cambrian plutonism was manifested within the parautochthon by synorogenic granites at ~509–507 Ma (Bold et al., 2016a). In addition to massive diorite and granodiorite plutons of the Dund Orthocomplex, smaller plugs of diorite are present in the southern portion of the Zavkhan terrane (Bold et al., 2016b).

In general, the Zavkhan Terrane underwent two long-lasting episodes of plutonism and associated crustal reworking to form granitic gneiss/migmatite complexes and diorite–granite intrusions: the earlier in the mid-Neoproterozoic ~856–755 Ma (Zhao et al., 2006; Yarmolyuk et al., 2008; Levashova et al., 2010; Kozakov et al., 2012; Bold et al., 2016a; Soejono et al., 2023); and the later in the Early Paleozoic ~515–482 Ma (Kozakov et al., 2002; Dijkstra et al., 2006; Jian et al., 2016; Soejono et al., 2023).

The next magmatic events occurred in Silurian and Permian time. In the autochthonous part of the terrane several intrusions have been recognized, including the Numrug granitoids emplaced at ~442 Ma in the Khasagt Mountains in the western part the Zavkhan Terrane as well as the Teel basalts at ~446 Ma and Tonkhil granitoids at ~286 Ma (Bold et al., 2016b; Kilian et al., 2016), recognized within the central part of the Zavkhan Terrane.

METHODOLOGY

FIELDWORK

In general, sampling for U-Pb age study was integrated with the available geological map of the Khasagt Mountains area (Enkhbayar et al., 2005), although it was also inspired by chronostratigraphic updating of neighbouring areas. Several coarse- and fine-grained granitoid type rocks and limited volcanic rocks were sampled from the Dund Orthocomplex, Bayanbulagand Bayanbogd intrusions (or massifs), in the south and (2) Namyn Bulag and the prolongation of Tonkil Intrusive Complexes, in the north (Fig. 2). They represent a diversity of the granitoids and other magmatic rocks recognized in the field.

In order to establish the age relationships between the plutonic versus volcanic and subvolcanic rocks, more than 20 localities were selected for age determination. However, in at least 8 cases (e.g., mafic volcanites and gabbro), no zircons were obtained for further investigation. Successfully analysed samples were collected in the area roughly located between the geographic coordinates of 47°00'00–46°40'00 north latitude and 95°00' 00–95°45'00 east latitude (Table 1 and Fig. 1B). The macroscopic features of the lithological varieties sampled in this study are shown in Figures 3 and 4.

U-Pb ZIRCON GEOCHRONOLOGY

Zircons from seventeen rock samples were separated at the Polish Geological Institute – National Research Institute (PGI-NRI) using separation procedures included crushing and pulverizing, followed by flotation through a magnetic separator, and flotation in heavy liquids to obtain a heavy mineral concentrate composed mostly of apatite and a few zircon crystals. The grains were hand-picked under a binocular microscope and glued on double-sided tape. Selected zircon grains were mounted in epoxy, together with *Temora-2* and 91500 zircon standards, and ground to about half their thickness, and sequentially polished using 6 µm and 1 µm diamond suspensions. All polished grains were imaged in reflected and transmitted light on a *Nikon ECLIPSE LV100POL* microscope, and in cathodoluminescence (CL) using a *HITACHI Su 3500* scanning electron microscope with a CL detector. Zircon was dated by the U-Pb method using the sensitive high-resolution ion microprobe SHRIMPIIe/MC, at PGI-NRI according to the analytical scheme described by Williams (1998).

The U-Pb ratios were measured under the following conditions: intensity of the primary O^{2-} ion beam at 3.5 nA. Before each analysis, the surface of the analysis site was pre-cleaned by rastering of the primary beam for 120 s, to reduce or eliminate surface common Pb. The sputtered area used for analysis was ~25 µm in diameter, and the analytical spot size of 20–23 µm. For each analysis, a raster (surface-cleaning) time of 2 minutes was used, and data were acquired over 6 scans through 9 the mass stations (i.e. $^{196}Zr_2O$, ^{204}Pb, 204.1 as a background, ^{207}Pb, ^{208}Pb, ^{238}U, ^{248}ThO, ^{254}UO). The *SQUID 2.50* software of Ludwig (2009) was used as the primary data processing platform. U-Pb ratios were normalized to the *Temora-2* zircon standard corresponding to a 416.78 ±0.3 Myr $^{206}Pb/^{238}U$ age (Black et al., 2003), accompanied by the reference zircons 91500 used for element concentrations U = 78 ppm (Wiedenbeck et al., 2004). Common Pb corrections were applied using the measured ^{204}Pb-correction Zircon isotopic age, and concordia diagrams were calculated/drawn using *Isoplot 3.0* (Ludwig, 2003). All data from individual analyses are tabulated with 1 uncertainty (Table S1), whereas pooled concordia age calculations were made as 2 . The tabulated data are all common-Pb corrected. The analytical points were selected within oscillatory-zoned external parts of grains in order to determine the main magmatic event. A few points, however, were placed in cores or central parts of crystals, to test the possible presence of inheritance. Volcanic zircon rims were preferentially measured in order to examine more closely the last stages of zircon crystallization. The total grain numbers from each sample correspond to the results given in the supplementary Table S1. The graphic presentation of all analyses on the traditional Wetherill concordia diagram for each sample, usually with the calculated intercept of the regression line with the concordia curve, is provided as a separate pdf file in the Supplement. Zircon U-Pb data were filtered by removing all measurements with elevated common lead (Pbc), and those with high analytical errors or/and discordance [calculated by SQUID from the ($^{206}Pb/^{238}U$) and ($^{207}Pb/^{206}Pb$) in the same way regardless of age range (<1 billion years and >1 billion years)]. In Table S1, these rejected analyses are marked by grey fonts. From the remaining data set, anomalously old zircons were interpreted as inherited or xenocrystic grains, while anomalously young, high-U or high common-Pb are dismissed as having been affected by Pb-loss or common-Pb contamination. Depending on the type of rock, different approaches to determining the Concordia age were used. For plutonic rocks, concordia age was defined based on the largest possible group of well-matched isotope ratios with the lowest possible MSWD value. In volcanic samples, to determine the maximum age of a volcanic eruption with no effects of the pre-eruptive juxtaposition of accessory antecrysts within the erupting melt during segregation (e.g., Bacon and Lowenstern, 2005; Miller et al., 2007), it was necessary to identify the most recent group of zircons, usually the youngest cluster of three or more single-grain data that overlap within 2 uncertainty (e.g., Dickinson and Gehrels, 2009; McKay et al., 2015; Nathwani et al., 2025).

U-Pb TITANITE GEOCHRONOLOGY

The selected titanite crystals encountered during the zircon separation process were used for auxiliary age determination. The selected titanite grains were mounted in epoxy with refer-

Table 1

General information on sampling

Sample ID	Rock type	Chemical R1-R2 nomenclature	Location according to the map	Coordinates Latiltude (N)	Coordinates Longitude (E)
1157	metamorphic	syeno-gabbro	Dund Ortho-complex	46°40'26.2"	95°40'16.2"
ASM03	plutonic	syenite	Dund Ortho-complex	46°41'49.3"	95°41'45.5"
ASM04	plutonic	granite	Dund Ortho-complex	46°41'45.7"	95°41'42.2"
ASM07	plutonic	tonalite	Dund Ortho-complex	46°43'12.0"	95°36'40.8"
ASM06	plutonic	granite	Dund Ortho-complex	46°43'10.1"	95°36'42.8"
ASM08	plutonic	granite	Dund Ortho-complex	46°43'11.9"	95°36'40.9"
552	plutonic	monzodiorite	Dund Ortho-complex	46°44'54.1"'	95°15'52.2"
ASM02	plutonic	gabbro	Baynbulag	46°41'53.5"	95°41'40.1"
551	volcanic	lati-basalt	Bayanbulag	46°44'54.1'	95°15'52.2"
048	subvolcanic	rhyodacite	Bayanbulag	46°52'21.5"	95°12'23.9""
270	subvolcanic	rhyolite	Bayanbogd	46°53'04.3"	95°10'30.2"
CSM01	plutonic	syenite	Tonkhil Complex	46°53'35.6"	95°26'08"
693	plutonic	alkali granite	Tonkhil Complex	46°56'45.7"	95°22'34.7"
CSM02	volcanic	rhyolite	Namyn Bulag	46°53'25"	95°26'07"
ASM21	plutonic	nepheline syenite	Namyn Bulag	46°53'54.4"	95°27'21.1"
815	volcanic	hawaite	Namyn Bulag	46°52'58"	95°25'35"
698	volcanic	alkali rhyolite	Namyn Bulag	46°58'33"	95°23'13"

ence Khan titanite (e.g., Heaman, 2009; Sato et al., 2016). Its uranium content of 584 ±95 ppm, according to ID–TIMS characteristics, and $^{206}Pb/^{238}U$ age of 518 ±2 Myr (Kinny et al., 1994), are commonly taken as reference values.

The titanite-bearing mount was polished, and examined using BSE images to select suitable targets for in situ single spot U-Pb SHRIMP analysis. The basic analytical procedure for titanite on the SHRIMP device described by Sato et al. (2016) has been slightly modified. A more detailed description of this protocol was given by Uher et al. (2019). The Khan titanite was used as the principal reference material for Pb*/U and Th*/Pb. The counts were acquired on both the sample and titanite standard during the whole analytical session.

The *SQUID2.50.11.01.03* software and attached *Isoplot/Ex version 3.00 Macro* program (Ludwig, 2009) were used for data processing. The SQUID2 calculates a 'calibration constant', for each analysis of the reference material and an error-weighted mean and standard error for all of these analyses, plus the error on the calibration, and the external error from the standard dataset. For each analysis of an unknown, a value for blank and its uncertainty is calculated. The ratio $^{204}Pb^*/^{206}Pb$, and the estimated $^{207}Pb^*/^{206}Pb$ age of the titanite, are used to correct for a common Pb composition calculated from the Stacey and Kramers (1975) model of bulk-crustal Pb isotope composition.

WHOLE-ROCK GEOCHEMISTRY

Chemical analyses of 16 whole-rock samples were performed at the PGI-NRI, Warsaw. The major-element compositions were analysed by wavelength dispersive X-ray fluorescence techniques on glass beads formed by fusing a sample with lithium metaborate $LiBO_2$; the Zr concentrations were determined on pressed powder pellets, using a *Philips PW2400* sequential spectrometer in both cases. Trace-element concentrations were determined by inductively coupled plasma mass spectrometry (ICP-MS) using a *Perkin Elmer ELAN DRC II* system (Perkin Elmer SCIEX Instruments, Waltham, MA, USA).

The samples were air-dried and ground, and then were decomposed with multi-acid digestion including hydrofluoric acid. The analytical accuracy and precision were found to be better than 1% for major elements, 5% for Zr and Th, and 10% for Sc, as checked by international standards and analysis of replicate samples.

RESULTS

PETROGRAPHY

The field observations indicate in general a weak tectonic involvement of the Dund Orthocomplex granites.The coarse- and fine-grained granitoid lithologies and limited volcanic rocks of the Dund Orthocomplex, Bayanbulagand Bayanbogd intrusions, from the parautochthonous area (Fig. 2) in the south (samples 1157, ASM02, ASM03, ASM04, ASM06, ASM07, ASM08 551, 552) and along the border (samples 270 0,48) as well as in Tonkhil West and Namyn Bulag intrusive complexes, belonging to the autochthonous area in the north (samples: 815, CSM02, CSM01, ASM21, 693, 698) were sampled for basic petrographic recognition of the rocks designated for U-Pb study. They represent the main granitoid type together with other rocks recognized in the field. Representative photographs of samples and photomicrographs of thin sections of the main types of granitoid and volcanic rocks recognized in this study are shown in Figure 5.

Sample 1157 (Fig. 4A), resembling a metasedimentary rock, differs from all the others from the Dund Orthocomplex. It represents equigranular felsic rocks with typical grain sizes of <1 mm, and is composed of a mixture of subhedral quartz, plagioclase, and K-feldspar (Fig. 5A), replaced by secondary epidote. As minor phases, subhedral biotite, albite that replaced plagioclase, muscovite and chlorite are also present. Accessory phases are opaque minerals, apatite, titanite and zircon. Widespread saussuritization is indicated by abundant mineral aggregates of very fine-grained epidote, sericite, this process commonly taking place during low-grade regional metamorphism of gabbros or basalts, both of which contain plagioclase as an essential component; thus, this sample has been classified as orthogneiss.

Two samples of very similar fine-grained granitod, ASM03 and ASM04 (not shown), are composed of quartz, K-feldspar, plagioclase and biotite. Accessory phases are the opaque minerals apatite, and zircon. Sample ASM04 is dominated by plagioclase in contrast to ASM03, where K-feldspar is more abundant but affected by widespread sericitization.

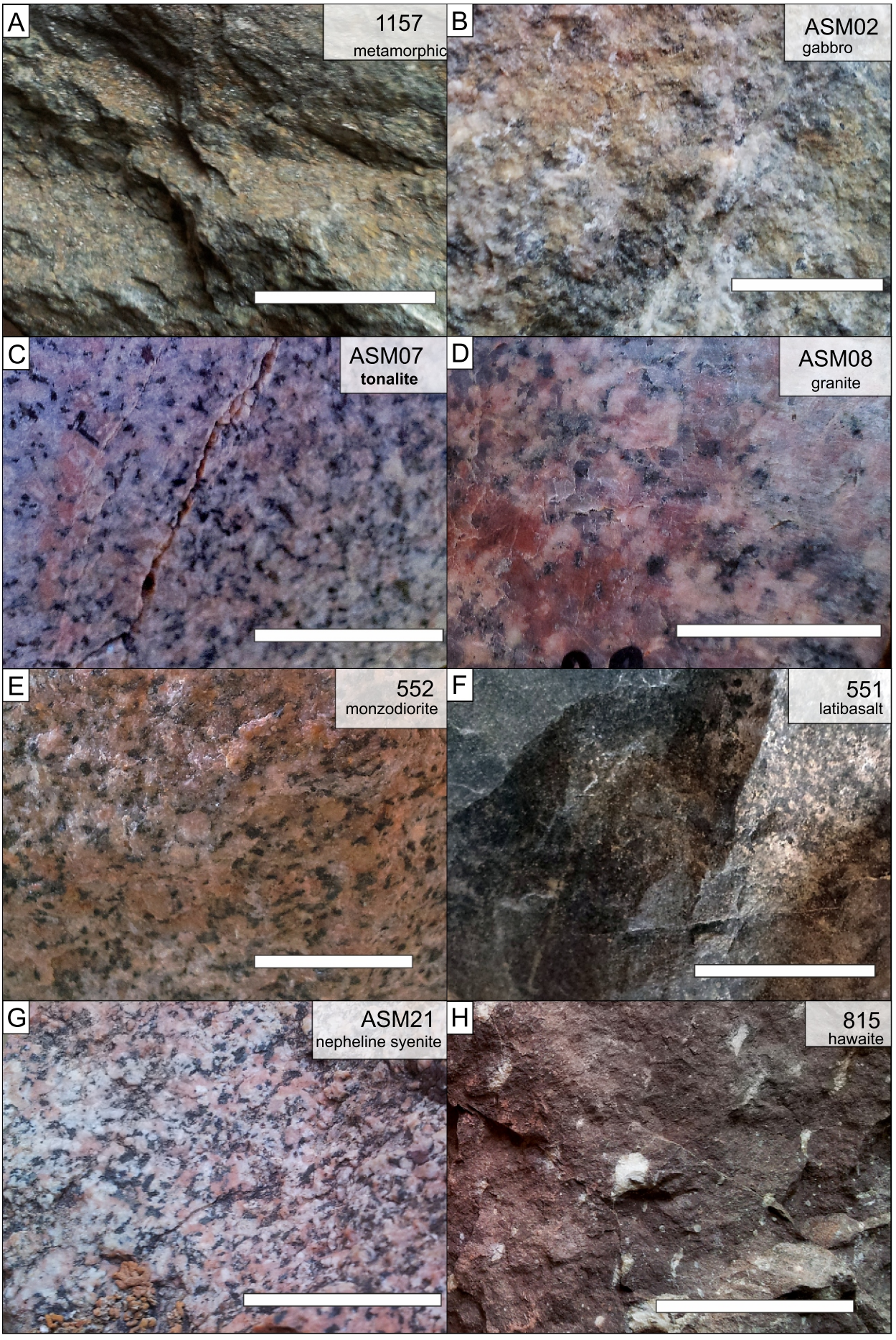


Fig. 4. Representative documentary photographs of the Khasagt Mountains rock samples selected for zircon separation and U-Pb geochronology

The scale bar is shown in the lower right corner as 5 cm

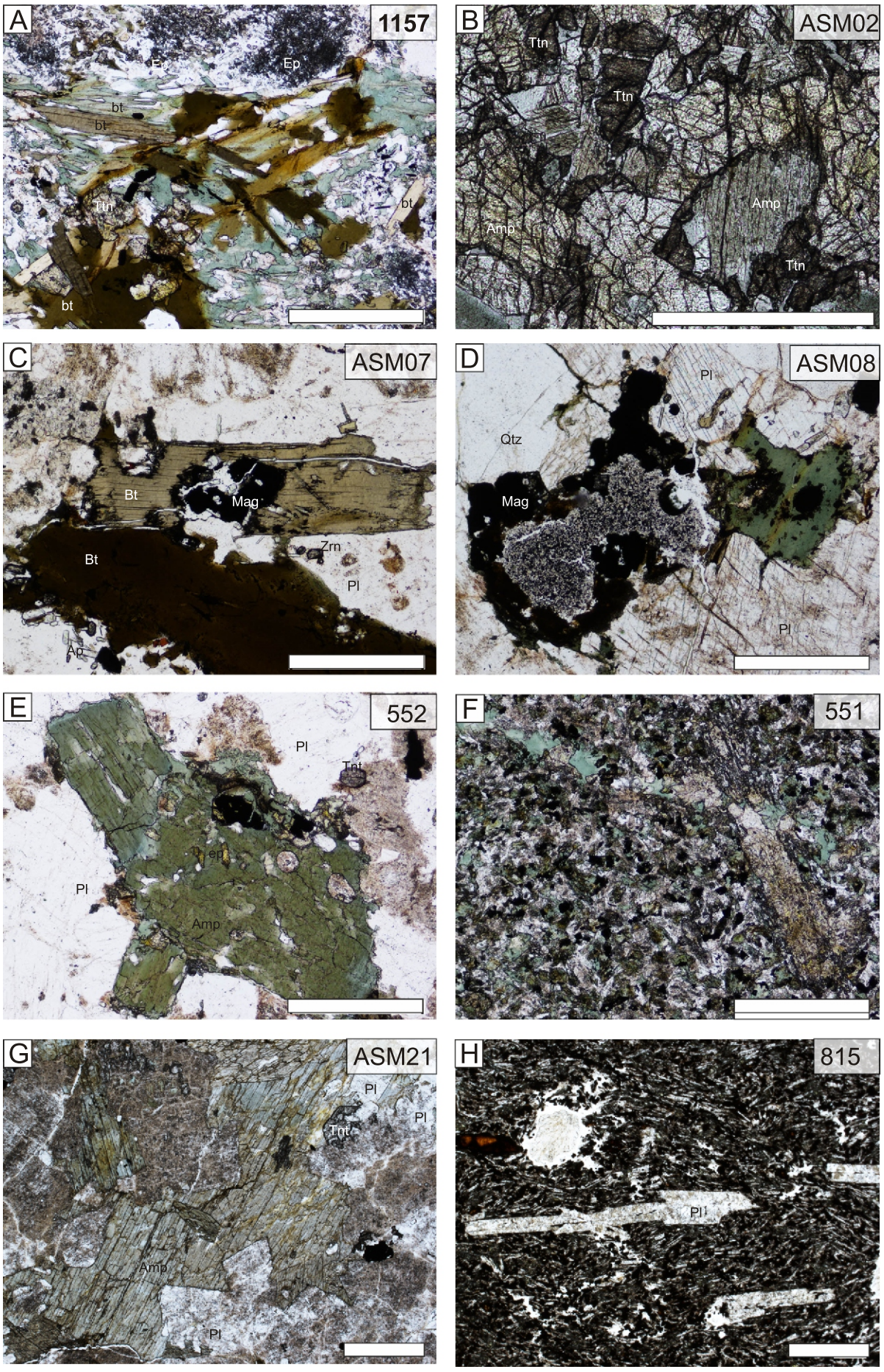


Fig. 5. Representative photomicrographs of the igneous rocks studied from the Khasagt Mountains showing typical mineral assemblages and textures

The scale bar for each micrograph is shown in the lower right corner as 0.5 mm. Abbreviations for names of rock-forming minerals: quartz (Qtz), plagioclase (Pl), amphibolite (Amp), biotite (Bt), titanite (Tnt), magnetite (Mag), epidote (Ep), apatite (Ap), zircon (Zrn)

Another sample, ASM02, from this area is a relatively mafic, fine-grained, gabbroic rock, dominated by amphibole, minor plagioclase and titanite as aggregates on the boundaries of amphibole crystals (Fig. 5B). Accessory phases are opaque minerals, apatite, and zircon.

In granitoids from the adjacent outcrop within the Dund Orthocomplex, a porphyritic texture recognized in thin sections is most characteristic. A red medium-grained granitoid sample ASM06 is composed of plagioclase phenocrysts, K- feldspar and quartz accompanied by a fine-grained generation of all these phases. Biotite is rare, and accessory minerals include apatite and zircon.

The similarly spotted red-pink medium-grained granitoid of sample ASM08 is dominated by large, partially sericitized plagioclase, K-feldspar and biotite crystals with numerous apatite and Fe-Ti oxides and zircon. Sample ASM07 is also characterized by a pink colour and medium-grained texture with dominant quartz, K-feldspar, plagioclase, biotite and Fe-Ti oxides. Accessory minerals are mainly zircon and apatite.

The medium-grained granitoid of sample 552 from the westernmost part of the Dund Orthocomplex is dominated by partially sericitized plagioclase and K-feldspar, amphibole, biotite and titanite, accompanied by apatite, Fe-Ti oxides and zircon.

Dark massive volcanic rocks in this area are represented by sample 551 with (Fig. 5F) an aphyric texture. The rock is composed of (Fig. 6J) fine-grained plagioclase, clinopyroxene, Fe-Ti oxides and apatite.

Outcrops located over 20 km to the north within the Namyn Bulag igneous body in the autochthonous area have yielded the medium-grained patchy granitoid of sample ASM21 (Fig. 5G) from the central part, composed of K-feldspar, altered plagioclase, amphibole, biotite and minor titanite, accessory apatite and zircon. The medium-grained pink granitoid sample 693 from the northernmost part contains altered K-feldspar, plagioclase, biotite, accessory apatite and zircon. Similary, the fine-grained light pink granitoid of CSM01 sampled at the edge of the massif is composed of K-feldspar, altered plagioclase, biotite with accessory apatite and zircon.

The volcanic components related to the Namyn Bulag intrusion are reprasented by a light, pink-coloured, partially porous volcanic rock of sample CSM02, which is composed of a fine-grained, groundmass with a few quartz xenocrysts showing local dissolution.

The massive, dark volcanic sample 815 is characterized by a reddish tint coming from hematite and a flow texture (Figs. 4H, 5H), highlighted by elongated amygdales (former vesicles) partially or completely infilled with secondary minerals. A few plagioclase phenocrysts are set within a finer- grained groundmass of strongly flow-aligned plagioclase laths and Fe oxides.

Dark porphyric volcanic rocks, located most north of sample 698, with abundant plagioclase phenocrysts and a few tiny xenoliths, show assimilation features such as irregular margins and embayments and bounded by an aphanitic groundmass, which suggests contamination during magma ascent or /and the presence of an older generation of the volcanic components.

U-Pb GEOCHRONOLOGY

Results of zircon U-Pb dating for seventeen samples from the Khasagt Mountains are reported in supplemental Table S1 and summarized in Table 2. Growth textures only observable in cathodoluminescence (CL) images are also shown. These images allow conclusions to be drawn of simple magmatic origin. Representative CL images of zircons with indicated microbeam pits and the U-Pb single spot ages obtained are shown on the right side of each concordia diagram (Fig. 6).

THE DUND ORTHOCOMPLEX

Sample 1157 – zircon

Zircons selected from sample 1157 contain short prismatic zircons not exceeding 100–150 μm, with usually euhedral to subhedral forms and well-preserved crystal faces. The CL imaging revealed relatively weak sector or oscillatory or sector zoning (Fig. 6A), usually attributed to kinetic factors and rapid environmental changes of crystal growth. The analysed interiors have low U and Th contents: 10 to 92 ppm and 6 to 79 ppm, respectively. The Th/U ratios range from 0.51 to 1.49, which is typical for magmatic zircons. The U-Pb measurements were focused on the middle parts of grains. A little data from 37 analyses revealed high Pbc contents (Table S1). They were omitted from the calculation of the age of the protolith. The remaining results provided $^{206}Pb/^{238}U$ ages ranging from 872 to 772 Myr. The concordia diagram (Fig. 6A) based on the most consistent analyses (n = 20) provided an age of 810.6 ±9. 0 Myr (MSWD = 0.119). The same twenty grains produced a weighted average $^{206}Pb/^{238}U$ age of 809.7 ±9.2 Myr (MSWD = 0.91).

Sample ASM04 zircon

The zircons of sample ASM04 are represented by relatively small (<100μm) euhedral to subhedral crystals with igneous concentric zoning (Fig. 6B). Thirty-eight grains were analysed (one spot per grain). They have variable U and Th contents: 51 to 231 ppm and 29 to 196 ppm, respectively. The Th/U values range from 0.44 to 1.21, typical for magmatic zircons. Part of the data obtained, including at least two of youngest dates, i.e. 656 and 690 Myr, revealed elevated contents of common lead (Pbc) in the range 2.31–13.57% Pbc. All these results were omitted. The rest yielded a range of radiogenic $^{206}Pb/^{238}U$ ages dispersed between 832 and 749 Myr. The most consistent group of analyses (n = 21/38) gave a concordia age of 810.3 ±6.3 Myr (MSWD = 1.3). The same twenty-one grains provided a weighted $^{206}Pb/^{238}U$ age average of 810.7 ± 6.4 Myr (MSWD = 0.57).

Sample ASM03 zircon

Syenite ASM03 has uniformly prismatic crystals ~50–100 μm in size. Their CL images show simple oscillatory zoning, characteristic of magmatic crystallization. They have low to moderate U and Th contents: 35 to 234 ppm and 17 to 350 ppm, respectively. The Th/U ratios range from 0.37 to 1.54, though usually oscillating around 0.99. The zircons with high Pbc (most commonly among within the youngest group) and high errors were omitted. The isotopic compositions plot as a single group with $^{206}Pb/^{238}U$ single spot ages ranging between 848 and 742 Myr. Eighteen selected analyses (Fig. 6C), provided a concordia age of 798 ±11 Myr (MSWD = 1.3). The same grains (n = 18/28) allowed calculation of a weighted average $^{206}Pb/2^{38}U$ age of 798 ± 14 Myr (MSWD = 0.38)

Sample ASM07 zircon

Sample ASM07 was represented by numerous but relatively small zircon grains <100ěm. They have moderate U and Th contents: 47 to 277 ppm and 40 to 316 ppm, respectively. The Th/U values range from 0.37 to1.35, typical for magmatic zircons. Forty-six single spot analyses revealed relatively uniform $^{206}Pb/^{238}U$ ages ranging from 822 to 771 Myr. Using of most of these analyses (n = 35/46) allowed definition (Fig. 6D) of a concordia age of 800.7 ±2.5 Myr (MSWD = 0.00047). The same number of grains yielded a weighted average $^{206}Pb/2^{38}U$ age of 800.7 ±3.2 Myr (MSWD = 1.5).

Sample ASM06 zircon

Crystals of varying sizes, with well-defined faces, were extracted from sample ASM06. They have moderate U and Th contents ranging from 75 to 239 ppm and 45 to 364 ppm, respectively. The Th/U ratios range between 0.48 and 1.19. All grains are characterized by magmatic zonation, without overgrowths. Thirty-seven analyses revealed single spot $^{206}Pb/^{238}U$ ages in the range from 816 to 778 Myr. Twenty-two selected analyses (Fig. 6E) yielded a concordia age of 797.7 ±3.2 Myr (MSWD = 3.0) and a weighted average of 796.7 ±3.5 Myr (MSWD = 0.78).

Sample ASM08 zircon

The zircon crystals extracted from ASM08 are generally euhedral and mostly prismatic. They have an igneous concentric zoning. The content of U ranges from 53 to 316 ppm though values are mostly > 100 ppm. The concentration of Th is mostly moderate but ranges from 28 to 349 ppm. The values of Th/U ratio are in the range of 0.49–1.34. Sixty-three zircon analyses yielded a range of $^{206}Pb/^{238}U$ ages scattered between 820 and 763 Myr. A selected, most uniform, group of forty-three analyses (Fig. 6F) provided a concordia age of 799.9 ±2.4 Myr (MSWD = 0.87) and weighted average of 799.0 ±2.9 Myr (MSWD = 1.2).

Sample 552 zircon

Sample 552 provided an abundance of zircon grains of similar euhedral shape. Cathodoluminescence imaging shows an oscillatory texture characterized by a concentric feature with narrow cyclic brightness variations. Only one xenocrystic core was recognized on the basis of CL imaging and confirmed by SHRIMP measurement. Fifty-nine zircon analyses yielded a range of radiogenic $^{206}Pb/^{238}U$ dates scattered between 840 and 785 Myr. They have moderate U and low Th contents: 37 to 251 ppm and 28 to 229 ppm, respectively. The Th/U ratios are in the range of 0.47–1.35 which is the most frequently reported range in these samples. The inherited core preserved a record of crystallisation at 2408 Ma (early Paleoproterozoic). Thirty-five selected, relatively consistent, isotopic ratios (Fig. 6G) provided a concordia age of 814.7±5.2 Myr (MSWD = 3.2). The same grains (n = 35/59) and their $^{206}Pb/^{238}U$ ages produced a weighted average of 814.3 ± 6.1 Myr (MSWD = 0.112).

THE BAYANBULAG INTRUSION

Sample ASM02 zircon

The zircons from sample ASM02 have generally euhedral to subhedral shapes, with the majority being prismatic or stubby. Cathodoluminescence imaging shows mostly simple oscillatory zoning. Some crystals contain fragments that resembled inherited cores, but their age and composition did not differ from the analyses of the rims. They have U and Th contents varying over a wide range from 39 to 610 ppm and from 20 to 776 ppm, respectively. The Th/U ratios range between 0.53 and 1.31. Thirty-three zircon analyses yielded a range of radiogenic $^{206}Pb/^{238}U$ ages scattered between 837 and 762 Myr. Most of the analyses (n = 26/33), provide a concordia (Fig. 6H) age of 809.7 ± 6 Myr (MSWD = 1.7). The same twenty six grains produced a weighted average of 808.7 ±7 Myr (MSWD = 0.45).

Sample ASM02 titanite

Apart from the zircon grains, two fractions of titanite were selected from sample ASM02. The titanite crystals were anhedral to subhedral (Fig. 6I), mostly having grain sizes of 30–200 μm in width and 50–300 μm in length, corresponding to the dimensions of grains associated with amphiboles and identified in thin section (Fig.5B). Fraction 1 consisted of brown to yellow clear titanites. The backscatter electron (BSE) imaging of the titanite grains revealed abundant mineral inclusions in this darker fraction. The inclusion-rich crystals were not suitable for analysis. The presence of inclusions limits the number of titanite grains and areas selected for dating. Fraction 2 consisted of light brown to brown usually medium-grained (<200 μm) grains. Only six grains were analysed. Three have very low-U contents in the range of 27–59 ppm and the other of 122–159 ppm; therefore, the age data obtained have relatively large uncertainties (>10% can be typical, Kohn, 2017). The Th/U ratios were in the range of 0.47–1.35, similar to those reported for the zircons. Titanite grains have a variable amount of common-Pb contamination (Pbc: 1.91–18.27%) resulting from the incorporation of Pb during their crystallization (referred to as initial Pb), which is a typical feature; therefore, these results are accepted.

The range of $^{206}Pb/^{238}U$ ages is scattered between 817 to 755 Myr. Age calculations from all these data (Fig. 6I) provided a concordia age of 785 ± 6.9 Myr (MSWD = 2.6). These six grains produced a weighted average of 779 ± 11 Myr (MSWD = 1.5).

Sample 551 zircon

Sample 551 of volcanic rock provided a sufficient quantity of small zircon grains (usually < 100 μm), with igneous, oscilatory or sector zoning and a lack of internal resorption surfaces. Twenty-five of them were analysed. However, some of these data were omitted due to elevated contents of Pbc of 1.5–4.5 %. They have moderate U and Th contents: 62 to 250 ppm and 41 to 300 ppm, respectively. The Th/U ratios range from 0.54 to 1.24. The accepted analyses indicate a range of $^{206}Pb/^{238}U$ ages scattered between 828 and 772 Myr. The selected, most consistent isotopic ratios (n = 19/26), allowed calculation of (Fig. 6J) a concordia age of 787.4 ±9.4 Myr (MSWD = 0.013). The same nineteen grains produced a weighted average of 787 ±10 Myr (MSWD = 0.42).

Sample 048 zircon

This sample provided relatively large zircon grains (>100 μm) and mostly stubby crystals, that all show concentric oscillatory zonation indicating typical magmatic cooling. The grains have moderate U and Th contents: 90 to 300 ppm and 36 to 281 ppm, respectively. The Th/U ratios are in a typical range of 0.38–1.20. Twenty-eight zircon analyses yielded a range of $^{206}Pb/^{238}U$ from 808 and 769 Myr. The selected, most consistent, isotopic ratios (n = 19/28), allowed to calculation of (Fig. 6K) a concordia age of 768.7 ±4.5 Myr (MSWD = 0.005). The same nineteen grains provided a weighted average age of 768.6 ±6.4.Myr (MSWD = 1.5).

THE BAYANBOGD INTRUSION

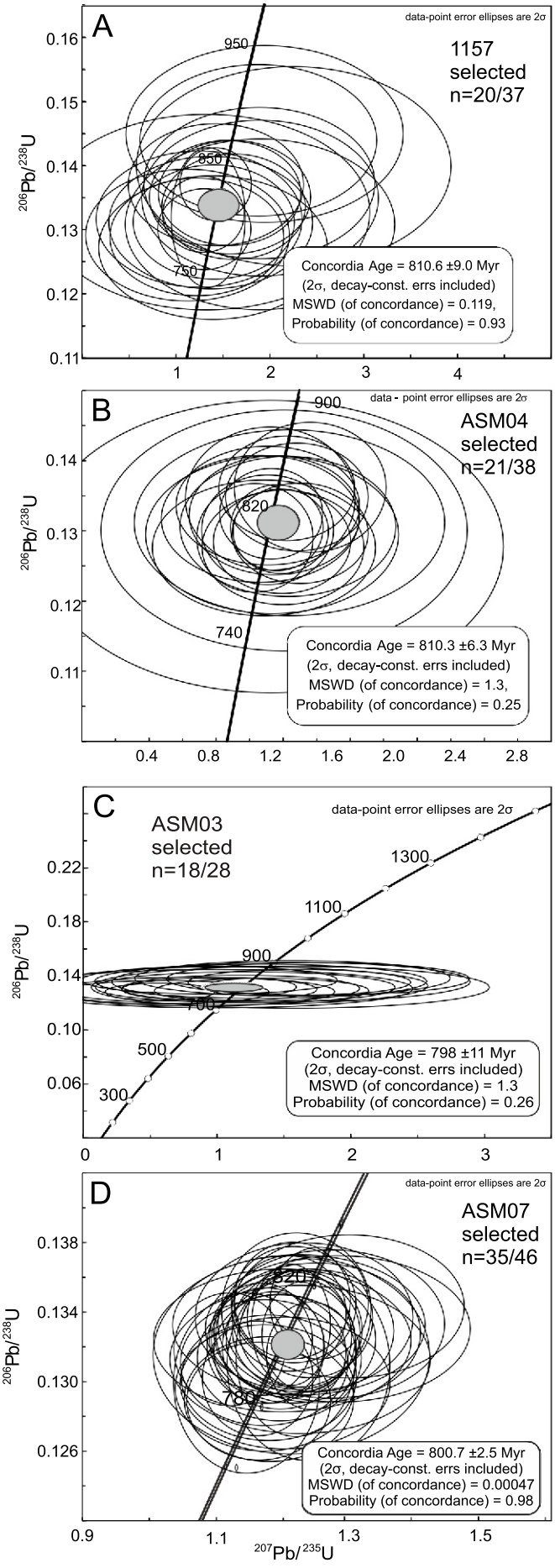
Sample 270 zircon

Sample 270 provided a limited number (<20) of euhedral zircon grains with very simple zonation visible in CL images. They have scattered U and Th contents: 27 to 257 ppm and 16 to 291 ppm, respectively. The value of Th/U ratios range from 0.50 to 1.16. Fifteen zircon analyses yielded a range of radiogenic $^{206}Pb/^{238}U$ ages scattered between 808 and 769 Myr. One of the grains analyzed twice (two spots) gave results in a similar range. Except for two data points with the lowest Pb contents, the rest of the data represent a relatively consistent group of isotopic ratios (n = 8/15), that allow constraint (Fig. 6L) of a concordia age of 774.5 ±5.5 Myr (MSWD = 0.41). The same eight grains produced a weighted average of 773.7 ±9.5 Myr (MSWD = 1.8).

THE WESTERNMOST TONKHIL COMPLEX

Sample CSM01 zircon

The large (<100 μm) zircon grains extracted from sample CSM01 show oscillatory zoning consisting of large (10–20 μm) almost rectangular 'growth bands' alternating with narrow (1–3 μm) cyclic layers in most cases. In some of the larger crystals, low-intensity luminous convolute bands are visible in the central part, indicating the initial stage of crystallization. They have moderate U and high Th contents: 34 to 392 ppm and 31



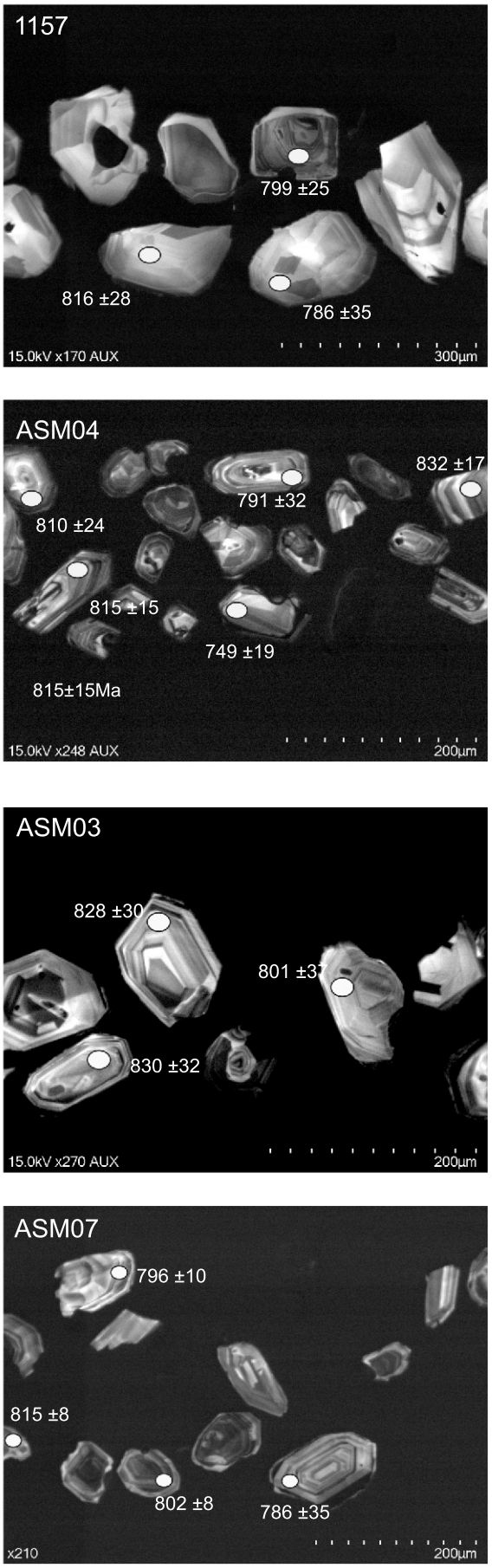
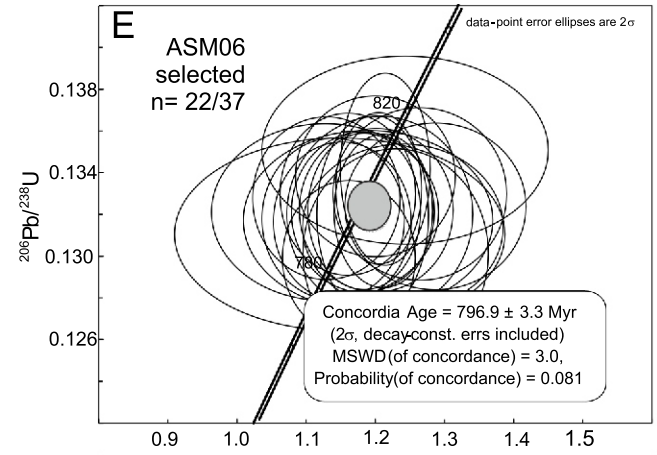
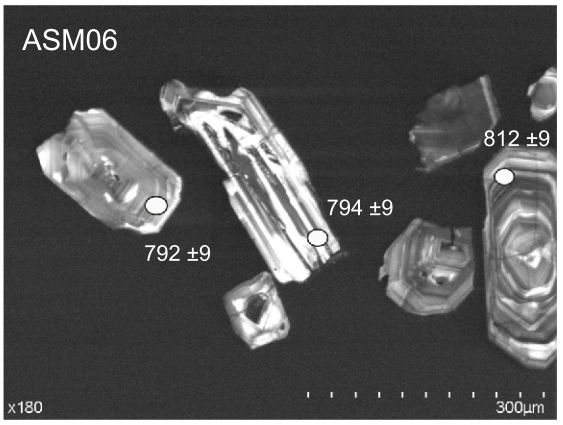
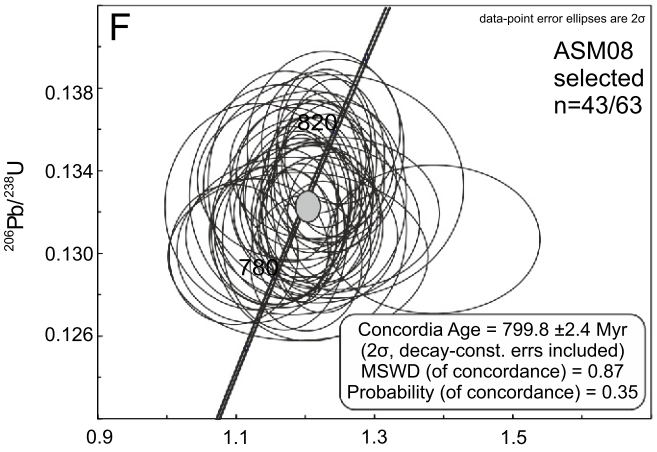


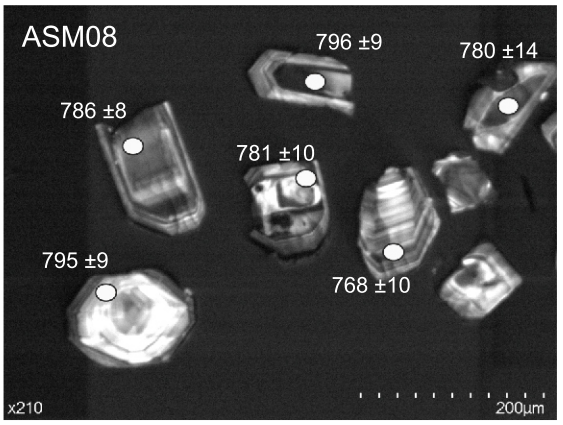
Fig. 6. U-Pb concordia plots diagrams and cathodoluminescence (CL) images of representative zircons and a BSE image of titanite from the igneous rocks of the Khasagt Mountains

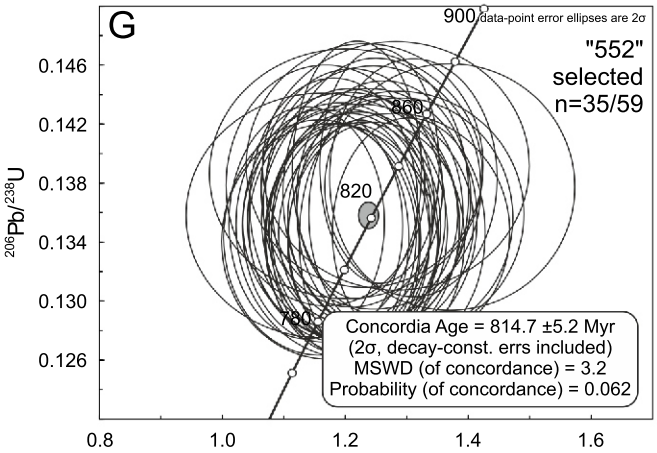
Sample arrangement from A to T as described in the text. White ellipses show analysis sites. Single-spot $^{206}Pb/^{238}U$ ages in Myr with 1 uncertainty are also indicated

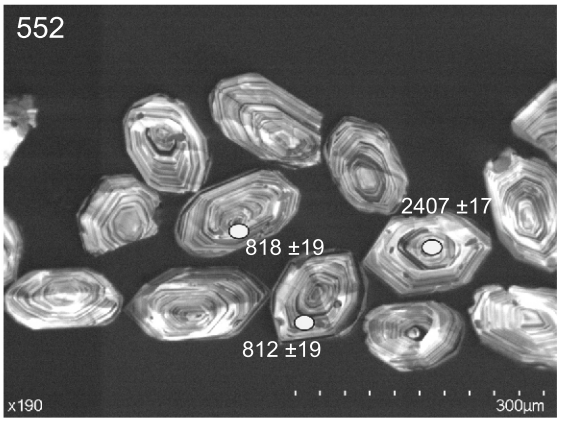

E
ASM06
selected
n= 22/37
data-point error ellipses are 2σ
820
780
Concordia Age = 796.9 ± 3.3 Myr
(2σ, decay-const. errs included)
MSWD (of concordance) = 3.0,
Probability(of concordance) = 0.081
$^{206}Pb/^{238}U$
0.138
0.134
0.130
0.126
0.9
1.0
1.1
1.2
1.3
1.4
1.5

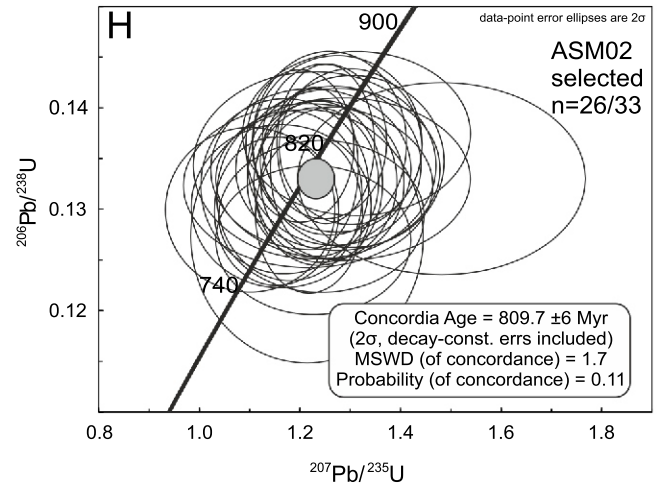

ASM06
812 ±9
794 ±9
792 ±9
x180
300µm


F
ASM08
selected
n=43/63
data-point error ellipses are 2σ
820
780
Concordia Age = 799.8 ±2.4 Myr
(2σ, decay-const. errs included)
MSWD (of concordance) = 0.87
Probability (of concordance) = 0.35
$^{206}Pb/^{238}U$
0.138
0.134
0.130
0.126
0.9
1.1
1.3
1.5


ASM08
796 ±9
780 ±14
786 ±8
781 ±10
795 ±9
768 ±10
x210
200µm


G
900
data-point error ellipses are 2σ
"552"
selected
n=35/59
860
820
780
Concordia Age = 814.7 ±5.2 Myr
(2σ, decay-const. errs included)
MSWD (of concordance) = 3.2
Probability (of concordance) = 0.062
$^{206}Pb/^{238}U$
0.146
0.142
0.138
0.134
0.130
0.126
0.8
1.0
1.2
1.4
1.6


552
2407 ±17
818 ±19
812 ±19
x190
300µm


H
900
data-point error ellipses are 2σ
ASM02
selected
n=26/33
820
740
Concordia Age = 809.7 ±6 Myr
(2σ, decay-const. errs included)
MSWD (of concordance) = 1.7
Probability (of concordance) = 0.11
$^{206}Pb/^{238}U$
0.14
0.13
0.12
0.8
1.0
1.2
1.4
1.6
1.8
$^{207}Pb/^{235}U$

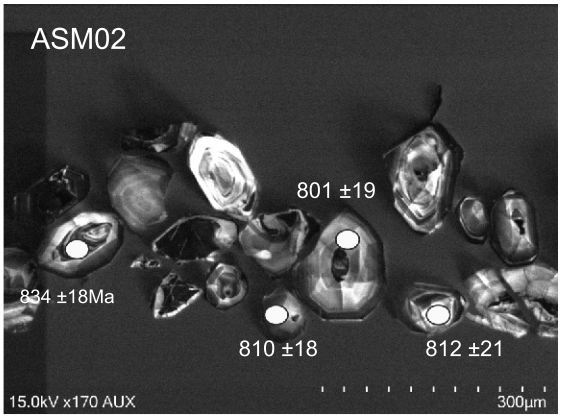

ASM02
801 ±19
834 ±18Ma
810 ±18
812 ±21
15.0kV x170 AUX
300µm

Fig. 6 cont.

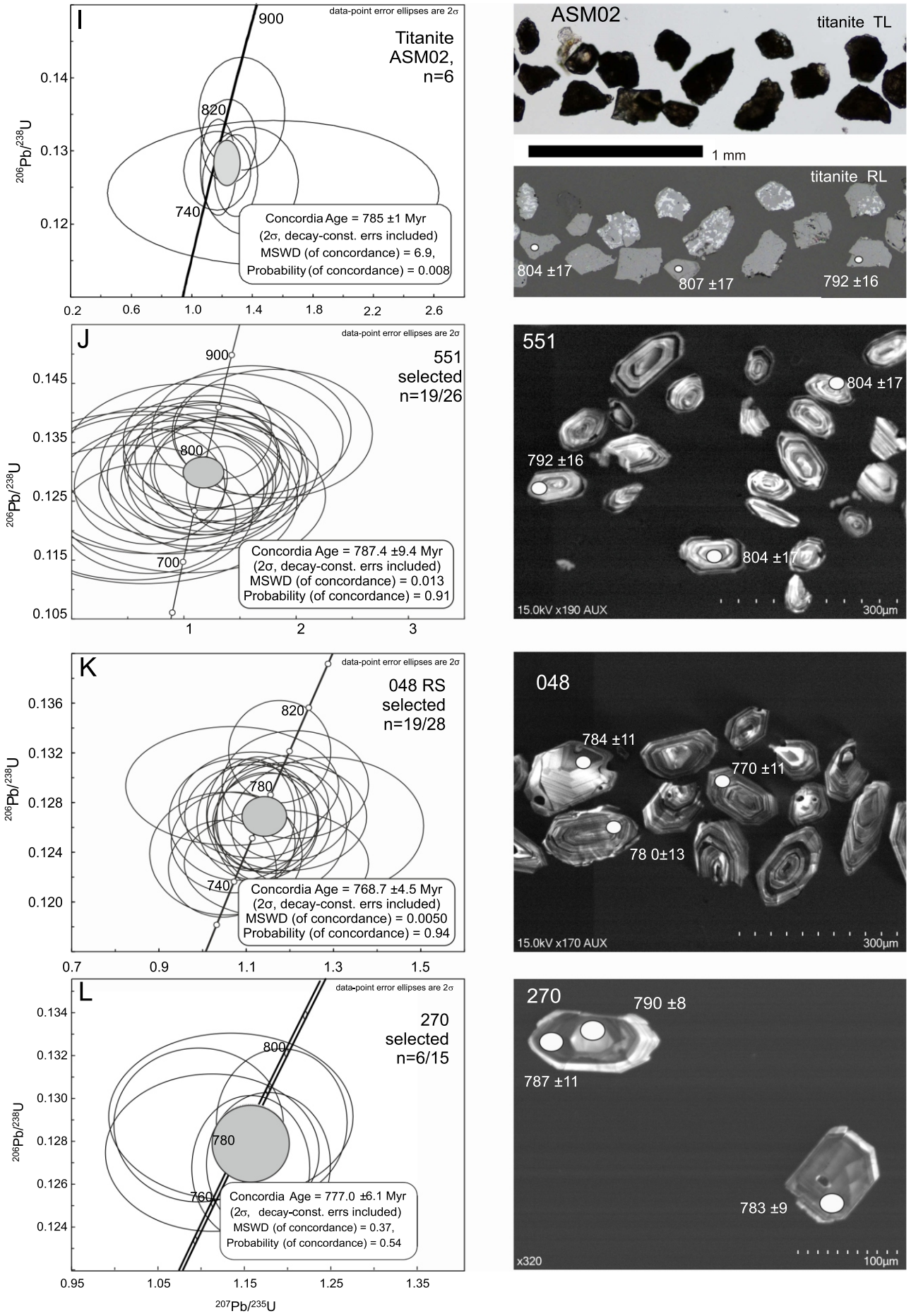
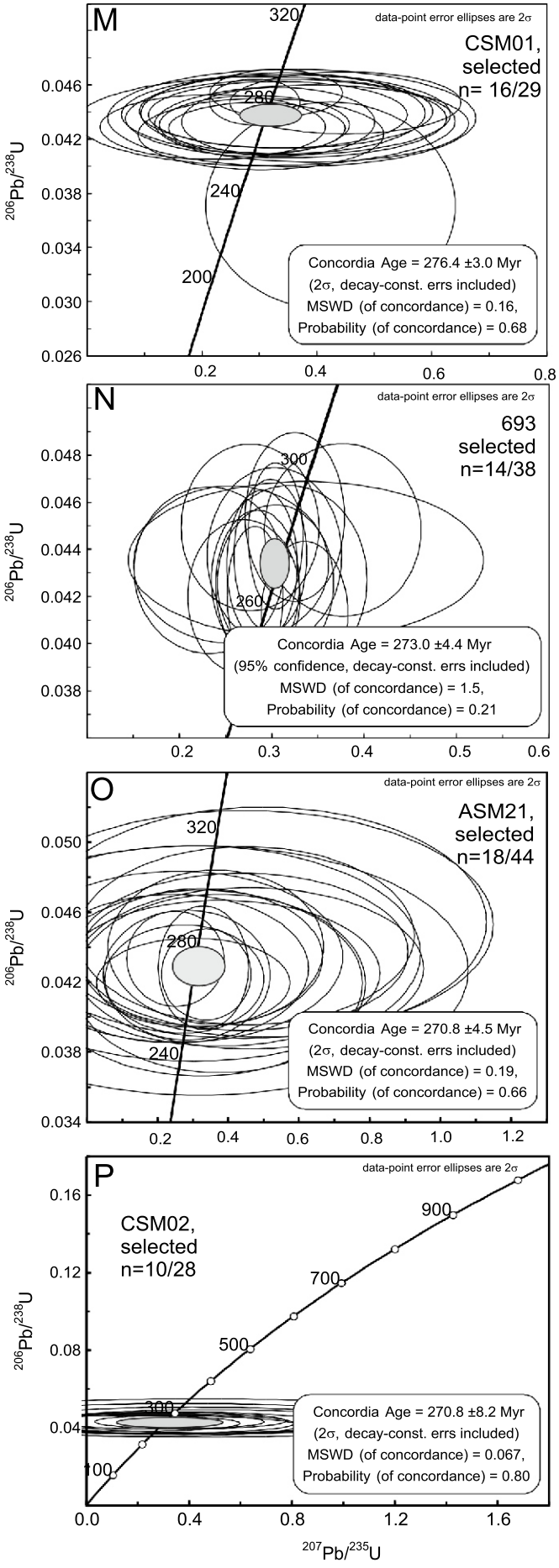
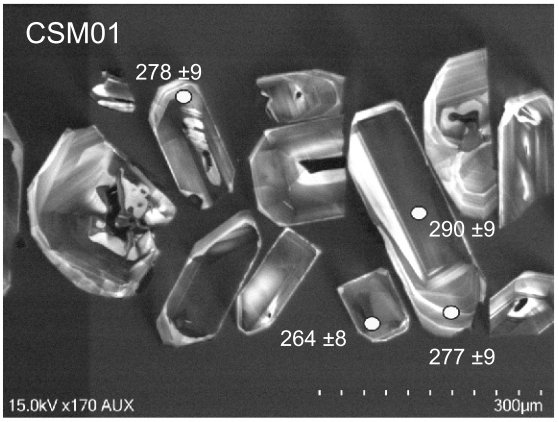
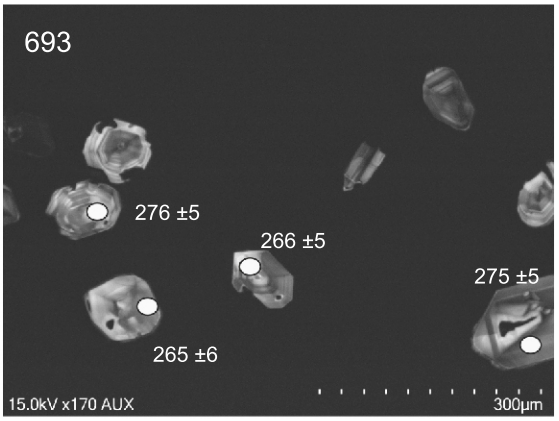
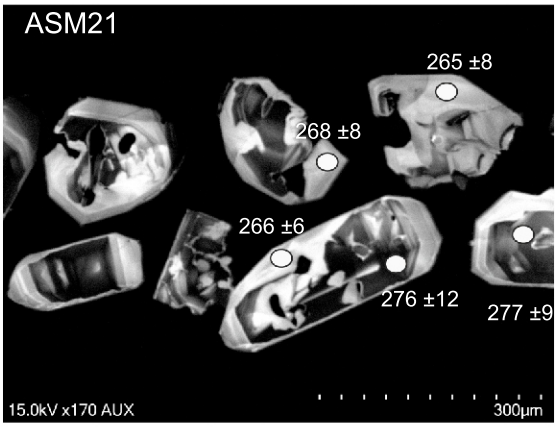

I
data-point error ellipses are 2σ
Titanite
ASM02,
n=6
900
820
740
Concordia Age = 785 ±1 Myr
(2σ, decay-const. errs included)
MSWD (of concordance) = 6.9,
Probability (of concordance) = 0.008
206Pb/238U
0.14
0.13
0.12
0.2
0.6
1.0
1.4
1.8
2.2
2.6
ASM02
titanite TL
1 mm
titanite RL
804 ±17
807 ±17
792 ±16
J
data-point error ellipses are 2σ
551
selected
n=19/26
900
800
700
Concordia Age = 787.4 ±9.4 Myr
(2σ, decay-const. errs included)
MSWD (of concordance) = 0.013
Probability (of concordance) = 0.91
206Pb/238U
0.145
0.135
0.125
0.115
0.105
1
2
3
551
804 ±17
792 ±16
804 ±17
15.0kV x190 AUX
300µm
K
data-point error ellipses are 2σ
048 RS
selected
n=19/28
820
780
740
Concordia Age = 768.7 ±4.5 Myr
(2σ, decay-const. errs included)
MSWD (of concordance) = 0.0050
Probability (of concordance) = 0.94
206Pb/238U
0.136
0.132
0.128
0.124
0.120
0.7
0.9
1.1
1.3
1.5
048
784 ±11
770 ±11
78 0±13
15.0kV x170 AUX
300µm
L
data-point error ellipses are 2σ
270
selected
n=6/15
800
780
760
Concordia Age = 777.0 ±6.1 Myr
(2σ, decay-const. errs included)
MSWD (of concordance) = 0.37,
Probability (of concordance) = 0.54
206Pb/238U
0.134
0.132
0.130
0.128
0.126
0.124
0.95
1.05
1.15
1.25
1.35
207Pb/235U
270
790 ±8
787 ±11
783 ±9
x320
100µm

Fig. 6 cont.


M
data-point error ellipses are 2σ
CSM01,
selected
n= 16/29
320
280
240
200
Concordia Age = 276.4 ±3.0 Myr
(2σ, decay-const. errs included)
MSWD (of concordance) = 0.16,
Probability (of concordance) = 0.68
N
data-point error ellipses are 2σ
693
selected
n=14/38
300
260
Concordia Age = 273.0 ±4.4 Myr
(95% confidence, decay-const. errs included)
MSWD (of concordance) = 1.5,
Probability (of concordance) = 0.21
O
data-point error ellipses are 2σ
ASM21,
selected
n=18/44
320
280
240
Concordia Age = 270.8 ±4.5 Myr
(2σ, decay-const. errs included)
MSWD (of concordance) = 0.19,
Probability (of concordance) = 0.66
P
data-point error ellipses are 2σ
CSM02,
selected
n=10/28
900
700
500
300
100
Concordia Age = 270.8 ±8.2 Myr
(2σ, decay-const. errs included)
MSWD (of concordance) = 0.067,
Probability (of concordance) = 0.80
206Pb/238U
207Pb/235U


CSM01
278 ±9
290 ±9
264 ±8
277 ±9
15.0kV x170 AUX
300µm


693
276 ±5
266 ±5
275 ±5
265 ±6
15.0kV x170 AUX
300µm


ASM21
265 ±8
268 ±8
266 ±6
276 ±12
277 ±9
15.0kV x170 AUX
300µm

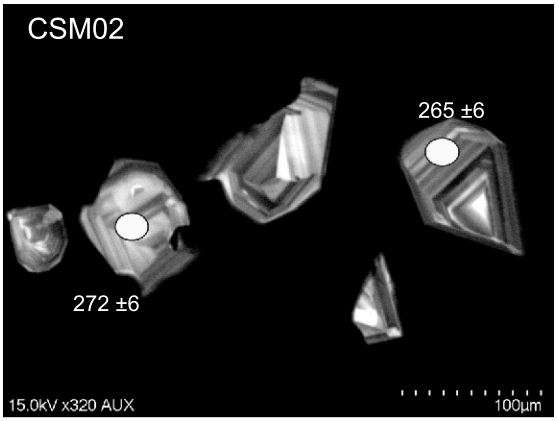

CSM02
265 ±6
272 ±6
15.0kV x320 AUX
100µm

Fig. 6 cont.

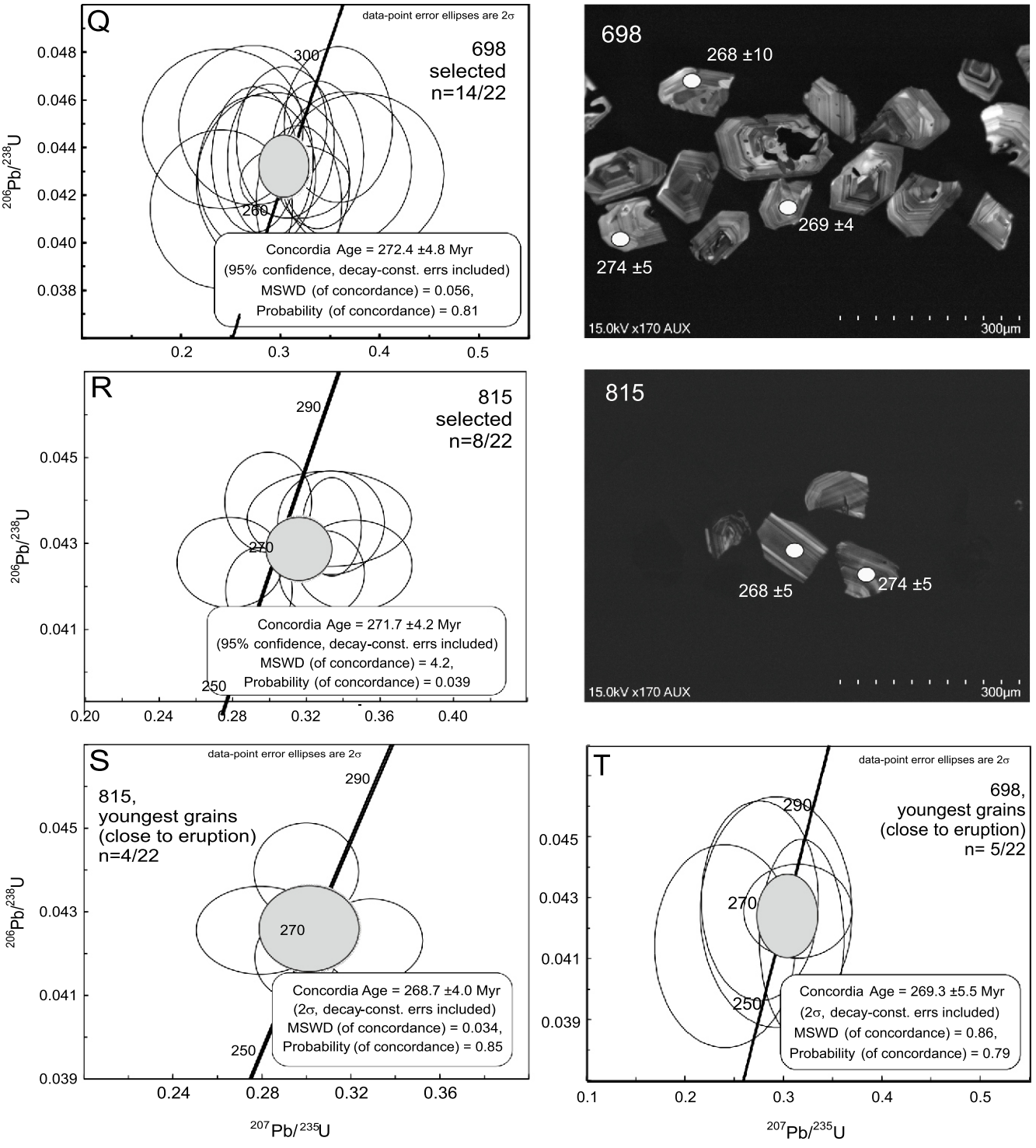


Fig. 6 cont.

to 1179 ppm, respectively. In consequence, the value of Th/U values is elevated, ranging from 0.85 to 3.10. Twenty-nine zircon analyses yielded a range of $^{206}Pb/^{238}U$ ages concentrated between 286 and 268 Myr. Several data points had to be omitted due to elevated contents of Pbc. The most consistent sixteen analyses selected (Fig. 6M) provide a well-defined concordia age of 276.2 ± 3.0 Myr (MSWD = 0.16). The same grains (n = 16/29), produced a weighted average of 276.4 ±3.5 Myr (MSWD = 0.99).

Sample 693 zircon

Mostly small grains (60–150 µm) extracted from sample 693 revealed euhedral forms and simple concentric to banded zonation. They have mostly low U and Th contents: 2 to 127 ppm and 2 to 218 ppm, respectively. The Th/U ratios range from 0.47 to 2.78. Thirty-eight zircon analyses yielded a range of radiogenic $^{206}Pb/^{238}U$ ages scattered between 304 and 254 Myr, thus some of these zircons can be considered as inherited. Some also have increased Pbc. The most consistent isotopic

Table 2

Summary of the U-Pb age determinations on zircon and titanite

Sample ID and location	Rock type [R1-R1] nomenclature	Concordia age [Myr] [MSWD]	Weighted average [Myr]	Number of spots /grains	Range of $^{206}Pb/^{238}U$ data [Myr]
PERMIAN					
„698" Namyn Bulag	volcanic [alkali rhyolite]	269.3 ±5.5 [0.86]	268.9 ±5.3 [0.16]	n=5/22	282→263 (*)
„815" Namyn Bulag	volcanic [hawaite]	268.7 ±4.0 [0.034]	268.1±7.0 [0.012]	n=4/22	293→264 (*)
„CSM02" Namyn Bulag	volcanic [rhyolite]	270.8 ±8.2 [0.067]	270.3 ±8 [0.18]	n=10/28	277→260 (*)
„ASM21" Namyn Bulag	plutonic [Ne syenite]	270.8 ±4.5 [0.19]	270.3 ±4.6 [0.28]	n=18/44	299→265
„693" Tonkhil Complex	plutonic [alkali granite]	273.0 ±4.4 [0.023]	273.0 ±2.5 [0.65]	n=14/38	304→254
„CSM01" Tonkhil Complex	plutonic [syenite]	276.4 ±3.0 [0.16]	276.4 ±3.5 [0.99]	n=16/29	286→268
TONIAN					
„1157" Dund Orthocomplex	metamorphic[]	810.6 ±9.0 [0.119]	809.7 ±9.2 [0.91]	n=20/37	872→772
„ASM04" Dund Orthocomplex	plutonic [granite]	810.3 ±6.3 [1.3]	810.7 ±6.4 [0.57]	n=21/38	832→749
„ASM03" Dund Orthocomplex	plutonic [syenite]	798 ±11 [1.3]	798 ±14 [138]	n=18/28	848→742
„ASM07" Dund Orthocomplex	plutonic [tonalite]	800.7 ±2.5 [0.0047]	800.7 ±3.2 [1.5]]	n=35/46	822→771
„ASM06" Dund Orthocomplex	plutonic [granite]	796.9 ±3.3 [3.0]	796.7 ±3.5 [0.78]	n=22/37	816→778
„ASM08" Dund Orthocomlex	plutonic [granite]	799.8 ±2.4 [0.87]	799.9 ±2.9 [1.2]	n=43/63	820→768
„552" Dund Orthocomplex	plutonic [monzodiorite]	814.7 ±5.2 [3.2]	814.3 ±6.1 [0.112]	n=35/59	840→785 (*)
„ASM02" Bayanbulag	plutonic [gabbro]	809.7 ±6 [1.7]	808.7 ±7 [0.45]	n=26/33	837→762
„ASM02" Titanite Bayanbulag	post-magmatic [gabbro]	785±11 [6.9]	779±11 [1.5]	n=6	817→755
„551" Bayanbulag	volcanic [lati-basalt]	787.4 ±9.4 [0.013]	787.4 ±10 [0.42]	n=19/25	828→772 (*)
„048" Bayanbulag	subvolcanic [syenogabbro]	768.7 ±4.5 [0.005]	768.6 ±6.4 [1.5]	n=19/28	803→746
„270" Bayanbogd	subvolcanic [rhyolite]	777.0 ±6.0 [0.37]	776 ±6.6 [0.55]	n=6/15	808→769

(*) inherited zircon grains more details within text and Table S1 in supplement. Appendix 1 in the supplement provides the Concordia diagrams with all analysed single spot results for each sample

ratios (Fig. 6N) were accepted and provide a concordia age of 273.0 ±4.4 Myr (MSWD = 1.5) for fourteen grains. The same number of spots (n = 14/38), produced a weighted average of 273 ±2.5 Myr (MSWD = 0.65)

Sample ASM21 zircon

The zircon grains extracted from sample ASM21 revealed euhedral forms but complex internal texture with distinct convoluted cores reflecting an early stage of crystallization, surrounded by uniformly bright, wide marginal zones. They have mostly low but scattered U and Th contents from 12 to 248 ppm and 5 to 495 ppm, respectively. The value of Th/U ratios are also spread between 0.47 and 2.23.

Forty-four zircon analyses were placed both in the cores and margins, yielding a range of $^{206}Pb/^{238}U$ ages scattered between 299 and 265 Myr. The most consistent eighteen analyses (Fig. 6O), provided a concordia age of 270.8 ±4.5 Myr (MSWD = 0.19). The same of grains produced a weighted average age of 270.3 ±4.6 Myr (MSWD = 0.28).

THE NAMYN BULAG INTRUSION

Sample CSM02 zircon

The rock contained very few small zircon grains (40–60 μm). The internal structure of the grains was simple with concentric zonation typical of felsic melts. They have low to moderate U and moderate and scattered Th contents from 65 to 204 ppm and from 33 to 514 ppm, respectively. The Th/U ratios remain in a range typical for magmatic zircons, from 0.5 to 1.77. Twenty-eight zircon analyses yielded a range of $^{206}Pb/^{238}U$ ages scattered between 277 and 260 Myr, but many of these provided

evidence of high Pbc (Table S1) contents. The most consistent analyses selected (n = 10/28), provided a concordia (Fig. 6P) age of 270.8 ±8.2 Myr (MSWD = 0.067). The same grains produced a weighted average of 270.3 ± 8.0 Myr (MSWD = 0.18).

Sample 815 zircon

This volcanic sample provided a limited number of small zircon grains with simple growth zonation. They have very low U and Th contents: 7 to 143 ppm and 4 to 111 ppm, respectively. The values of Th/U ratios range from 0.62 tp 1.83. Twenty-two zircon analyses yielded a range of $^{206}Pb/^{238}U$ ages scattered between 293 and 264 Myr with two clearly older ones standing out from the rest: of 304 Myr, and 347 Myr (discordant). Omitting these, the rest of the analyses (n = 8/22), defined (Fig. 6R) a concordia age of 271.7 ±4.2 Myr with relatively poor MSWD = 4.2. The single spot age results are highly dispersed. For volcanic zircon samples, the youngest results are usually considered as the best estimate of eruption time. The youngest zircons (n = 4) yielded (Fig. 6S) a concordia age of 268.7 ±4.0 Myr (MSWD = 0.034). The same four grains produced a weighted average of 268.1 ±7 Myr (MSWD = 0.0115).

Sample 698 zircon

Apart from the xenocrysts identified in this volcanic rock (two grains), the remaining volcanic zircons (Table S1) have very low U and low Th contents: 14 to 82 ppm and 16 to 140 ppm, respectively. The Th/U ratios range from 0.43 to 1.76. Twenty-two zircon analyses yielded a range of $^{206}Pb/^{238}U$ ages scattered between 282 and 263 Myr. One xenocrystic grain with an Archean core of 2883 Myr and Neoproterozoic rim of 624 Myr was also detected. The main volcanogenic zircon group was not uniform, but relatively consistent numerous analyses selected (n = 14/22) defined (Fig. 6Q) a concordia age of 272.4 ±4.8 Myr (MSWD = 0.056). However, to estimate the age of the eruption, only the youngest five zircons (n = 5/22) were used. They yielded (Fig. 6T) a well-defined concordia age of 269.3 ±5.5 Myr (MSWD = 0.86). The same five grains produced a weighted average of 268.9 ±5.3 Myr (MSWD = 0.16).

WHOLE-ROCK COMPOSITION AND ROCKS CLASSIFICATION

Compilation of Harker diagrams which plot major oxides and selected trace elements (Nb, Th, Zr, Sc, La, Y, Sr, Rb) against SiO_2 of the both age groups are provided as an Appendix to illustrate the variation within the suite.

GEOCHEMISTRY OF THE TONIAN ROCKS (DUND ORTHOCOMPLEX, BAYANBULAG AND BAYANBOGD INTRUSIONS)

The samples collected (Table 1 and Fig. 2) from the Tonian Dund Orthocomplex (8 samples), the Bayanbulag intrusion (2 samples) and the Bayanbogd intrusion (2 samples) are dominated by granitoids with minor subvolcanic to volcanic rocks. There is also one metamorphic rock sample (1157) with an igneous protolith (as shown by the zircon internal features). These granitoids have varied composition (Table 3), expressed by a wide range of the main oxides with SiO_2 (50.47–75.47 wt.%), MgO (0.17–6.13 wt.%), CaO (1.18–6.13 wt.%) and total alkalis ($Na_2O + K_2O$=4.5–10.8 wt.%) combined with variable Al_2O_3 (13.66–20.14 wt.%), Fe_2O_{3T} (0.89–6.93 wt.%) and low TiO_2 (0.52–0.84 wt.%) contents. The Na_2O/K_2O ratios (1.01–3.31) are higher than 1. The Mg# values are represented by three clusters of 20–30, 37–43 and 64 (ASM02). On the TAS classification diagram after Middlemost (1994), they show a basic/intermediate to acidic composition (Fig. 7A), plotting mostly as quartz monzonite and granite. The mafic sample of ASM02 falls on the border of the gabbroic diorite field, while the orthogneiss sample (1157) has a monzodioritic composition. The alkaline type rock sample (ASM03) plots in the quartz monzonite field. All three show (Fig. 7B) metaluminous characteristics with the aluminous saturation index A/CNK ranging from 0.60 to 0.92, while the others have clearly peraluminous features (*sensu* Maniar and Piccoli, 1989). Only three samples (i.e. ASM04, ASM06, ASM07) have A/CNAK > 1.1. A wide range of rock compositions is clearly illustrated by the R1–R1 multicationic classification (De la Roche et al., 1980), where the rock samples plot into the gabbro, monzodiorite, tonalite and granite fields. There is also evidence of more alkaline composition with plots in the syenogabbro and nepheline syenite fields (Fig. 7C). These rocks clearly show a bimodal character in plots on a (Na_2O+K_2O) vs. SiO_2 diagram (Fig. 7A). The mafic samples (gabbros) have relatively low Na_2O contents in the range of 2.8–3.7 wt.%, but the granitoids tend to have high Na_2O contents up to 7–9.5 wt.% (Fig.7D). In consequence, the Na_2O/K_2O ratio ranges from 1.08 to 10.85 while the K_2O/Na_2O ratio does not exceed 1, ranging from 0.09 to 0.99. This dominant sodic affinity (sodium series), nevertheless, could be partly linked to element mobility. The granitoids of the Khasagt Mountains can be classified as mostly alkaline-calcic and alkalic to calcic and ferroan to weakly magnesian (Fig. 7E, F). To account for alteration and metasomatic influence a classification scheme based on the immobile elements was used. Since Winchester and Floyd (1977) proposed the Zr/TiO_2-Nb/Y diagram, it has been extensively applied for the nomenclature of altered volcanic rocks. It also has a modified (Pearce, 1996) equivalent (i.e. Zr/Ti-Nb) for plutonic rocks. These plots (Fig. 8A, B) classified the plutonic samples as alkali granite syenite and granite/granodiorite (with no gabbro composition) but the volcanic samples as subalkaline basalt and rhyolite.

The chondrite-normalized rare earth element (REE) patterns of most samples, both plutonic and volcanogenic, are mutually comparable (Fig. 8C, D). They feature moderate light REE enrichment La_N/Yb_N = 6.7–25 with only one value of 40, and a relatively flat heavy REE segment in most samples expressed by Gd_N/Yb_N = 1.2–2.96. The granites mostly do not have negative Eu anomalies. Usually weak to moderate positive Eu anomalies (Eu/Eu* = 1.05–1.52) were observed in the granitic samples 552, ASM07, 048 and metamorphic 1157. Plagioclase is the mineral thought to be responsible for the development of the Eu anomaly. Usually, positive Eu anomalies are typical of anorthosites, which consist of cumulus plagioclase. Thus, slightly positive Eu anomalies (Eu/Eu* = 1.06–1.52) suggest a minor role of plagioclase fractionation, or even, considering the predominant immobile character of REE elements, the effects of post-magmatic modification.

GEOCHEMISTRY OF THE PERMIAN IGNEOUS ROCKS (TONKHIL AND NAMYN BULAG INTRUSIVE COMPLEXES)

New age data (Table 2) revealed the Permian igneous rocks in the northern part of the Khasagt Mountains. Their chemistry is described on the basis of samples from the Namyn Bulag Complex (Fig. 2) and from an area that may be the westernmost part (continuation) of the Tonkhil Complex known for its Permian rocks (see Kilian et al., 2016). In the case of both plutonic and volcanic rocks, the SiO_2 contents, ranging from ~49 to 77 wt.% (Fig. 7A), reflect a bimodal character of magmatism. On the total-alkalis *versus* silica diagram (TAS) after Le Maitre et al. (1989) the volcanic samples indicate trachybasaltic (sample 815) and rhyolite composition (sample 698). The plutonic samples plot within the quartz monzonite field (sample: ASM21 and CSM01) and the granite field (sample 693). The rocks are metaluminous to weakly peraluminous

Table 3

Whole-rock geochemistry and geochemical ratios

Sample ID	1157	ASM03	ASM04	ASM06	ASM07	ASM08	552	ASM02
Lab ID	10/19/5	10/19/8	10/19/2	10/19/9	10/19/6	10/19/3	10/19/16	10/19/7
Rock type	metamorphic	plutonic	plutonic	plutonic	plutonic	plutonic	plutonic	plutonic
TAS	monzodiorite	Q– monzonite	Q–monzonite	granite	Q–monzonie	granite	Q–monzonite	diorite
R1 vs R2	syenogabbro	syenite	granite	granite	tonalite	granite	monzodiorite	gabbro
[wt.%]								
SiO_2	54–35	62–85	67–54	75–47	64–77	72–74	63–1	50–47
TiO_2	0–274	0–38	0–32	0–134	0–264	0–133	0–234	0–459
Al_2O_3	22–32	19–38	17–42	13–66	20–14	15–12	19–75	16–96
Fe_2O_3	5–32	0–89	2–52	1–36	1–8	1–37	2–28	6–93
MnO	0–089	0–028	0–068	0–029	0–075	0–051	0–056	0–149
MgO	1–17	0–26	0–41	0–17	0–55	0–21	0–49	6–13
CaO	7–69	2–69	1–88	1–18	3–31	1–47	4–21	11–08
Na_2O	6–51	9–52	4–25	3–75	6–03	4–8	5–02	2–84
K_2O	0–6	1–26	4–22	3–47	2–06	3–9	3–44	1–7
P_2O_5	0–202	0–116	0–1	0–032	0–104	0–046	0–162	0–081
(SO_3)	<0.01	<0.01	<0.01	<0.01	<0.01	<0.01	<0.01	<0.01
(Cl)	0–02	0–029	0–017	0–023	0–023	0–02	0–027	0–023
(F)	<0.01	0–01	<0.01	<0.01	0–02	<0.01	<0.01	<0.01
LOI	1–3	2–4	1–0	0–6	0–6	<0.5	1–0	3–1
SUM	99–7	99–82	99–68	99–85	99–73	99–78	99–73	99–66
CIA	46–8	46–9	53–8	53–1	52–6	50–6	50–1	38–9
Mg# [Mg/Mg+Fe]	30–3	36–7	24–4	19–8	37–7	23–3	29–9	63–7
A/NK	1–97	1–14	1–51	1–38	1–48	1–25	0–65	2–6
A/CNK	0–88	0–88	1–16	1–13	1–11	1–02	1–01	0–64
Na_2O/K_2O	10–7	7–6	1	1–1	2–9	1–2	1–5	1–7
A.I.agpaitic index	0–51	0–88	0–66	0–73	0–6	0–8	0–61	0–38
[ppm]								
Ba	557	646	1568	528	1030	1025	914	625
Co	6	3	<3	5	<3	4	6	21
Cr	25	7	28	<5	<5	47	<5	232
Ga	22	11	18	13	19	15	18	14
Hf	<3	4	4	3	4	<3	<3	<3
Nb	6	9	12	15	10	11	7	7
Ni	<3	<3	<3	<3	<3	<3	<3	43
Sr	1097	236	339	125	868	245	731	462
U	<2	<2	<2	<2	<2	<2	<2	<2
V	99	41	15	<5	10	16	27	139
Zr	142	221	225	114	203	115	108	81
Pb	9	3	16	18	11	14	12	4
Rb	9	24	69	103	44	65	77	26
K/Rb	562	448	514	282	392	499	376	561
Sc	10–7	8–6	3–6	3–1	4–5	4–3	3–0	45–9
Th	1–42	11–8	9–23	10–19	3–22	6–00	4–2	1–76
Y	12–8	14–2	12–2	23–3	14–0	15–5	6–1	14–1
Sr/Y	87–1	16–6	27–8	5–1	62	15–8	119–8	32–8
La	32–4	43–6	59–4	27–0	18–7	21–5	23–0	15–8
Ce	55–9	89–2	113–2	54–6	33–6	41–5	34–7	31–9
Pr	6–4	10–2	12–2	6–7	4–1	5	3–6	4–0
Nd	23–0	36–2	40–3	24–2	16–3	18–1	12–1	16–0
Eu	2–69	1–79	1–72	0–85	2–19	1–2	0–94	1–12
Sm	3–73	6–11	5–71	4–96	3–32	3–37	1–87	3–35
Gd	2–88	4–28	3–68	4–11	3–11	2–8	1–49	3–1
Tb	0–39	0–59	0–48	0–68	0–47	0–44	0–2	0–44
Dy	2–35	3–12	2–63	4–32	2–88	2–8	1–15	2–78
Ho	0–49	0–57	0–49	0–89	0–58	0–59	0–23	0–58
Er	1–38	1–48	1–28	2–72	1–61	1–76	0–65	1–58
Tm	0–18	0–19	0–17	0–42	0–22	0–27	0–09	0–22
Yb	1–15	1–15	0–99	2–76	1–35	1–84	0–61	1–36
Lu	0–18	0–18	0–15	0–42	0–19	0–28	0–1	0–21
Sum REE	133–1	198–7	242–4	134–6	88–6	101–5	80–7	82–4
La_N/Yb_N	18–78	25–28	40	6–52	9–23	7–79	25–14	7–75
Gd_N/Yb_N	2	2–97	2–96	1–19	1–84	1–21	1–95	1–82
La_N/Gd_N	9–41	8–52	13–5	5–49	5–03	6–42	12–91	4–26
Eu/Eu*	2–52	1–08	1–15	0–58	2–1	1–2	1–73	1–07
Zr+Nb+Ce+Y	181–5	333–4	362–4	206–9	260–6	183	155–8	134
T sat zircon [°C]	716	771	820	769	798	754	733	620

Tabl. 3 cont.

Sample ID	270	48	551	815	ASM21	CSM01	693	698
Lab ID	10/19/1	10/19/10	10/19/4	10/19/12	10/19/13	10/19/15	10/19/14	10/19/11
Rock type	subvolcanic	volcanic	volcanic	volcanic	plutonic	plutonic	plutonic	volcanic
TAS	rhyolite	rhyolite	basalt	trachy-basalt	Q-monzonite	Q-monzonite	granite	rhyolite
R1 vs R2	rhyolite	rhyodacite	lati-basalt	hawaite	Ne-syenite	syenite	alkali granite	alkali rhyolite
[wt.%]								
SiO_2	69.32	71.29	49.8	49.14	55.99	59.16	74.41	77.01
TiO_2	0.327	0.243	2.008	1.484	1.054	1.445	0.184	0.265
Al_2O_3	15.61	14.9	15.78	19.27	18.57	18.76	13.75	11.89
Fe_2O_3	2.55	2.38	12.34	11.72	3.2	4.7	1.14	1.32
MnO	0.057	0.039	0.205	0.158	0.061	0.111	0.017	0.016
MgO	0.9	0.77	4.83	4.01	0.76	1.16	0.16	0.13
CaO	0.98	2.07	8.08	7.35	2.53	2.93	0.35	0.24
Na_2O	7.18	5.38	3.67	5.23	6.1	6.17	4.69	3.16
K_2O	1.32	1.62	1.14	0.52	4.56	4.65	5.06	5.01
P_2O_5	0.114	0.055	0.579	0.319	0.345	0.484	0.05	0.02
(SO_3)	<0.01	<0.01	<0.01	<0.01	<0.01	<0.01	<0.01	<0.01
(Cl)	0.048	0.025	0.023	0.022	0.026	0.021	0.039	0.025
(F)	<0.01	<0.01	<0.01	<0.01	<0.01	<0.01	<0.01	<0.01
LOI	1.5	1.1	1.5	0.7	6.3	<0.5	<0.5	0.8
SUM	99.85	99.77	99.61	99.59	99.48	99.49	99.85	99.85
CIA	51	50.9	41.8	46.1	48.7	47.8	49.9	51.8
Mg# [Mg/Mg+Fe]	41.2	39.1	43.7	40.4	32.00	32.8	21.8	16.3
A/NK	1.18	1.41	2.17	2.1	1.24	1.24	1.04	1.12
A/CNK	1.04	1.04	0.72	0.86	0.95	0.91	0.99	1.08
Na_2O/K_2O	5.4	3.3	3.2	10.1	1.3	1.3	0.9	0.6
A.I.agpaitic index	0.85	0.71	0.46	0.48	0.81	0.81	0.96	0.89
[ppm]								
Ba	444	819	452	2736	215	2079	394	14
Co	7	8	27	6	29	8	<3	7
Cr	<5	6	<5	<5	167	<5	<5	<5
Ga	13	12	19	21	19	23	17	18
Hf	4	4	4	<3	3	<3	6	9
Nb	8	6	15	23	12	28	21	45
Ni	<3	<3	15	<3	87	<3	<3	<3
Sr	173	309	468	894	791	804	105	35
U	<2	<2	<2	<2	<2	<2	<2	4
V	29	27	321	50	115	67	8	<5
Zr	136	107	201	253	179	325	258	341
Pb	4	7	5	8	<3	12	15	23
Rb	34	35	35	59	6	60	114	156
K/Rb	328	389	275	725	689	646	369	269
Sc	6.0	4.8	35.2	5.9	21.1	7.9	1.7	4.4
Th	5.71	6.39	2.07	1.58	1.19	2.57	6.58	16.99
Y	20.2	9.7	31.7	20.1	22.4	25.4	11.6	54.5
Sr/Y	8.6	31.9	14.8	35.3	44.5	31.7	9.1	38.5
La	29.3	22.7	29.6	49.8	17.7	65.1	18.8	66.1
Ce	58.4	38.3	63.9	98.5	38.8	126.0	36.9	137.9
Pr	7	4	8.5	12	5.4	15.4	4.2	16.8
Nd	25.8	13.0	35.4	44.2	23.0	56.8	13.4	57.0
Eu	1.24	0.85	2.47	3.2	1.85	3.5	0.43	0.48
Sm	4.78	2.06	7.37	7.02	5.3	9.24	2.13	11.01
Gd	3.77	1.63	7.07	5.65	5.08	7.06	1.6	8.51
Tb	0.58	0.26	1.03	0.74	0.76	0.94	0.29	1.51
Dy	3.73	1.68	6.38	4.31	4.52	5.33	1.94	9.8
Ho	0.78	0.36	1.31	0.81	0.9	1.00	0.42	2.07
Er	2.32	1.08	3.62	2.14	2.43	2.61	1.37	6.33
Tm	0.34	0.16	0.49	0.27	0.32	0.32	0.23	0.95
Yb	2.27	1.06	3.00	1.58	1.97	1.83	1.56	6.11
Lu	0.37	0.17	0.43	0.23	0.29	0.27	0.25	0.9
Sum REE	140.7	87.3	170.6	230.5	108.3	295.4	83.5	325.5
La_N/Yb_N	8.6	14.28	6.58	5.99	21.01	23.72	8.03	7.21
Gd_N/Yb_N	1.32	1..23	1.88	2.06	2.85	3.08	0.82	1.11
La_N/Gd_N	6.5	11.65	3.5	2.91	7.37	7.71	9.83	6.5
Eu/Eu*	0.9	1.43	1.05	1.1	1.56	1.33	0.72	0.15
Zr+Nb+Ce+Y	222.6	196	311.6	252.4	394.6	504.4	327	578.4
T sat zrn [°C]	765	749	701	743	757	802	825	867

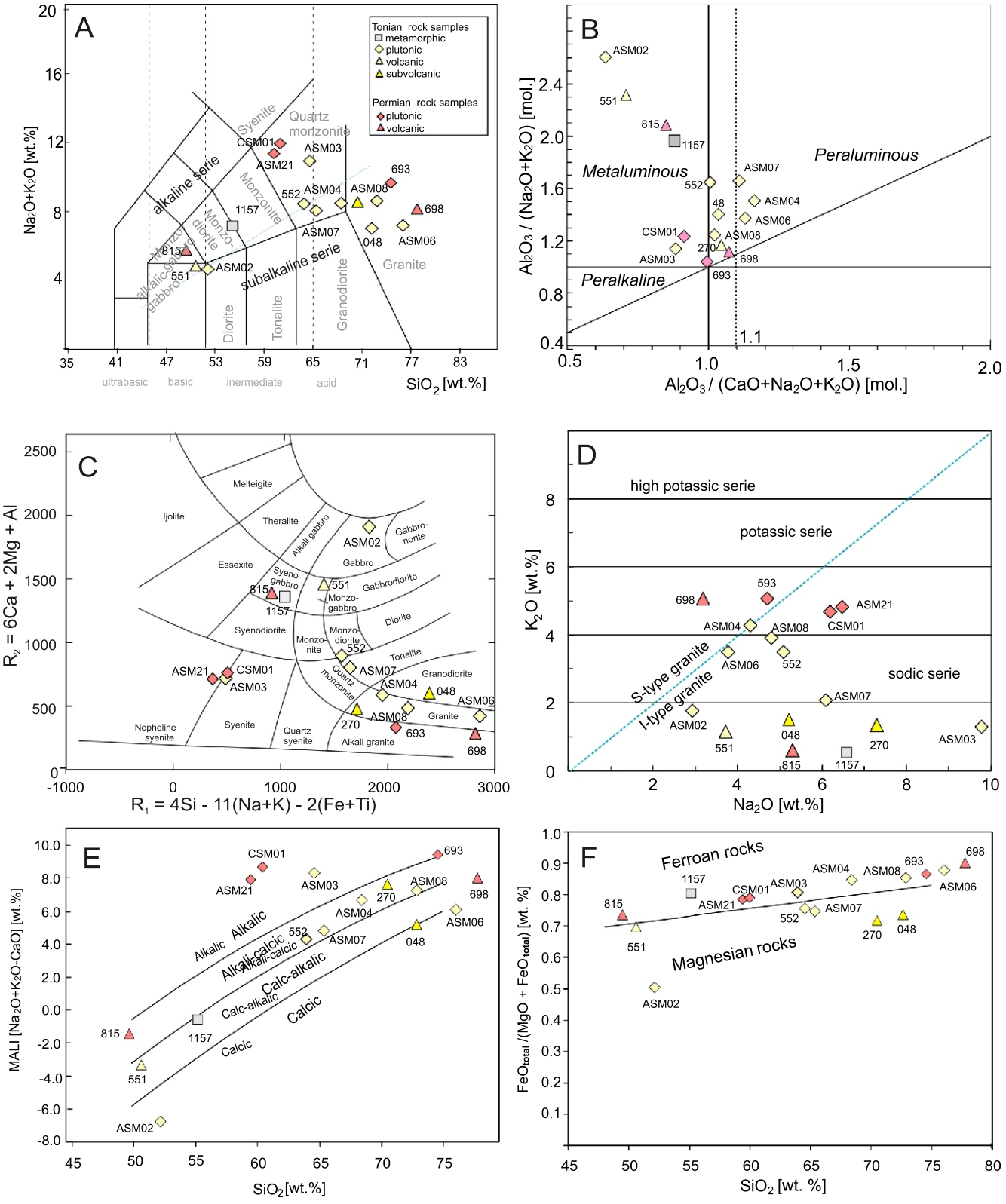


Fig. 7. Whole-rock classification of the Khasagt Mountains crystalline rocks

A – total alkali–silica (TAS) diagram after Middlemost (1994) with the alkaline/subalkaline boundary according to Irvine and Baragar (1971); **B** – A/NK vs. A/CNK diagram (Maniar and Piccoli, 1989) showing the peraluminous to metaluminous character of the samples; **C** – diagram based on the multicationic parameters R1 and R2 (after De la Roche et al., 1980); **D** – Na_2O vs. K_2O wt.% diagram after Middlemost (1975) with fields of the high-potassium, potassium and sodium series, and discrimination of I-type and S-type granitic rocks (after Chappell and White, 2001); **E** – MALI vs. SiO_2 discrimination (Frost et al., 2001); **F** – FeO total/(FeO total + MgO) vs. SiO_2 discrimination diagram indicating fields for ferroan and magnesian granites (Frost et al., 2001)

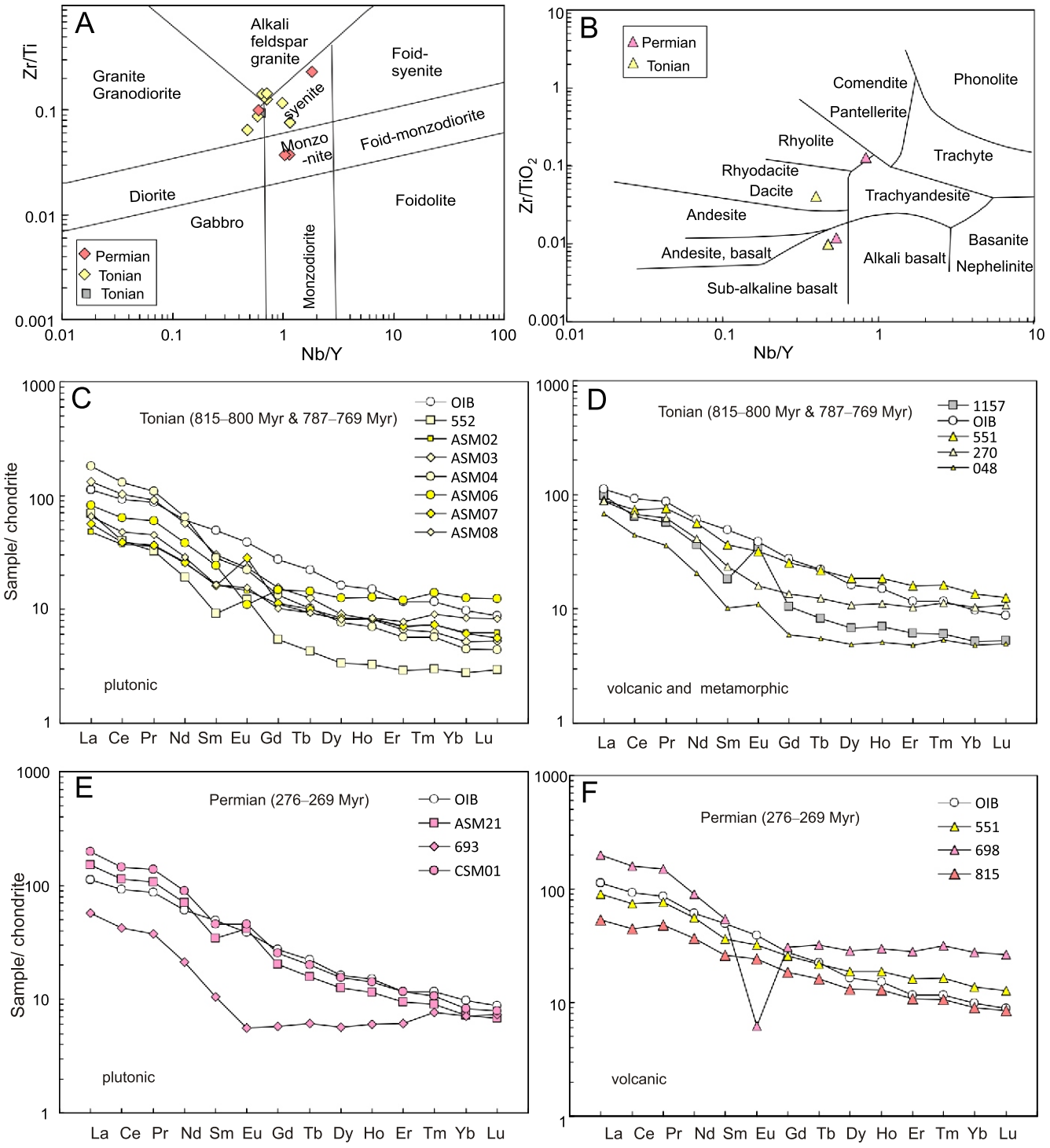


Fig. 8. Trace element characteristics of the Khasagt Mountains crystalline rocks

A – Zr/Ti *versus* Nb/Y diagram for plutonic rocks (Pearce ,1996); **B** – Zr/TiO_2 *versus* Nb/Y for volcanic rocks after Winchester and Floyd (1977); **C** – chondrite-normalized REE patterns for the Tonian group of granitoids; **D** – chondrite- normalized REE distribution patterns for the Tonian orthogneiss and volcanic, subvolcanic rocks; **E** – chondrite-normalized REE distribution patterns for the Permian granitoids; **F** – chondrite-normalized REE distribution patterns for the Permian volcanic rocks (Tonian volcanic sample is shown for comparison). Chondrite-normalizing values after Nakamura (1974)

with the aluminous saturation index A/CNK ranging from 0.89 to 1.08 (Fig. 7B). In terms of the R1 vs. R2 classification diagram (De la Roche et al., 1980), the plutonic rocks plot in the alkali granite, syenite and close to the border of the nepheline syenite fields. The volcanic samples are located in the alkali rhyolite and hawaite fields (Fig. 7C). They represent both potassic and sodic series (Fig. 7D). The K_2O/Na_2O ratio range varies between 0.1 and 1.59 (but Na_2O/K_2O from 0.63 to10.64). The Mg# values show two clusters, of 16–22 and 32–40. The Permian granitoids of the Khasagt Mountains can be classified (Fig. 7E, F) as alkalic and ferroan but the volcanic rocks are alkalicalcic and ferroan. Using a classification scheme based on immobile elements proposed by Pearce (1996) the plutonic rocks are monzogranite and syenite (Fig. 8A, B). The volcanic rocks can be classified as subalkaline basalt and trachyandesite.

The chondrite-normalized rare earth element (REE) patterns, of both plutonic and volcanogenic samples, show moderate variation in their characteristics (Fig. 8E, F). Chondrite-normalized REE patterns in the volcanic samples are weakly to strongly fractionated. The light REE enrichment is evident from La_N/Yb_N = 6.0–23.7. The heavy REE segments are flat in most samples expressed by Gd_N/Yb_N = 0.8–3.1. The granites have weak positive Eu anomalies (Eu/Eu* = 1.33–1.56). The felsic alkali rhyolite (sample 698), as a strongly fractionated rock, reveals a negative Eu anomaly (Eu/Eu* = 0.15). On the whole, the HREE pattern of all the rocks clusters around 10 times chondrite for those of granitic composition, and 30–10 times for the volcanic rocks.

DISCUSSION

The new U-Pb age and whole-rock geochemical data of the granitoids and volcanic to subvolcanic rocks (Figs. 1 and 2), collected in the southwestern part of the Zavkhan Terrane in Western Mongolia, have informed on several crucial questions about the age and origin of these rocks. The explored area of the Khasagt Mountains is dominantly composed of late Tonian granitoids and early Permian granitoids and volcanic-sedimentary sequences. The Permian sequences are limited to the northernmost part of study area. The traditional application of zircon U-Pb geochronology in igneous rocks includes determining the emplacement age, but there are also attempts (e.g., McKay et al., 2018) to identify distinctive geochemical signatures of zircon reflecting specific tectonic settings. The use of zircon Th/U ratios can provide insight into tectonic processes.

ZIRCON (Th/U) COMPOSITIONAL SIGNATURES

U and Th concentrations in zircons are collected as part of U-Pb age determinations on SHRIMP analyses and provide a wealth of information that is useful in understanding rock-forming processes and conditions. The composition (and texture) of grains from the Khasagt Mountains does not show any evidence for metamorphic crystallization, which should be expressed by (well-defined) overgrowths and low Th/U ratios i.e. Th/U <0.1 (Rubatto, 2002; Hoskin and Schaltegger, 2003). Apart from one case of a xenocryst in a volcanic rock (689),the Th/U ratios from both age groups are represented by values between 0.4 and 2.0 (Fig. 9A), which meets a common criterion for zircons from igneous rocks (Kirkland et al., 2015). Most of the Tonian data plot close to or below the Th/U = 1 line (Fig. 9) suggest a similar magmatic system. There is no systematic variation of Th/U among the plutonic versus volcanic samples within this age group. Low zircon Th/U values correlate with convergent arc magmatism (McKay et al., 2018). Some general observations (Xie et al., 2022), hav esuggested that low zircon Th/U values (<1.0) tend to be from melts generated in a compressional arc front setting. However, the presence of numerous grains with a value >1 does not allow them to be classified as obvious arc zircons.

The Permian zircon samples are characterized by wide range and higher Th/U values up to 3.5, which are probably related to more evolved, fractionated or/and alkaline melts. Zircons from the alkaline rocks are characterized by Th/U >1 (Belousova et al., 2002). The alkaline nature of the grains, recognized on the basis of SHRIMP measurements (Table S1), indicate their affinity to a rift-related tectonic setting. Recently, it has been suggested (e.g., McKay et al., 2018; Xie et al., 2022), that magmatism coeval with extensional tectonism tends to produce zircons with a wider range of Th/U values, including significant populations of elevated Th/U zircons (>1.0).

These features, identified mainly in zircons from samples of the Permian rocks, indicate the extensional nature of the magmatism in the northern part of the Khasagt. Apart from the tectonic stress regime (McKay et al., 2018), the Th/U parameter in zircon also empirically links to the silica content of the host melt and crystallization temperatures (Kirkland et al., 2015). The zircon data collected from the Khasagt Mountains indicate that zircons with more uniform Th/U values, in the range of 0.5–1.5, are associated with more mafic rocks (e.g., ASM02, Bayanbulag intrusion), although some felsic rocks (e.g., ASM03, ASM04, the Dund Orthocomplex) also contain zircons with this Th/U range (Fig. 9C). Moreover, there is no simple (i.e.positive or negative) correlation of Th/U with the whole-rock zircon saturation temperature (T_{Zr}, Watson and Harrison, 1983). Observed T_{Zr} variations rather result from the rock type. They correspond well to averaged temperatures of fractionated I-type or A-type granite (King et al.,1997). Therefore, it seems that theTh/U ratio measured in igneous zircons may become a promising discriminator of the stress regime, that is related to the regional tectonic setting (i.e extension).

GEOCHEMICAL INDICATORS OF TECTONIC SETTING

The Neoproterozoic igneous rocks in the Zavkhan Terrane have commonly been interpreted as of island arc or/and continental margin affinity, and as reworked Early Precambrian continental crust (e.g., Kozakov et al., 2021 and references within). Recent considerations of geochemistry related to the early Neoproterozoic magmatism highlight a number of possible complications in assessing the tectonic environment based solely on geochemical data (Soejono et al., 2023 and references therein). Similarly, the record of geochemical variability from the Khasaght Mountains study area seems to be diagnostically unclear.

Normal mid-ocean ridge basalt (N-MORB)-normalized trace element patterns, (presented with precisely identified sample ID and age (see Fig.10) clearly highlight the presence of a negative Nb anomaly, that is a general indicator of arc-like melts. Nevertheless, cases of contamination by continental crust or lithosphere may also expressed by this anomaly (e.g., Förster et al., 1997). They lead to misidentification of contaminated rocks from other settings as arc-related.

The late Tonian granitoids (Fig.10A) are similar to each other. They also show positive K, negative P, and deeply negative Ti anomalies inferred from the low TiO_2 (<0.45 wt.%). These characteristics are commonly interpreted as a subduction-like signature (e.g., low Nb, low Ta and low Ti). The formation of the Dund Ortocomplex and Bayanbulag (and Bayanbogd) intrusions have been linked to similar tectonic settings. This may suggest their co-magmatic genesis. Moreover,

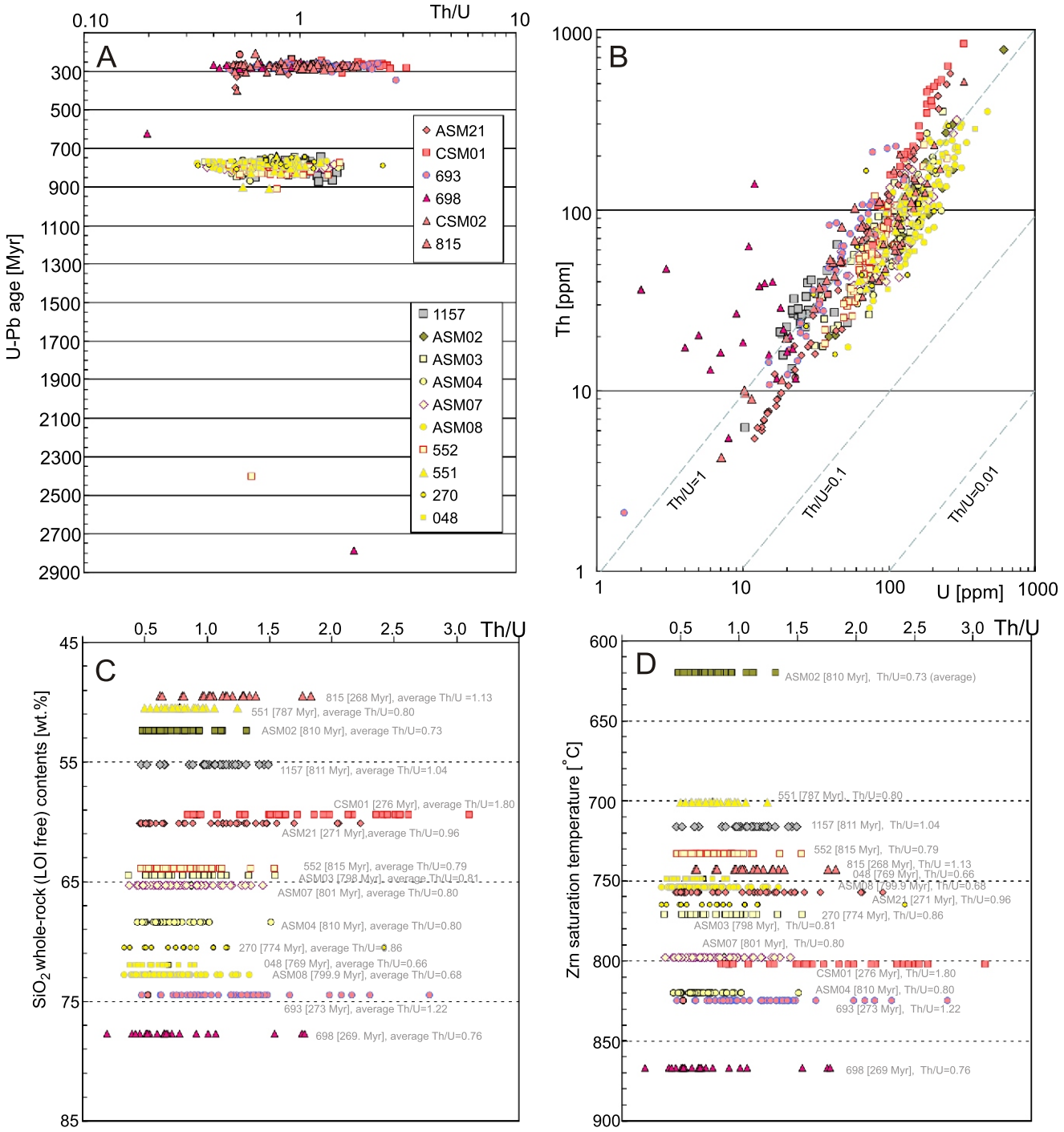


Fig. 9. Th/U discrimination diagrams of the zircon crystals analysed from the Khasagt Mountains

A – U-Pb age *versus* Th/U; **B** – U versus Th; **C** – whole-rock silica concentrations *versus* Th/U; **D** – whole-rock zircon saturation temperature (T_{Zr}, Watson and Harrison, 1983) diagrams. All data provided by SHRIMP single-spot analyses of grains. The sample $^{206}Pb/^{238}U$ age and Th/U average is indicated

the subvolcanic 048 and metamorphosed 1157 samples (Fig. 10B) resemble the granitoid characteristics (similar enrichments in Rb, Th, and LREE; with a comparable or lower magnitude of negative Nb anomaly and lower P and Ti depletion).

This is in contrast to the characteristics of the Permian granitoids and volcanics (Fig. 10C, D), where heterogeneity of N-MORB)-normalized patterns is observed. The Nb, K and P, Ti anomalies are not well-defined, showing neither distinct enrichments nor depletions. The use of discrimination diagrams with canonical trace element arrangements (*sensu* Pearce et al., 1984) leads to indication of the setting as a volcanic arc (Fig. 11A, B) or continental-arc magmatism, but with significantly dispersed plots, also towards the within-plate field, that could be related (Föster et al., 1997) to a complex or polyphase orogeny or associated in space and time with an extensional regime. Numerous studies in various tectonic settings have examined immobile Th and Nb elements as a proxy for crustal imputs (Pearce, 2008).The whole-rock concentrations of these

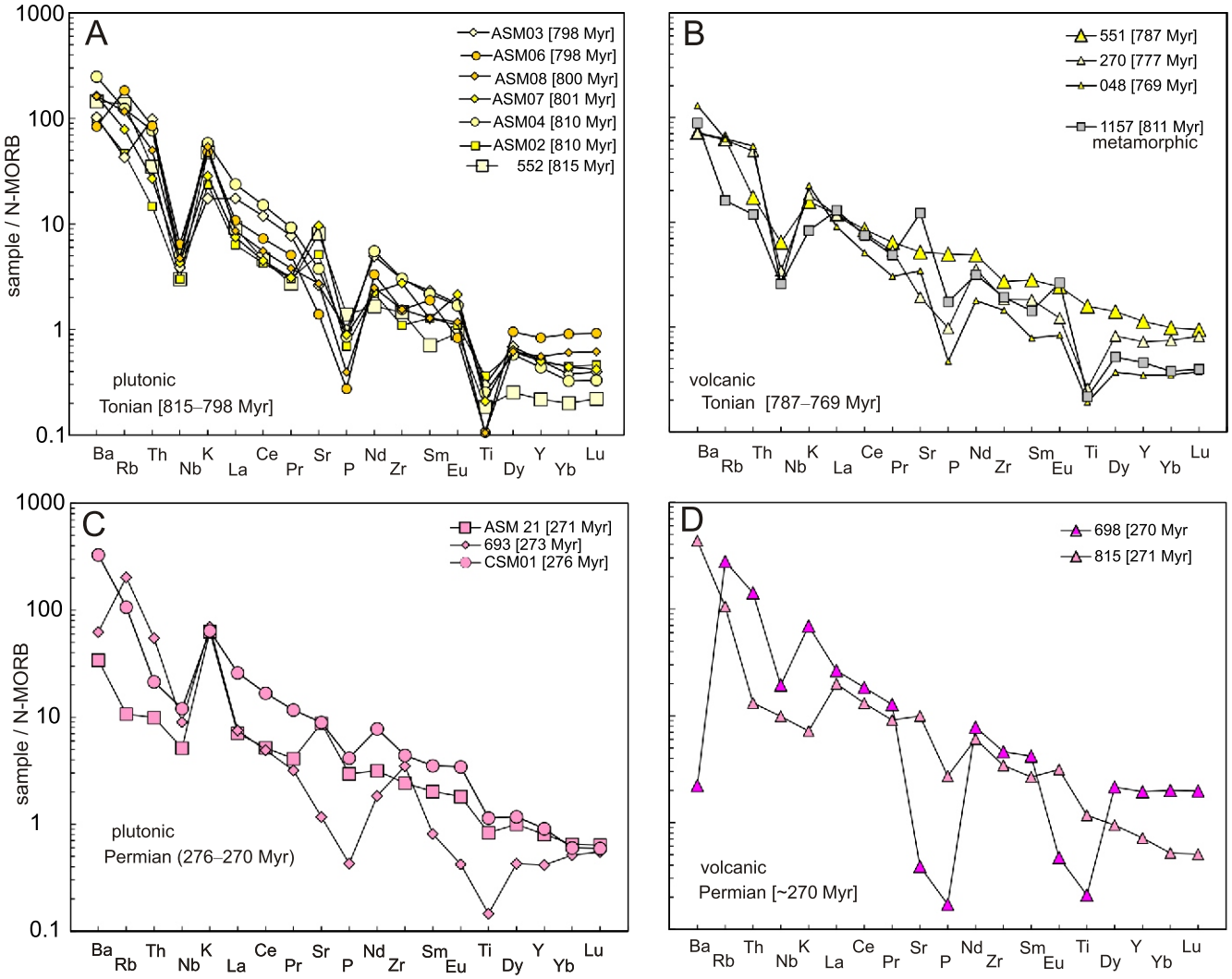


Fig. 10. Whole-rock incompatible elements normalized to N-MORB (normal mid-ocean ridge basalt; diagrams comparing patterns of the plutonic versus volcanic rocks: (A) Tonian samples (B) Permian samples

N-MORB values after **Sun and McDonough (1989)**

elements normalized to N-MORB (in order to have a direct idea of enrichment or depletion with respect to N-MORB) are among many details related to a backarc or forearc setting and allow discrimination of a melt type generated at divergent versus at convergent plate settings (Saccani, 2015). Althought generally applied to more mafic melts, this diagram exposes two distinct geochemical trends. The variations on the Th_N vs Nb_N diagram (Fig. 11E) indicate distinct plots of the Permian samples within the field of a divergent regime (within-plate setting or subduction-unrelated setting and rifted margins). This is in contrast to the Tonian samples plotted within the range of convergent plate settings (e.g., continental margin, volcanic arc or polygenetic crust island arc). However, among the geochemical dataset described from the Khasagt Mountains, the mafic components are not fully representative. Their age has not been determined, with no zircons separated from at least 4–6 samples collected in the field. Despite a lack of the geochemical documentation a number of occurrences of mafic rocks were identified in the field, as evidence of bimodal magmatism. This can occur in diverse tectonic settings including continental rift zones (e.g., Deering et al., 2011), oceanic island arcs (e.g., Gribble et al., 1996) and continental arcs (e.g., Wang et al., 2019), back-arc basins (e.g., Stern et al., 1996) and post-collision extensional regimes (e.g., Ersoy et al., 2008). A bimodal association with the participation of alkali granites is considered as a strong indicator of rifting processes (Bonin et al., 1998; Bonin, 2007). Both age groups in the Khasagt Mountains reveal (Fig. 7E) geochemical indicators of an alkaline nature, expressed by high Nb/Y ratios on classification diagrams (Fig. 8A, B) and by the agpaitic index (A.I.; Table 3), in the range of 0.81–0.96 (Permian) or 0.6–08 (Tonian). The alkalinity of the igneous rocks was identified (Figs. 8A, B and 11G, H) using combinations of Th/Yb, Nb/Yb, and La/Yb in diagrams of Nb/Yb-Th/Nb and Nb/Zr-La/Yb (after Li et al., 2025).

Some of the Tonian and all Permian granitoids tend to plot close to the division line between I-type and A-type granitoids or in the A-type discrimination field (Fig. 11C). They represent a higher (than common I-type rocks) degree of fractionation or lower degree of partial melting expressed by the sum of the HFSE (Zr+Y+La+Ce) being higher than 350 ppm (Whalen et al.,1987). A similar compositional trend towards A-type rocks has been documented by whole-rock analyses (Fig. 11C) of the granitoids previously dated by Yarmolyuk et al. (2008) and Soejono et al. (2023). Their potential A-type affinity, however,

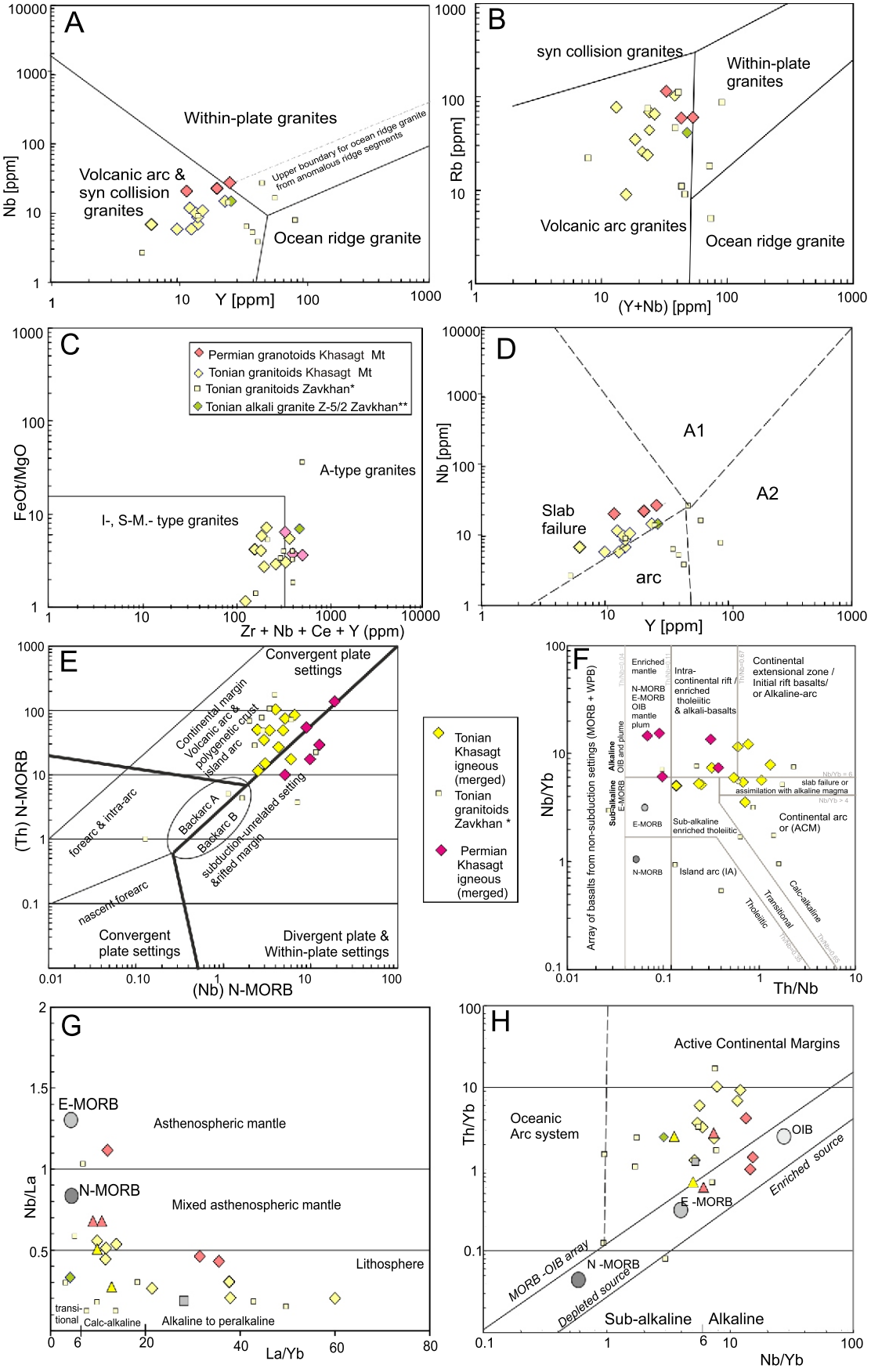


Fig. 11. Geochemical discrimination to constrain the tectonic setting type and magma source characteristics

A, **B** – tectonic discrimination diagrams after Pearce et al. (1984); **C** – Zr+Nb+Ce+Y *versus* FeOt/MgO after Whalen et al. (1987); **D** – Nb-Y and discrimination plot modified by Whalen and Hildebrand (2019) with fields of arc, slab failure-influenced granitoids versus A1- and A2-type granitoid; **E** – Th_N vs. Nb_N diagram (Saccani, 2015) with values normalized to the N-MORB composition (Sun and McDonought, 1989); F – newly constructed Nb/Yb vs. Th/Nb diagram (Li et al., 2025) providing more accurate magmatic alkalinity discrimination; **G** – Nb/La vs. La/Yb diagram to distinguish between lithospheric and asthenospheric mantle sources adopted from Hollocher et al. (2012); with alkaline range after Li et al. (2025); **H** – Nb/Yb *versus* Th/Yb discrimination diagram after Pearce (2008), including values characteristic of E- and N-MORB = Enriched and Normal Mid-Ocean Ridge Basalts; OIB = Oceanic Island Basalts

has not been discussed previously. Only the late Paleozoic granitoids in the northwestern Trans-Altai Zone (Hanžl et al., 2023) were interpreted as alkaline post-orogenic plutons, with A2-type granite affinity (*sensu* Elby, 1992). The diagnostic sum (Zr+Y+La+Ce) for these rocks ranges from 327 to 578 ppm, similar to the range of A-type granites (>350 ppm) *sensu* Whalen et al. (1987). A current approach to classification of granitoids (Bonin, 2007) retains the term A-type to define a group of rocks that may include ferroan, alkaline to alkali-calcic, metaluminous, slightly peraluminous, and peralkaline varieties.

Recently, the classic volcanic arc granitoids of Pearce et al. (1984) have been divided into volcanic arc and slab-failure fields (Whalen and Hildebrand, 2019). Based on this discrimination (Fig. 11D) , some of the Neoproterozoic Permian samples fall on the border between the slab failure and arc fields, which may result from the simultaneous influence of several factors. This could be consistent with their occurrence as small plutons rather than arcuate belts. It also suggests that the parental magma of these rocks presumably experienced extensive contamination or assimilation with alkaline magma (Fig. 11F). This is consistent with the latest ideas on whole-rock and isotopic geochemistry (Soejono et al., 2023), emphasing that a hybrid magmatic suite in the Zavkhan Terrane originated from the interaction between basic, mantle-derived and felsic, crustally-derived magmas, with geochemical signatures of an intra-plate, extensional (rift) setting and a signal of an ancient, possibly arc-related crust.

The whole-rock data collected from the the Khasaght Mountains area revealed also an alkaline nature of the rocks. A newly developed “Nb/Yb-Th/Nb” discriminator (Fig. 11F), designed to be applicable to both mafic and felsic igneous rocks simultaneously (Li et al., 2025) points to an alkaline signature (i.e.Nb/Yb >4), of both late Tonian and early Permian magmatism, indicating rifting-related geochemical features, similar to initial rift melts, continental extensional zones or intracontinental rifts. This final diagram has been used as a supporting tool rather than the primary method for geotectonic discrimination.

The complex geochmical signature that blurred recogniton of the tectonic setting has resulted from a developing rift, that dissected a pre-existing arc or active margin domain (as indicated by sizeable negative Nb–Ti anomalies in N-MORB-normalised spider plots).

TEMPORAL VARIATION OF MAGMATIC EPISODES IN THE KHASAGT MOUNTAINS

The results of age investigations of the south-western part of the Khasagt Mountains area (summarized by Table 2), indicated a spectrum of U-Pb ages forming two main groups: a dominant and widespread late Tonian group, and an early Permian group (Fig. 12A).discovered in the northern part of the area. This important U-Pb zircon age group supports a link between theTonkhil Complex with alkaline granites, suggesting a prolongation of the alkaline bodies towards the west.

LATE TONIAN PUNCTATED EPISODE

The geochronological data from eleven samples of the Khasagt Mountains, western Mongolia, yielded crystallization ages varying from 815 to 769 Myr. This range partially overlaps (Fig. 12B) with those reported by Bold et al. (2016a, b) i.e. ~811–787 Myr, by Soejono et al. (2023) i.e. 840–800 Myr and by Kozakov et al. (2021) i.e. 840–720 Myr.

Exploration of the southern part of the Zavkhan Terrane in the Khasagt Mountains completes the age recognition in two adjacent sub-areas (NW: Buduun–Urgamal complexes and SE Zalaa Uul Teeg Uul Complex) previously realized by Soejono et al. (2023). The Khasagt Mountains, a study area including the Dund Orthocomplex, Bayanbulag (and Bayanbogd) intrusions, provides a slightly younger time frame of 810–770 Myr (Table 2). The older early Neoproterozoic magmatic episode is known from other parts of the Zavkhan Terrane e.g. the 960–931 Myr Mélange zone (Kovach et al., 2021) and at ~840–800 Myr, from the Zavkhan Formation and Zalaa Uul Complex in the south-east. The compilation of these results indicate punctuated magmatic pulses, that were most intense at ~810–800 Ma, followed by a period of little activity at ~787–769 Ma, related mainly to volcanic or subvolcanic activity.

This relatively younger magmatic pulse at 787–769 Ma influenced the surrounding older massifs, slowing their cooling. Some of the granitoids (including sample ASM02) include a titanite phase, usually crystallised during late-stage magmatic evolution. The Th/U ratio is commonly used to discriminate the formation environment of titanite with Th/U (>1) indicating a magmatic origin and Th/U (<0.4) a hydrothermal origin (Aleinikoff et al., 2002). Variations of Th/U values in the range of 0.4–1.9 recorded in the ASM02 titanite crystals however suggest rather an intermediate origin.Titanite as a reactive mineral is prone to (re)crystallization via multiple mechanisms such as: igneous growth, diffusion-related retrograde metamorphic reactions and crystallization in the presence of fluids (Lei et al., 2021). The ASM02 titanite is interpreted as having crystallized from sub-solidus fluids (as a so-called “hydrothermal titanite”, e.g. Erdmann et al. (2019) in contrast to titanite crystallized in unequivocal magmatic conditions. Hydrothermally crystallized titanite typically forms irregular rims on magmatic crystals (Fig. 3B). The ASM02 titanite grains record a time of crystallization of 785 Ma. Thus, an interval of at least 23 Myr between the zircon and titanite ages is visible (Table 2). The titanite age is consistent with the time of the second mostly volcanic pulse (sample 551, 270) in the Khasagt region. Therefore, a titanite U-Pb age is not interpreted in terms of thermochronology (as a simple cooling age) of sample ASM02, but it indicates rather thermal resetting or (re)crystallisation corresponding with the emplacement of the adjacent massifs. In this particular southernmost part of the Zavkhan terrane, late Tonian magmatic rocks were emplaced over ~46 Myr.

EARLY PERMIAN EPISODE

In the Khasagt Mountains no plutonic or volcanic rocks of Permian age have previously been determined. The U-Pb geochronology of six zircon samples revealed an Early Permian emplacement age. The new data indicate a brief plutonic pulse at 276–271 Ma overlapping with a volcanic pulse at 271–269 Ma. A Permian age of the intrusive rocks (~286 Myr) was previously documented only in the isolated Tonkhil complex (46.8786°N, 95.7105°E) by Kilian et al. (2016) and concurrently referred to by Bold et al. (2016a, b). Thus our results (Table 2) indicate an extended occurrence of Permian rocks slightly farther west (i.e. 46.5258°N, 95.2535°E, sample 815). Among the zircons analysed in this Permian group (n = 183), only one case of an inherited grain was identified (rim of 624 Myr and core of 2 883 Myr) in an effusive alkali rhyolite (sample 698).

The volcanic rocks typically show dispersed U-Pb single-spot zircon ages, indicating that the underlying magmatic system has been dated and not the eruption itself The grains

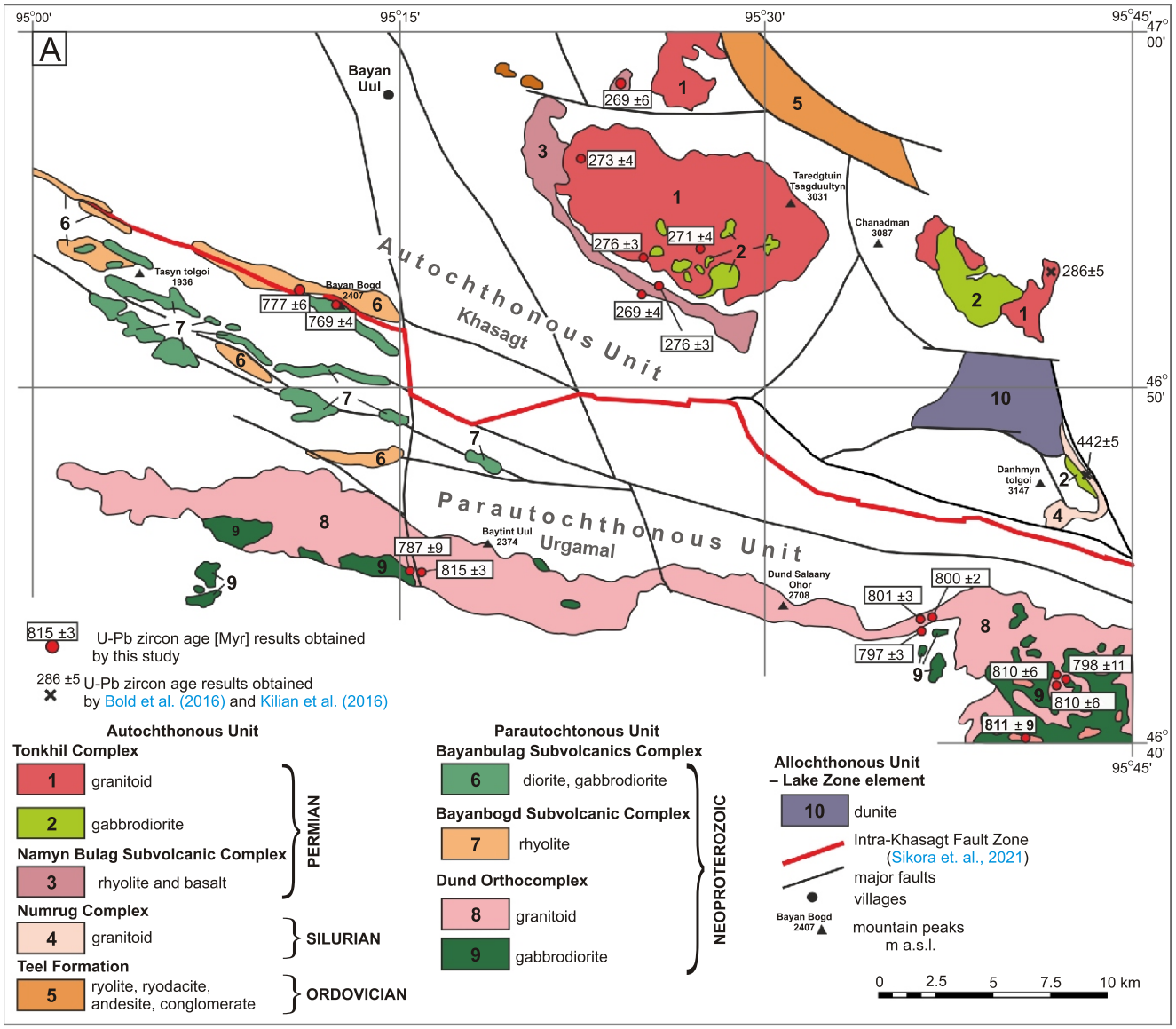


Fig. 12. Graphic summary of U-Pb zircon age results from the Khasagt area

A – geological map of the crystalline rocks showing the age and distribution of igneous rocks the Khasagt area; **B** – compilation diagram including newly obtained age data and the previous age data from the Zavkhan terrane with generalized tectonic interpretations for the early Neoproterozoic and Permian magmatism. U-Pb age data taken from this study and from Yarmolyuk et al. (2008), Levashova et al. (2010), Bold et al. (2016a, b), Zhao et al. (2017), Kozakov et al. (2021), Khukhuudei et al. (2022), Soejono et al. (2023)

from this sample show some scatter in their age distribution. This is interpreted as the occurrence of antecrystic and autocrystic zircons (Miller et al., 2011). The youngest autocrystic zircons (~270 Myr) are thus interpreted as better constraining the eruption age. In order to date the timing of the eruption, the youngest U-Pb zircon (at least three examples) overlapping on concordia diagram are usually considered (e.g., Chamberlain et al., 2014). Depending on the approach used in the case of volcanic zircons, significant age differences can be obtained, as indicated by concordia diagrams (Fig. 6Q, R vs. S, T), where the age difference reaches ~3 Myr.

Nevertheless, even pre-eruptive zircons (antecrysts of sample 815 and 698) can provide important information about activity within the volcanic system. Their ages of 272 Myr correlate well with the age of the rhyolite (CSM02). However, the youngest zircons in the alkaline rhyolite (sample 698) and hawaite (sample 815) clearly indicate continued volcanic activity up to 267 Ma. This may suggest that both intrusions and volcanism were almost simultaneous and intense during an interval of 8 Myr (276–268 Ma). For the Khasagt Mountains, this was an unexpected finding, since the rocks forming these massifs were formerly attributed to the Devonian (Enkhbayar et al., 2005). Early Permian (and minor late Carboniferous) granitic rocks emplaced at ~290–280 Ma have been discovered in the Khan-Bogd area of southern Mongolia (Zhou et al., 2023).

THE REGIONAL CONTEXT FOR TWO MAGMATIC EVENTS

RODINIA RIFTING

Early Neoproterozoic igneous rocks are relatively widespread among the Mongolian microcontinents (e.g., Kozakov et al., 2021, Skuzovatov, 2021, Soejono et al., 2023), indicating the significance of crust-forming events at this time. Several terranes in the central segment of the CAOB preserved a record of crust-forming magmatic activity at 960–930 Ma, 880–850 Ma and 810–790 Ma (Kozakov et al., 2021 and reference therein), with igneous suites formed in oceanic island arc, mature continental margin, and rift-related extensional settings, providing evidence that these were microcontinental blocks involved in the main stages of Rodinia evolution. According to the geochemical characteristics described above of the Khasagt Mountains rocks together with previously completed studies of adjacent areas (Yarmolyuk et al., 2008; Soejono et al., 2023), the late Tonian magmatism in the Zavkhan Terrane was connected with of gradual disintegration of Rodinia. Several authors concluded (Li et al., 2003 and references therein), that there were two major phases of widespread bimodal magmatism in South China during the Neoproterozoic. The first one, at ~830–795 Ma, started before the continental rifting but continued into the first two stages of the rifting. Initiation of continental rifting in South China has been thought to be represented by magmatism at 825 Ma (Li et al., 2008). The time span between 780 and 745 Ma was critical in the geological history of the Rodinia supercontinent, because rifting processes in this interval embraced an extensive territory (e.g., Li et al. 2008; Kheraskova et. al., 2010). Evidence of intraplate magmatism within the age ranges of 830–795 Myr and 780–745 Myr (U-Th-Pb method, including a SHRIMP dataset) has been detected in the Yangtze blocks in southern China, Tarim, and Australia as well as in Baltica (Wang and Li, 2003; Li et al., 2008; Lu et al., 2008; Zhang et al., 2009; Callegari et al., 2023).

The new data from the Khasagt Mountains region (southernmost margin of the Zavkhan Terrane) provides further evidence of this magmatic activity, indicating the timing of late Tonian extension (Fig. 12A). The oldest pulse is recorded by the granites (samples 552 and ASM04) of the Dund Orthocomplex at ~815–810 Ma and gabbro at ~810 Ma (sample ASM02) in the Bayanbulag intrusion, followed by the emplacement at ~800 Ma of the granites (samples ASM08, ASM06), tonalite (sample ASM07) and syenite (sample ASM03) within the Dund Orthocomplex. A subsequent pulse is represented by the volcanic rocks (sample 551) of the Bayanbulag intrusion at ~787 Ma and by dykes of rhyolitic composition (270 Bayanbogd intrusion) and syenogabbro (048 Bayanbulag) intruded along the tectonic border between ~774–769 Ma.

The Tonian magmatic activity was recorded in several regions of the Mongolian Collage almost simultaneously (e.g., Soejono et al., 2023). The nature of the magmatic rocks could potentially be different (although it is not always possible to verify this geochemically) e.g the marginal part of the Tuva–Mongolian microcontinent (north of Khasagt Mountains) has been interpreted as evolved on an active continental margin (Kuzmichev and Larionov, 2011). However most of the continental blocks of the central CAOB were affected by rifting and massive intra-plate magmatism during the break-up of Rodinia.

Based on comparison of the magmatic evidence (Kozakov et al., 2021; Soejono et al., 2023 and this study), the Zavkhan Terrane (Fig. 12B), with an undoubtedly peri-Rodinian palaeogeographic position, is dominated by a record of rift–alkaline magmatism. Afterwards, the Rodinian passive margin was transformed into an immense series of magmatic-arc belts during a prolonged Ediacarian to Paleozoic orogenic evolution, dominated by Silurian, Devonian and Carboniferous accretionary complexes and arc-related volcanic and volcaniclastic rocks (e.g., Badarch et al., 2002; Xiao et al., 2003; Windley et al., 2007; Lehmann et al., 2010), finaly assembled as a part of the CAOB.

LATE CARBONIFEROUS–EARLY PERMIAN RIFTING

The Late Paleozoic tectonic evolution of the CAOB is considered to be the turning point for the termination of terrane amalgamation (e.g., Liu et al., 2025). However, tdebate about the tectonic setting of the region during this interval is still not resolved. After the final amalgamation of the CAOB, in southern Mongolia and northern Inner Mongolia a few magmatic pulses of Late Carboniferous–Early Permian age with different characteristics have been recognized as widespread across the various part of the CAOB (e.g., Yarmolyuk et al., 2000; Badarch et al., 2002; Byamba, 2009; Jahn et al., 2009; Kröner et al., 2010; Žáček et al., 2016).

The recently recognized regional geological characteristics (Zhou et al., 2023 and references therein), that provide a key to the Carboniferous–Permian periods in southern Mongolia, suggest that magmatic activity can be roughly divided into three stages: Early Carboniferous (350–325 Ma), Late Carboniferous (320–305 Ma), and Early Permian (300–280 Ma). During the Early Carboniferous (350–325 Ma), southern Mongolia developed as a common arc-type magmatic arc having a southwards migration trend. During the Late Carboniferous (320–305 Ma), southern Mongolia was dominated by high-silica granites, especially alkaline feldspar granites and syenites (315–310 Ma), which were produced by the re-melting of earlier arc-crust, indicating the cessation of significant consumption of subducted oceanic plates. During the Early Permian (300–280 Ma), extension-related magmatic rocks, such as A-type granites, bimodal volcanic rocks and basic dikes, were developed.

This last magmatic pulse clearly corresponds to the geochemical characteristics of the Early Permian igneous rocks exposed in the Khasagt Mountains. In general, in the area of the Zavkhan Terrane, Permian plutons are mapped in a few places

e.g. an age of 286 ±5 Myr was documented by a single dated sample from the coarse-grained alkaline granites of the Tonkhil Complex (Killian et al., 2016). Thus, the new U-Pb zircon age data from the Khasagt Mountains provide further evidence of the common occurrence of Permian magmatism in this part of Zavkhan Terrane. The early Permian mostly bimodal magmatism propagated progressively from the continent margin towards the interior, and has commonly been ascribed to a continental-rift setting (Yarmolyuk et al., 2008; Zhang et al., 2008; Jahn et al., 2009; Buriánek et al., 2012).

The spatial association of the oval Permian granitic plutons along E–W trending magnetic lineaments suggests the presence of Permian rift zones (Guy et al., 2014 and reference therein). However, in other parts of the CAOB, magmatism typical of a volcanic arc was active at the same time (e.g., Economos et al., 2012; Li et al., 2021), as was indicated by the tectonic evolution of the Middle-Late Permian orogenic belt in the eastern part of the CAOB on the basis of the geochemical characteristics of magmatic rocks in the Changchun-Kaiyuan area displaying an arc affinity, related to the southwards subduction of the Paleo-Asian Ocean (Zhang et al., 2023).

CONCLUSION

A new approach including whole-rock trace element geochemistry and systematic U-Pb zircon and titanite geochronology has been applied to the igneous rocks exposed in the Khasagt Mountains, at the southernmost margin of the Zavkhan Terrane (Western Mongolia). Based on the new results as well as on comparison to previously published studies from other complexes of the composite Zavkhan Terrane or/and Mongolian Collage of the CAOB, the following conclusions can be drawn:

1. Outcrops in the Khasagt Mountains area provide evidence of two prominent magmatic episodes at the margin of the Zavkhan Terrane.
2. The late Tonian at ~815–800 Ma saw the emplacement of granites, monzodiorites and gabbros, followed by a subsequent pulse at 787–769 Ma with volcanic latibasalt and subvolcanic rhyolite and rhyodacite intrusions;
3. In the northern part of the Khasagt region, an Early Permian igneous episode has been documented between 276–268 Ma by alkaline granites and volcanic rocks;
4. The whole-rock trace element contents revealed the alkaline nature (i.e.Nb/Yb >4), of both late Tonian and early Permian rocks, indicating also other geochemical features including high Th/U ratios in the zircons, typical of an extensional regime and/or rift;
5. Most of the late Tonian and all Permian granitoids tend to be close to A-type affinity expressed by the sum of incompatible elements (Zr+Y+La+Ce) being higher than 350 ppm. The intrusive rocks show an alkaline character with A.I. in the range of 0.61–0.88 and elevated La/Yb and Nb/Yb values;
6. This case study of data from the Khasagt Mountains highlights the significance of using multiple geochemical discriminators, as each of them brings new and useful aspects;
7. These integrated data indicate that the late Tonian magmatic pulses in the southern part of Khasagt Mountains were related to an early stage of global rifting processes occurring diachronously across the Rodinia supercontinent;
8. The Early Permian episode in northern part of the Khasagt region forms a link between magmatic complexes described as the Tonkhil Complex (alkaline granites), indicating the prolongation of the alkaline complexes towards the west corresponding to the late Paleozoic alkaline Central Asian rift system.

Acknowledgements. Part of this work was co-financed by the National Fund for Environmental Protection and Water Management, pursuant to Grant Agreement No. 289/2018 for SM. Analytical work on SHRIMP was performed under project 19.9914.1301.00.0. This publication was prepared with the support of project 62.9012.2517.00.0. The authors would like to thank Igor Soejono and a second anonymous reviewer for their constructive comments, which significantly contributed to improving this manuscript.

REFERENCES

Aleinikoff, J.N., Wintsch, R.P., Fanning, C.M., Dorais, M.J., 2002. U-Pb geochronology of zircon and polygenetic titanite from the Glastonbury Complex, Connecticut, USA: an integrated SEM, EMPA, TIMS, and SHRIMP study. Chemical Geology, **188**: 125–147; https://doi.org/10.1016/S0009-2541(02)00076-1

Bacon, C.R., Lowenstern, J.B., 2005. Late Pleistocene granodiorite source for recycled zircon and phenocrysts in rhyodacite lava at Crater Lake, Oregon. Earth and Planetary Science Letters, **233**: 277–293; https://doi.org/10.1016/j.epsl.2005.02.012

Badarch, G., Cunningham, W.D., Windley, B.F., 2002. A new terrane subdivision for Mongolia: implications for the Phanerozoic crustal growth of central Asia. Journal of Asian Earth Sciences, **21:** 87–110; https://doi.org/10.1016/S1367-9120(02)00017-2

Belousova, E.A., Walters, S., Griffin, W.L., O'Reilly, S.Y., Fisher, N.I., 2002. Zircon trace-element compositions as indicators of source rock type. Contributions to Mineralogy and Petrology, **143:** 602–622; https://doi.org/10.1007/s00410-002-0364-7

Black, L.P., Kamo, S.L., Allen, C.M., Aleinikoff, J.A., Davis, D.W., Korsch, J.R., Foudolis, C., 2003. TEMORA 1: a new zircon standard for Phanerozoic U-Pb geochronology. Chemical Geology, **200:** 155–170; https://doi.org/10.1016/S0009-2541(03)00165-7

Bold, U., Crowley, J.L., Smith, E.F., Sambuu, O., Macdonald, F.A., 2016a. Neoproterozoic to early Paleozoic tectonic evolution of the Zavkhan Terrane of Mongolia: implications for continental growth in the Central Asian Orogenic Belt. Lithosphere, **8:** 729–750; https://doi.org/10.1130/L549.1

Bold, U., Smith, E.F., Rooney, A.D., Bowring, S.A., Buchwaldt, R., Dudás, F., Ramezani, J., Crowley, J.L., Schrag, D.P., Macdonald, F.A., 2016b. Neoproterozoic stratigraphy of the Zavkhan Terrane of Mongolia: the backbone for Cryogenian and Early Ediacaran chemostratigraphic records. American Journal of Science, **316**: 1–63; https://doi.org/10.2475/01.2016.01

Bonin, B., 2007. A-type granites and related rocks; evolution of a concept, problems and prospects. Lithos, **97:** 1–29; https://doi.org/10.1016/j.lithos.2006.12.007

Bonin, B., Azzouni-Sekkal, A., Bussy, F., Ferrag, S.,1998. Alkali-calcic and alkaline postorogenic (PO) granite magmatism: petrologic constraints and geodynamic settings. Lithos, **45:** 45–70; https://doi.org/10.1016/S0024-4937(98)00025-5

Broussolle, A., Chen, M., Long, X., Zhang, L., 2024. External geodynamic evolution of the Mongolian Accretionary Collage: Insights from petro-chronology of zircon. Journal of Asian Earth Sciences, **259**, 105914; https://doi.org/10.1016/j.jseaes.2023.105914

Burashnikov, V.V., 1990. Tectonics of the Urgamal zone, early Calidonides of western Mongolia. Ph.D. Thesis, Russian Academy of Sciences, Moscow, Russia.

Byamba, J., 2009. Late Paleozoic to Early Mesozoic structures (in Mongolian). In: Geology and Minerals of Mongolia: Lithosphere Plate Tectonics (eds. J. Byamba, J. Badamgarav, A. Bayasgalan, N. Arvisbaatar, E.H. Turutanov, B. Dorjsuren, D. Tomurhuu, G. Dejidmaa, D. Dorjnamjaa, T. Mahbadar and A. Amarjargal): 353–358. Soyombo Printing, Ulaanbaatar.

Callegari, R., Kośmińska, K., Barnes, C., Klonowska, I., Barker, A., Rousku, S., Nääs, E., Kooijman, E., Witt-Nilsson, P., Majka, J., 2023. Early Neoproterozoic magmatism and Caledonian metamorphism recorded by the Mårma terrane, Seve Nappe Complex, northern Swedish Caledonides. Journal of the Geological Society, **180**, jgs2022-092; https://doi.org/10.1144/jgs2022-092

Cawood, P., Kröner, A., Collins, W., Kusky, T.M., Mooney, W.D., Windley, B.F., 2009. Accretionary orogens through Earth history. Geological Society Special Publications, **318**: 1–36; https://doi.org/10.1144/SP318.1

Cawood, P.A., Martin, E.L., Murphy, J.B., Pisarevsky, S.A., 2021. Gondwana's interlinked peripheral orogens. Earth and Planetary Sciences Letters, **568**, 117057; https://doi.org/10.1016/j.epsl.2021.117057

Chamberlain, K.J., Wilson, C.J., Wooden, J.L., Charlier, B.L.A., Ireland, T.R., 2014. New perspectives on the Bishop Tuff from zircon textures, ages and trace elements. Journal of Petrology, **55:** 395–426; https://doi.org/10.1093/petrology/egt072

Chappell, B.W., White, A.J.R., 2001. Two Contrasting Granite Types: 25 Years Later. Australian Journal of Earth Sciences, **48:** 489–499; https://doi.org/10.1046/j.1440-0952.2001.00882.x

Cocks, L.R.M, Trond, H., Torsvik, T.H. 2005. Baltica from the late Precambrian to mid-Palaeozoic times: The gain and loss of a terrane's identity. Earth-Science Reviews, **72**: 39–66; https://doi.org/10.1016/j.earscirev.2005.04.0

Cocks, L.R.M, Trond, H., Torsvik, T.H., 2007. Siberia, the wandering northern terrane, and its changing geography through the Palaeozoic. Earth-Science Reviews, **82:** 29–74; https://doi.org/10.1016/j.earscirev.2007.02.001

De la Roche, H., Leterrier, J., Grandclaude, P., Marchal, M., 1980. A classification of volcanic and plutonic rocks using R1-R2 diagrams and major element analyses. Its relationships with current nomenclature. Chemical Geology, **29:** 183–210; https://doi.org/10.1016/0009-2541(80)90020-0

Deering, C.D. Bachmann, O., Dufek, J., Gravley, D.M., 2011. Rift-related transition from andesite to rhyolite volcanism in the Taupo Volcanic Zone (New Zealand) controlled by crystal–melt dynamics in Mush Zones with variable mineral assemblages. Journal of Petrology, **52:** 2243–2263; https://doi.org/10.1093/petrology/egr046

Dergunov, A.B., 2001. Tectonics. Magmatism and Metallogeny of Mongolia. Routledge, London.

Dijkstra, A.H., Brouwer, F.M., Cunningham, W.D., Buchan, C., Badarch, G., Mason, P.R., 2006. Late Neoproterozoic proto-arc ocean crust in the Dariv Range, Western Mongolia: a supra-subduction zone end-member ophiolite. Journal of the Geological Society, **163:** 363–373; https://doi.org/10.1144/0016-764904-156

Dickinson W.R., Gehrels G.E., 2009. Use of U-Pb ages of detrital zircons to infer maximum depositional ages of strata: a test against a Colorado Plateau Mesozoic database. Earth and Planetary Science Letters, **288**: 115–125; https://doi.org/10.1016/j.epsl.2009.09.013

Dobretsov, N.L., Buslov, M.M., Vernikovsky, V.A., 2003. Neoproterozoic to early Ordovician evolution of the Paleo-Asian Ocean: Implications to the break-up of Rodinia. Gondwana Research, **6:** 143–159; https://doi.org/10.1016/S1342-937X(05)70966-7

Economos, R.C., Paterson, S.R., Said, L.O., Ducea, M.N., Anderson, J.L., Padilla, A.J., 2012. Gobi–Tianshan connections: field observations and isotopes from an early Permian arc complex in southern Mongolia. GSA Bulletin, **124:** 1688–1701; https://doi.org/10.1130/B30324.1

Eby, G.N., 1992. Chemical subdivision of the A-type granitoids: Petrogenetic and tectonic implications. Geology, **20:** 641–644; https://doi.org/10.1130/0091-7613(1992)020<0641:CSOTAT>2.3.CO;2

Énhbayar, B., Batbold, D., Monhnasan, C.Z., Sumhuu, D., Ohirhuayat, C,Z., Barsbold, C., 2005. Govi-Altaj ajmagijn Bayan Uul, Jargalan sumdin nutagt 2003–2004 (sheets L-46-47 A, B, W, G –L, 46–48 A, B) (in Mongolian). Archive of Mineral Resources and Petroleum Authority of Mongolia, Ulaan-Baatar, 5660.

Erdmann, S., Wang, R., Huang, F., Scaillet, B., Zhao, K., Liu, H., Chen, Y., Faure, M., 2019. Titanite: A potential solidus barometer for granitic magma systems. Comptes Rendus Géoscience, **351:** 551–561; https://doi.org/10.1016/j.crte.2019.09.002

Ersoy, Y., Helvac, C., Sözbilir, H., Erkül, F., Bozkurt, E., 2008. A geochemical approach to Neogene–Quaternary volcanic activity of western Anatolia: An example of episodic bimodal volcanism within the Selendi Basin, Turkey. Chemical Geology, **255:** 265**–**282; https://doi.org/10.1016/S0024-4937(97)00032-7

Frost, B.R., Barnes, C.G., Collins, W.J., Arculus, R.J., Ellis, D.J., Frost, C.D., 2001. A geochemical classification for granitic rocks. Journal of Petrology, **42**: 2033–2048; https://doi.org/10.1093/petrology/42.11.2033

Förster, H.J., Tischendorf, G., Trumbull, R.B., 1997. An evaluation of the Rb vs. (Y + Nb) discrimination diagram to infer tectonic setting of silicic igneous rocks. Lithos, **40**: 261–293; https://doi.org/10.1016/S0024-4937(97)00032-7

Ganbat, A., Tsujimori, T., Miao, L., Safonova, I., Pastor-Galán, D., Anaad, Ch., Baatar, M., Aoki, S., Aoki, K., Savinskiy, I., 2021. Late Paleozoic–Early Mesozoic granitoids in the Khangay-Khentey basin, Central Mongolia: Implication for the tectonic evolution of the Mongol-Okhotsk Ocean margin, Lithos, **404–405,** 106455; https://doi.org/10.1016/j.lithos.2021.106455

Gribble, R.F., Stern, R.J., Bloomer, S.H., Stüben, D., O'Hearn, T., Newman, S., 1996. MORB mantle and subduction components interact to generate basalts in the southern Mariana Trough back-arc basin, Geochimica et Cosmochimica Acta, **60:** 2153–2166; https://doi.org/10.1016/0016-7037(96)00078-6

Guy, A., Schulmann, K., Munschy, M., Miehe J.M., Edel, J.B., Lexa, O., Fairhead, D., 2014. Geophysical constraints for terrane boundaries in southern Mongolia. Journal of Geophysical Research B: Solid Earth, **119**: 7966–7991; https://doi.org/10.1002/2014JB011026

Guy, A., Schulmann, K., Soejono, I., Holzrichter, N., Lexa, O., Munschy, M., 2021. Structures and geodynamics of the Mongolian tract of the Central Asian Orogenic Belt constrained by potential field analyses. Gondwana Research, **92**: 26–53; https://doi.org/10.1016/j.gr.2020.11.016

Han, B.F., Guo, Z.J., Zhang, Z.C., Zhang, L., Chen, J.F., Song, B., 2010. Age, geochemistry, and tectonic implications of a late Paleozoic stitching pluton in the North Tian Shan suture zone, western China. GSA Bulletin, **122**: 627–640; https://doi.org/10.1130/B26491.1

Hanžl, P., Janoušek, V., Hrdličková, K., Buriánek, D., Gerel, O., Altanbaatar, B., Hora, J.M., Čoupek, P., 2023. From magmatic arc to a post-accretionary setting: Late Palaeozoic granitoid plutons in the northwestern Trans-Altai Zone, Mongolia. Journal of Geosciences, **68:** 25–66; https://doi.org/10.3190/jgeosci.366

Heaman, L.M., 2009. The application of U-Pb geochronology to mafic, ultramafic and alkaline rocks: an evolution of the three mineral standards. Chemical Geology, **261:** 43–52; https://doi.org/10.1016/j.chemgeo.2008.10.021

Hollocher, K., Robinson, P., Walsh, E., Roberts, D., 2012. Geochemistry of amphibolite-facies volcanics and gabbros of the Stȓren nappe in extensions west and southwest of Trondheim, Western Gneiss Region, Norway: a key to correlations and paleotectonic settings. American Journal of Science, **312:** 357–416; https://doi.org/10.2475/04.2012.01

Hoskin, P.W.O., Schaltegger, U., 2003. The composition of zircon and igneous and metamorphic petrogenesis. Reviews in Mineralogy and Geochemistry, **51:** 27–62; https://doi.org/10.2113/0530027

Irvine, T.N., Baragar, W.R.A., 1971. A guide to the chemical classification of the common volcanic rocks. Canadian Journal of Earth Sciences, **8**: 523–548; https://doi.org/10.1139/e71-055

Jahn, B.M., 2004. The Central Asian Orogenic Belt and growth of the continental crust in the Phanerozoic. Geological Society Special Publications, **226**: 73–100; https://doi.org/10.1144/GSL.SP.2004.226.01.05

Jahn, B.M., Litvinovsky, B.A., Zanvilevich, A.N., Reichow, M., 2009. Peralkaline granitoid magmatism in the Mongolian-Transbaikalian Belt: evolution, petrogenesis and tectonic significance: Lithos, **113:** 521–539; https://doi.org/10.1016/j.lithos.2009.06.015

Janoušek, V., Jiang, Y.D., Buriánek, D., Schulmann, K., Hanžl, P., Soejono, I., Kröner, A., Altanbaatar, B., Erban, V., Lexa, O., Ganchuluun, T., Košler, J., 2018. Cambrian Ordovician magmatism of the Ikh-Mongol Arc System exemplified by the Khantaishir Magmatic Complex (Lake Zone, south-central Mongolia). Gondwana Research, **54**: 122–149; https://doi.org/10.1016/j.gr.2017.10.003

Jian, P., Kröner, A., Jahn, B.M., Windley, B.F., Shi, Y., Zhang, W., Zhang, F., Miao, L.,Tomurhuu, D., Liu, D., 2014. Zircon dating of Neoproterozoic and Cambrian ophiolites in West Mongolia and implications for the timing of orogenic processes in the central part of the Central Asian Orogenic Belt. Earth-Science Reviews, **133:** 62–93; https://doi.org/10.1016/j.earscirev.2014.02.006

Jiang, Y.D., Schulmann, K., Sun, M., Štípskŕ, P., Guy, A., Janoušek, V., Lexa, O., Yuan, C., 2016. Anatexis of accretionary wedge, Pacific type magmatism and formation of vertically stratified continental crust in the Altai Orogenic Belt. Tectonics, **35:** 3095–3118; https://doi.org/10.1002/2016TC004271

Jiang, Y.D., Schulmann, K., Kröner, A., Sun, M., Lexa, O., Janoušek, V., Burianek, D., Yuan, C., Hanžl, P., 2017. Neoproterozoic-Early Paleozoic Peri-Pacific accretionary evolution of the Mongolian Collage System: insights from geochemical and U-Pb zircon data from the Ordovician sedimentary wedge in the Mongolian Altai. Tectonics, **36:** 2305–2330; https://doi.org/10.1002/2017tc004533

Khain, E.V., Bibikova, E.V., Kröner, A., Zhuralev, D.Z., Sklyarov, E.V., Fedotova, A.A., Kravchenko-Berezhnoy, I.R., 2002. The most ancient ophiolite of the Central Asian fold belt: U-Pb and Pb-Pb zircon ages for the Dunzhugur complex, Eastern Sayan, Siberia, and geodynamic implications. Earth and Planetary Sciences Letters, **199:** 311–325; https://doi.org/10.1016/S0012-821X(02)00587-3

Khain, E.V., Bibikova, E.V., Sal'nikova, E.B., Kröner, A., Gibsher, A.S., Didenko, A.N., Degtyarev, K.E., Fedotova, A.A., 2003. The Palaeo-Asian Ocean in the Neoproterozoic and early Palaeozoic: new geochronologic data and palaeotectonic reconstructions. Precambrian Research, **122:** 329–358; https://doi.org/10.1016/S0301- 9268(02)00218-8

Kheraskova, T.N., Bush, V.A., Didenko, A.N., Samygin, S.G., 2010. Breakup of Rodinia and Early Stages of Evolution of the Paleoasian Ocean. Geotectonics, **44:** 1–24.

Khukhuudei, U., Timothy Kusky, T., Windley, B.F., Otgonbayar, O., Wang, L., 2022. Ophiolites and ocean plate stratigraphy (OPS) preserved across the Central Mongolian Microcontinent: a new mega-archive of data for the tectonic evolution of the Paleo-Asian Ocean. Gondwana Research, **105:** 51–83; https://doi.org/10.1016/j.gr.2021.12.008

Kilian, T.M., Swanson-Hysell, N.L., Bold, U., Crowley, J., Macdonald, F.A., 2016. Paleomagnetism of the Teel basalts from the Zavkhan terrane: implications for Paleozoic paleogeography in Mongolia and the growth of continental crust. Lithosphere, **8:** 699–715; https://doi.org/10.1130/L552.1

King, P.L., White, A.J.R., Chappell, B.W., Allen, C.M., 1997. Characterization and origin of aluminous a-type granites from the Lachlan fold belt, southeastern Australia. Journal of Petrology, **38**: 371–391; https://doi.org/10.1093/petroj/38.3.371

Kinny, P.D., McNaughton, N.J., Fanning, C.M., Maas, R., 1994. 518 Ma sphene (titanite) from the Khan pegmatite, Namibia, southwest Africa: a potential ion-microprobe standard. Abstract, 8th International Conference on Geochronology, Cosmochronology and Isotope Geology. U.S. Geological Survey Circular, **1107**: 171.

Kirkland, C.L., Smithies, R.H., Taylor, R.J.M., Evans, N., McDonald, B., 2015. Zircon Th/U ratios in magmatic environs. Lithos, **212–215**: 397–414; https://doi.org/10.1016/j.lithos.2014.11.021

Kohn, M.J., 2017. Titanite petrochronology. Review in Mineralogy and Geochemistry, **83**: 419–441; https://doi.org/10.2138/rmg.2017.83.13

Kovach, V.P., Kozakov, I.K., Salnikova, E.B., Yarmolyuk, V.V., Kozlovsky, A.M., Terent'eva, L.B., 2013. Crustal growth stages in the Songino block of the early Caledonian superterrane in Central Asia: II. Geochemical and Nd-Isotope Data. Petrology, **21**: 409–426; https://doi.org/10.1134/S0869591113050020

Kovach, V.P., Kozakov, I.K., Wang, K.-L., Plotkina, Y.V., Lee, H.-Y., Chung, S.-L., 2019. Age and sources of terrigenous rocks of Basal Formation of the Tsagaan-Olom Group of the Dzabkhan Terrane: results of U-Th-Pb geochronological, Lu-Hf and Sm-Nd isotopic studies. Stratigraphy and Geological Correlation, **27:** 555–572; https://doi.org/10.1134/S0869593819050046

Kovach, V.P., Kozakov, I., Kröner, A., Salnikova, E., Wang, K.L., Lee, H.Y., Plotkina, J., Gorokhovsky, B., Adamskaya, E., Tolmacheva, E., Shpakovich, L., 2021. Early Neoproterozoic crustal growth and microcontinent formation of the north–central Central Asian Orogenic Belt: new geological, geochronological, and Nd–Hf isotopic data on the Mélange Zone within the Zavkhan Terrane, western Mongolia. Gondwana Research, **91**: 254–276; https://doi.org/10.1016/j.gr.2020.12.022

Kozakov, I.K., Sal'nikova, E.B., Khain, E.V., Kovach, V.P., Berezhnaya, N.G., Yakovleva, S.Z., Plotkina, Y.V., 2002. Early Caledonian crystalline rocks of the Lake zone in Mongolia: Formation history and tectonic settings as deduced from U-Pb and Sm-Nd datings. Geotectonics, **36**: 156–166.

Kozakov, I.K., Kozlovsky, A.M., Yarmolyuk, V.V., Kovach, V.P., Bibikova, E.V., Kirnozova, T.I., Plotkina, Y.V., Zagornaya, N.Y., Fugzan, M.M., Erdenejargal, C., Lebedev, V.I., Eenjin, G., 2011. Crystalline complexes of the Tarbagatai block of the Early Caledonian superterrane of Central Asia. Petrology, **19:** 426–444; https://doi. org/10.1134/S0869591111040047

Kozakov, I.K., Yarmolyuk, V., Kovach, V., Bibikova, E., Kirnozova, T., Kozlovskii, A., Plotkina, Y.V., Fugzan, M., Lebedev, V., Erdenezhargal, C., 2012. The Early Baikalian crystalline complex in the basement of the Dzabkhan microcontinent of the Early Caledonian orogenic area, Central Asia. Stratigraphy and Geological Correlation, **20:** 231–239; https://doi.org/10.1134/S0869593812030057

Kozakov, I.K., Kovach, V.P., Bibikova, E.V., Kirnozova, T.I., Lykhin, D.A., Plotkina, Y., Tolmacheva, E.V., Fugzan, M.M., Erdenezhargal, C., 2014. Late Riphean episode in the formation of crystalline rock complexes in the Dzabkhan microcontinent: geological, geochronologic, and Nd isotopic-geochemical data. Petrology, **22:** 480–506; https://doi.org/10.1134/S0869593808040023

Kozakov, I.K., Kovach, V.P., Sal'nikova, E.B., Didenko, A.N., Plotkina, Y.V., Fedoseenko, A.M., 2021. Formation of the Neoproterozoic continental crust in the structures of the central segment of the Central Asian Fold Belt. Petrology, **29:** 195–220; https://doi:10.1134/S0869591121020053

Kröner, A., (ed.), 2015. The Central Asian Orogenic Belt Geology, Evolution, Tectonics, and Models. Beitrage zur regionalen Geologie der Erde, **32**.

Kröner, A., Lehmann, J., Schulmann, K., Demoux, A., Lexa, O., Tomurhuu, D., Štípská, P., Otgonbator, D., Liu, D.Y., Wingate, M.T.D., 2010. Lithostratigraphic and geochrono- logical constraints on the evolution of the Central Asian Orogenic Beltin SW Mongolia: Early Paleozoic rifting followed by late Paleozoic accretion. American Journal of Science, **310:** 523–574; https://doi.org/10.2475/07.2010.01

Kröner, A., Kovach, V., Belousova, E., Hegner, E., Armstrong, R., Dolgopolova, A., Seltmann, R., Alexeiev, D., Hoffmann, J., Wong, J., 2014. Reassessment of continental growth during the accretionary history of the Central Asian Orogenic Belt. Gondwana Research, **25:** 103–125; https://doi.org/10.1016/j.gr.2012.12.023

Kröner, A., Kovach, V., Alexeiev, D., Wang, K.-L., Wong, J., Degtyarev, K., Kozakov, I., 2017. No excessive crustal growth in the Central Asian Orogenic Belt: further evidence from field relationships and isotopic data. Gondwana Research, **50:** 135–166; https://doi.org/10.1016/j.gr.2017.04.006

Kuzmichev, A.B., Larionov, A.N., 2011. The Sarkhoi Group in East Sayan: Neoproterozoic (~770–800 Ma) volcanic belt of the Andean type. Russian Geology and Geophysics, **52:** 685–700; https://doi.org/10.1016/j.rgg.2011.06.001

Le Maitre, R.W., Bateman, P., Dudek, A.J., Keller, M.J., 1989. A Classification of Igneous Rocks and Glossary of Terms. Blackwell, Oxford.

Lehmann, J., Schulmann, K., Lexa, O., Corsini, M., Kröner, A., Štípská, P., Tomurhuu, D., Otgonbator, D., 2010. Structural constraints on the evolution of the Central Asian Orogenic Belt in SW Mongolia. American Journal of Sciences, **310:** 575–628 https://doi.org/10.2475/07.2010.02

Lei, X.-F., Jiang, S.-Y., Su, H.-M., Ying, Y.-C., 2021. Hydrothermal titanite U–Pb age and geochemistry as a reliable chronometer and genetic tracer for quartz vein-type tungsten deposit at Qipangou of Qinling orogenic belt, Central China. Ore Geology Reviews, **135**, 104246; https://doi.org/10.1016/j.oregeorev.2021.104246

Levashova, N.M., Kalugin, V.M., Gibsher, A.S., Yff, J., Ryabinin, A.B., Meert, J.G., Malone, S.J., 2010. The origin of the Baydaric microcontinent, Mongolia: Constraints from paleomagnetism and geochronology. Tectonophysics, **485:** 306–320; https://doi.org/10.1016/j.tecto.2010.01.012

Levashova, N.M., Meert, J.G., Gibsher, A.S., Grice, W.C., Bazhenov, M.L., 2011. The origin of microcontinents in the Central Asian Orogenic Belt: Constraints from paleomagnetism and geochronology. Precambrian Research, **185:** 37–54; https://doi.org/10.1016/j. precamres.2010.12.001

Li, H., Godang, S., Saputro, S.P., 2025. Revealing Unmapped Tectonic Settings through Geochemical Fingerprinting of Th-Nb-Yb. Lithosphere, **2,** 125; https://doi.org/10.2113/2025/lithosphere2025

Li, Z.-X., Li, X.H., Kinny, P.D., Wang, J., Zhang, S., Zhou, H., 2003. Geochronology of Neoproterozoic syn-rift magmatism in the Yangtze Craton, South China and correlations with other continents: evidence for a mantle superplume that broke up Rodinia. Precambrian Research, **122:** 85–109; https://doi.org/10.1016/S0301-9268(02)00208-5

Li, Z.X., Bogdanova, S.V., Collins, A.S., Davidson, A., De Waele, B., Ernst, R.E., Vernikovsky, V., 2008. Assembly, configuration, and break-up history of Rodinia: A synthesis. Precambrian Research, **160:** 179–210; https://doi.org/10.1016/j.precamres.2007.04.021

Li, P., Sun, M., Shu, C., Yuan, C., Jiang, Y., Zhang, L., Cai, K., 2019. Evolution of the Central Asian Orogenic Belt along the Siberian margin from Neoproterozoic-Early Paleozoic accretion to Devonian trench retreat and a comparison with Phanerozoic eastern Australia. Earth-Science Reviews, **198,** 102951; https://doi.org/10.1016/j.earscirev.2019.102951

Li, P., Sun, M., Narantsetseg, T., Jourdan, F., Hu, W., Yuan, C., 2021. First structural observation around the hinge of the Mongolian Orocline (Central Asia): Implications for the geodynamics of oroclinal bending and the evolution of the Mongol-Okhotsk Ocean. GSA Bulletin, **134:** 1994–2006; https://doi:10.1130/b36200

Long, X., Xu, B., Yuan, Ch., Zhang, Ch., Zhang, L., 2019. Precambrian crustal evolution of the southwestern Tarim Craton, NW China: Constraints from new detrital zircon ages and Hf isotopic data of the Neoproterozoic metasedimentary rocks. Precambrian Research, **334,** 105473; https://doi.org/10.1016/j.precamres.2019.105473

Lu, S.N., Li, H.K., Zhang, C.L., Niu, G.H., 2008. Geological and geochronological evidence for the Precambrian evolution of the Tarim Craton and surrounding continental fragments. Precambrian Research, **160:** 94–107; https://doi.org/10.1016/j.precamres.2007.04.02

Ludwig, K.R., 2003. User's Manual for Isoplot 3.6 (February 2012 Revision). Berkeley Geochronology Center Special Publication, **4**. Retrieved from http://sourceforge.net/projects/isoplot

Ludwig, K.R, 2009. SQUID 2.50*:* A User's Manual. Berkeley Geochronology Center Special Publication.

Maniar, P.D., Piccoli, P.M.,1989. Tectonic discrimination of granitoids. GSA Bulletin, **101**: 635–643; https://doi.org/10.1130/0016-7606(1989)101<0635:TDOG>2.3.CO

Mao, Q.G., Xiao, W.J., Fang, T.H., Windley, B.F., Sun, M., Ao, S.J., Zhang, J.E, Huang, X.K., 2014. Geochronology, geochemistry and petrogenesis of Early Permian alkaline magmatism in the Eastern Tianshan: implications for tectonics of the Southern Altaids. Lithos**, 190–191**: 37–51; https://doi.org/10.1016/j.lithos.2013.11.011

McKay, M.P., Weislogel, A.L., Fildani, A., Brunt, R.L., Hodgson, D.M., Flint, S.S., 2015. U-Pb zircon tuff geochronology from the Karoo Basin, South Africa: Implications of zircon recycling on stratigraphic age controls. International Geology Review, **57**: 393–410; https://doi.org/10.1080/00206814.2015.1008592

McKay, M.P., Jackson Jr, W.T., Hessler, A.M., 2018. Tectonic stress regime recorded by zircon Th/U. Gondwana Research, **57:** 1–9; https://doi.org/10.1016/j.gr.2018.01.004

Middlemost, E.A.K., 1975. The basalt clan. Earth-Science Reviews, **11**: 337–364; https://doi.org/10.1016/0012-8252(75)90039-2

Middlemost, E.A.K., 1994. Naming Materials in the Magma/Igneous Rock System. Earth-Science Reviews, **37:** 215–244; https://doi.org/10.1016/0012-8252(94)90029-9

Miller, J.S., Matzel, J.E., Miller, C.F., Burgess, S.D., Miller, R.B. 2007. Zircon growth and recycling during the assembly of large, composite arc plutons. Journal of Volcanology and Geothermal Research, **167**: 282–299; https://doi.org/10.1016/j.jvolgeores.2007.04.019, 2007

Miller, C.F., Furbish, D.J., Walker, B.A., Claiborne, L.I., Koteas, G.C., Bleick, H.A., Miller, J.S., 2011. Growth of plutons by incremental emplacement of sheets in crystal-rich host: Evidence from Miocene intrusions of the Colorado River region, Nevada, USA: Tectonophysics, **500**: 65–77; https://doi.org/10.1016/j.tecto.2009.07.011

Mossakovsky, A., Ruzhentsev, S.V., Samygin, S.G., Kheraskova, T., 1993. Central Asian fold belt: geodynamic evolution and history of formation. Geotectonics, **6:** 3–33.

Mossakovsky, A., Ruzhenysev, S., Samygin, S., Kherskova, T., 1994. Central Asian fold belt: geodynamic evolution and formation history. Geotectonics, **27:** 445–474.

Naemura, K., Erdenejargal, C., Javkhlan, T.O., Kato, T., Hirajima, T., 2020. Geochronology and tectonic implications of the Urgamal eclogite, western Mongolia. Journal of Mineralogical and Petrological Science, **115:** 357–364; https://doi.org/10.2465/jmps.191126

Nakamura, N., 1974. Determination of REE, Ba, Fe, Mg, Na and K in Carbonaceous and Ordinary Chondrites. Geochimica et Cosmochimica Acta, **38:** 757–775; https://doi.org/10.1016/0016-7037(74)90149-5

Nathwani, C., Szymanowski, D., Tavazzani, L., Markovic, S., Virmond, A., Chelle-Michou, C., 2025. Controls on zircon age distributions in volcanic, porphyry and plutonic rocks. Geochronology, **7:** 15–33; https://doi.org/10.5194/gchron-7-15-2025

Parfenov, L.M., Khanchuk, A.I., Badarch, G., Miller, R.J., Naumova, V.V., Nokleberg, W.J., Ogasawara, M., Prokopiev, A.V., Yan, H., 2003. Preliminary Northeast Asia Geodynamics Map, sheet 2, scale 1:5,000,000. U.S. Geological Survey, Open File Report, 03–205.

Pearce, J.A., 1996. A user's guide to basalt discrimination diagrams. Geological Association of Canada, Short Course Notes, **12:** 79–113.

Pearce, J.A., 2008. Trace element characteristics of lavas from destructive plate boundaries. In: Andesites: Orogenic Andesites and Related Rocks (ed. R.S. Thorpe): 525–548. John Wiley & Sons, Chichester.

Pearce, J.A., Harris, N.W. Tindle, A.G., 1984. Trace element discrimination diagrams for the tectonic interpretation of granitic rocks. Journal of Petrology, **25:** 956–983; https://doi.org/10.1093/petrology/25.4.956

Peřestý, V., Soejono, I., Schulmann, K., Ruffet, G., Kylander, R.C.A., Sláma, J., Štípská, P., Maierová, P., Aguilar, C., Hanžl, P., Kašpar, A., 2025. Late Cambrian syn-intrusive thickening of the Ikh Mongol Arc domains in the Mongolian Collage. Tectonics, **44**, e2024TC008437; https://doi:10.1029/2024TC008437

Rojas-Agramonte, Y., Kröner, A., Demoux, A., Xia, X., Wang, W., Donskaya, T., Liu, D. Sun, M., 2011. Detrital and xenocrystic zircon ages from Neoproterozoic to Palaeozoic arc terranes of Mongolia: Significance for the origin of crustal fragments in the Central Asian Orogenic Belt. Gondwana Research, **19:** 751–763; https://doi.org/10.1016/j.gr.2010.10.004

Rubatto, D., 2002. Zircon trace element geochemistry: partitioning with garnet and the link between U-Pb ages and metamorphism. Chemical Geology, **184:** 123–138; https://doi.org/10.1016/S0009-2541(01)00355-2

Ruzhentsev, S.V., Burashnikov, V.V., 1996. Tectonics of the western Mongolian Salairides. Geotectonics, **29**: 379–394.

Saccani, E., 2015. A new method of discriminating different types of post-Archean ophiolitic basalts and their tectonic significance using Th-Nb and Ce-Dy-Yb systematics. Geoscience Frontiers, **6**: 481–501; https://doi.org/10.1016/j.gsf.2014.03.006

Safonova, I., Seltmann, R., Kröner, A., Gladkochub, D., Schulmann, K., Xiao, W., Kim, J., Komiya, T., Sun, M., 2011. A new concept of continental construction in the Central Asian Orogenic Belt. Episodes, **34**: 186–196; https://doi.org/10.18814/epiiugs/2011/v34i3/005

Sato, K., Siga, O.Jr., Basel, M.A.S., Tassinari, C.C.G., Onoe, A.T., 2016. SHRIMP U-Th-Pb analyses of titanites: analytical techniques and examples of terranes of the South-Southeast of Brazil– Geoscience Institute of the University of São Paulo. Geologia Universidade de São Paulo. Série Científica, **16:** 3–18.

Schulmann, K., Paterson, S., 2011. Asian continental growth. Nature Geoscience, **4**: 827–829; https://doi.org/10.1038/ngeo1339

Schulmann, K., Edel, J.B., Lexa O., Xiao W., Trebinova D., Spikings R., Schaltegger U., Derkowski A., Szczerba M., 2023. Paleomagnetic, tectonic and geochronological constraints for Permian–Triassic oroclinal bending of the Mongolian collage. National Science Review, **10**, nwac184; https://doi.org/10.1093/nsr/ nwac184

Şengör, A.M.C., Natal'in, B.A., Burtman, V.S., 1993. Evolution of the Altaid tectonic collage and Paleozoic crustal grow thin Eurasia. Nature, **364:** 299–307; https://doi.org/10.1038/364299a0

Şengör, A.C., Sunal, G., Natal'in, B.A., Van der Voo, R., 2022. The Altaids: A review of twenty-five years of knowledge accumulation. Earth-Science Reviews, **228**, 104013; https://doi:10.1016/j.earscirev.2022.104013

Sikora, R., 2015. Wyniki badań i mezoskopowa analiza tektoniczno-strukturalna w rejonie Hasagt (in Polish). In: Raport z prac geologicznych przeprowadzonych w rejonie Hasagt (Mongolia) w latach 2009–2013 (eds. A. Wójcik et al.). CAG, nr arch. I:3319/2021, Warszawa.

Sikora, R., Wójcik, A., Szczerba, M., Bazarnik, J., Madej, S., 2021. K-Ar dating of deformation of metasedimentary rocks from the Yargait Formation of the Zavkhan terrane (Khasagt Mountains, Mongolia) – preliminary results (in Polish with English summary). Przegląd Geologiczny, **69**: 448–453; https://doi.org/10.7306/2021.29

Skuzovatov, S., 2021. Nature and (in-)coherent metamorphic evolution of subducted continental crust in the Neoproterozoic accretionary collage of SW Mongolia. Geoscience Frontiers, **12,** 101097; https://doi.org/10.1016/j.gsf.2020.10.004

Soejono, I., Janoušek, V., Perestý, V., Schulmann, K., Svojtka, M., Hanžl, P., Hora, J.M., Míkovŕ, J., Štípskŕ, P., Guy, A., Collett, S., Otgonbaatar, D., 2023. From Rodinian passive margin to peri-Siberian continental arc: evidence from the multiphase Neoproterozoic–early Paleozoic magmatic record of the Zavkhan Block in the Mongolian Collage. Gondwana Research, **121:** 344–367; https://doi.org/10.1016/j.gr.2023.05.001

Soejono, I., Collett, S., Schulmann, K., Štípská, P., Míková, J., Peřestý, V., Novotná, N., Guy, A., 2025. Neoproterozoic paleogeography and displacement of the Mongolian blocks constrained by detrital zircon ages and Hf isotopic systematics (Zavkhan Block, W Mongolia). Precambrian Research, **417**, 107657; https://doi.org/10.1016/j.precamres.2024.107657

Stacey, J.S., Kramers, I.D., 1975. Approximation of terrestrial lead isotope evolution by a two-stage model. Earth and Planetary Science Letters, **26:** 207–221; https://doi.org/10.1016/0012-821X(75)90088-6

Stern, R.J., Bloomer, S.H., Martinez, F., Yamazaki, T. Harrison, T.M., 1996. The composition of back-arc lower crust and upper mantle in the Mariana Trough: a first report. Island Arc, **5:** 354–372; https://doi.org/10.1111/j.1440-1738.1996.tb00036.x

Suess, E., 1901. Das Antlitz der Erde, vol. III (Dritter Band. Erste Hälfte). F. Tempsky, Prag and Wien, and G. Freytag, Leipzig.

Suess, E., 1908. The Face of the Earth, **3**. Clarendon Press, Oxford.

Sun, S.S., McDonough, W.F., 1989. Chemical and isotopic systematics of oceanic basalts: implications for mantle composition and processes. Geological Society Special Publications, **42:** 313–345; https://doi.org/10.1144/GSL.SP.1989.042.01.19

Turkina, O.M., 2002. Tonalite–trondhjemite of subduction-related complexes (Late Riphean plagiogranites) on the SW margin of the Siberian craton. Russian Geology and Geophysics, **43**: 418–431.

Uher, P., Broska, I., Krzemińska, E., Ondrejka, M., Mikuš, T., Vaculovič, T., 2019. Titanite composition and SHRIMP U-Pb dating as indicators of post-magmatic tectono-thermal activity: Variscan I-type tonalites to granodiorites, the Western Carpathians. Geologica Carpathica, **70:** 449–470; https://doi.org/10.2478/geoca-2019-0026

Van der Voo, R., van Hinsbergen, D.J.J., Domeier, M., Spakman, W., Torsvik, T.H., 2015. Latest Jurassic-earliest Cretaceous closure of the Mongol-Okhotsk Ocean: a paleomagnetic and seismological-tomographic analysis. GSA Special Paper, **513**: 589–606; https://doi.org/10.1130/2015.2513(19)

Wang, J., Li, Z.X., 2003. History of Neoproterozoic rift basins in South China: Implications for Rodinia break-up. Precambrian Research, **122:** 141–158; https://doi.org/10.1016/S0301-9268(02)00209-7

Wang, T., Niu, M-l., Wu, Q., Li, X., Cai, Q., Zhu, G., 2019. Episodic bimodal magmatism at an active continental margin due to Paleo-Pacific Plate subduction: A case study from the southern segment of the Tan-Lu Fault Zone, eastern China. Lithos, **328–329:** 159–181; https://doi.org/10.1016/j.lithos.2019.01.025

Watson, E.B., Harrison, T.M., 1983. Zircon saturation revisited: temperature and composition effects in a variety of crustal magma types. Earth and Planetary Science Letters, **64**: 295–304; https://doi:10.1016/0012-821X(83)90211-X

Whalen, J.B., Hildebrand, R.S., 2019. Trace element discrimination of arc, slab failure, and A-type granitic rocks. Lithos, **348–349,** 105179; https://doi.org/10.1016/j.lithos.2019.105179

Whalen, J.B., Currie, K.L., Chappell, B.W., 1987. A-type granites: geochemical characteristics, discrimination and petrogenesis. Contribution to Mineralogy and Petrology, **95:** 407–419.

Wiedenbeck, M., Hanchar, J.M., Peck, W.H., Sylvester, P., Valley, J., Whitehouse, M., Kronz, A., Morishita, Y., Nasdala, L., Fiebig, J., Franchi, I., Girard, J.-P., Greenwood, R.C., Hinton, R., Kita, N., Mason, P.R.D., Norman, M., Ogasawara, M., Piccoli, P.M., Rhede, D., Satoh, H., Schulz-Dobrick, B., Skĺr, Ř., Spicuzza, M.J., Terada, K., Tindle, A., Togashi, S., Vennemann, T., Xie, Q., Zheng, Y.-F., 2004. Further Characterisation of the 91500 Zircon Crystal. Geostandards and Geoanalytical Research, **28:** 9–39.

Wilhem, C., Windley, B.F., Stampfli, G.M., 2012. The Altaids of Central Asia: a tectonic and evolutionary innovative review. Earth-Science Reviews, **113:** 303–341; https://doi.org/10.1016/j.earscirev.2012.04.001

Williams, I.S., 1998. U-Th-Pb Geochronology by Ion Microprobe. Reviews in Economic Geology, **7:** 1–35.

Winchester, J.A., Floyd, P.A., 1977. Geochemical discrimination of different magma series and their differentiation products using immobile elements. Chemical Geology, **20:** 325–343; https://doi.org/10.1016/0009-2541(77)90057-2

Windley, B.F., Alexeiev, D., Xiao, W., Kröner, A., Badarch, G., 2007. Tectonic models for accretion of the Central Asian Orogenic Belt. Journal of the Geological Society, **164:** 31–47; https://doi.org/10.1144/0016-76492006-022

Xiao, W., Windley, B.F., Hao, J., Zhai, M., 2003. Accretion leading to collision and the Permian Solonker suture, Inner Mongolia, China: Termination of the Central Asian Orogenic Belt. Tectonics, **22,** 106; https://doi.org/10.1029/2002TC001484

Xiao, W., Kröner, A., Windley, B., 2009. Geodynamic evolution of Central Asia in the Paleozoic and Mesozoic. International Journal of Earth Sciences, **98**: 1185–1188; https://doi.org/10.1007/s00531-009-0418-4

Xiao, W.J., Windley, B.F., Sun, S., Li, J., Huang, B.C., Han, C.M., Yuan, C., Sun, M., Chen, H.L., 2015. A tale of amalgamation of three Permo-Triassic collage systems in central Asia: oroclines, sutures, and terminal accretion. Annual Review of Earth and Planetary Sciences, **43**: 477–507; https://doi.org/10.1146/annurev-earth-060614-105254

Xiao, W., Windley, B. F., Han, C., Liu, W., Wan, B., Zhang, J., **Ao, S., Zhang, Z., Song, D., 2018.** Late Paleozoic to early Triassic multiple roll-back and oroclinal bending of the Mongolia collage in Central Asia. Earth-Science Reviews, **186**: 94–128; https://doi.org/10.1016/j.earscirev.2017.09.020

Xie, W., Lu, Y., Chen, L.-M., Song, X.-Y., Deng, Y.-F., Zhao, Y., 2022. Zircon Th/U ratios suggest a post-collision extensional setting for the Permian Ni-Cu sulfide deposits in the Eastern Tianshan, NW China, Ore Geology Reviews, **144**, 104837; https://doi.org/10.1016/j.oregeorev.2022.104837

Yakubchuk, A. 2008. Re-deciphering the tectonic jigsaw puzzle of northern Eurasia. Journal of Asian Earth Sciences, **32:** 82–101; https://doi.org/10.1016/j.jseaes.2007.10.009

Yang, J.H., Cawood, P.A., Du, Y.S., Huang, H., Huang, H.W. Tao, P., 2012. Large Igneous Province and Magmatic Arc Sourced Permian-Triassic Volcanogenic Sediments in China. Sedimentary Geology, **261–262:** 120–131; https://doi.org/10.1016/j.sedgeo.2012.03.018

Yarmolyuk, V.V., Degtyarev, K.E., 2019. Precambrian Terranes of the Central Asian Orogenic Belt: Comparative Characteristics, Types, and Peculiarities of Tectonic Evolution. Geotectonics, **53**: 1–23; https://doi.org/10.1134/S0016852119010096

Yarmolyuk, V.V., Vorontsov, A.A., Ivanov, V.G., Kovalenko, V.I., Baikin, D.N., Sandimirova, G.P., 2000. Stages of Bimodal and Alkaline Granit Magmatism in the Western Transbaikal Region: Geochronological Data on Rocks from the Tugnui Depression. Doklady Earth Sciences, **373**: 811–815.

Yarmolyuk, V.V., Kovalenko, V., Anisimova, I., Sal'nikova, E., Kovach, V., Kozakov, I., Kozlovsky, A., Kudryashova, E., Kotov, A., Plotkina, Y., Terent'eva, L., Yakovleva, S., 2008. Late Riphean alkali granites of the Zabhan microcontinent: evidence for the timing of Rodinia breakup and formation of microcontinents in the Central Asian Fold belt. Doklady Earth Sciences, **420:** 583–588; https://doi.org/10.1134/S1028334X08040132

Yarmolyuk, V.V., Kozlovsky, A.M., Lebedev, V.I., 2017. Neoproterozoic magmatic complexes of the Songino block (Mongolia): a problem of formation and correlation of Precambrian terranes in the Central Asian Orogenic Belt. Petrology, **25:** 365–395; https://doi.org/ 10.1134/S0869591117040051

Žáček, V., Burianek, D., Pecskay, Z., Skoda, R., 2016. Astrophyllite-alkali amphibole rhyolite, an evidence of Early Permian A-type alkaline volcanism in the western Mongolian Altai. Journal of Geosciences, **61:** 93–103; https://doi.org/10.3190/jgeosci.205

Žáček, V., Buriánek, D., Pécskay, Z., Škoda, R., 2019. Anorogenic Early Permian dykes in the western Mongolian Altai – petrography, geochemistry and K-Ar geochronology. Journal of Geosciences, **64:** 37–58; https://doi.org/10.3190/jgeosci.280

Zhang, N., Liu, Z., Xu, Z., Li, G., Dong, X., Liu, J, Li, W., 2023. Tectonic evolution of the Middle-Late Permian orogenic belt in the eastern part of the CAOB: Implications from the magmatism in the Changchun-Kaiyuan area. Geological Magazine, **160**: 1875–1892; https://doi.org/10.1017/S001675682300078

Zhang, Y.Q., Xu, L.Q., Kang, X.L., Bao, Y., 2009. Age dating of alkali granite in Jingesitai area of Dong Ujimqin Banner, Inner Mongolia, and its significance (in Chinese with English summary). Geology in China, **36:** 988–995.

Zhao, G., Wang, Y., Huang, B., Dong, Y., Li, S., Zhang, G., Yu, S., 2018. Geological reconstructions of the East Asian blocks: From the breakup of Rodinia to the assembly of Pangea. Earth-Science Reviews, **186:** 262–286; https://doi.org/10.1016/j.earscirev.2018.10.003

Zhao, J.H., Zhou, M.F., 2007. Geochemistry of Neoproterozoic mafic intrusions in the Panzhihua district (Sichuan Province, SW China): implications for subductionrelated metasomatism in the upper mantle. Precambrian Research, **152:** 27–47; https://doi.org/10.1016/j.precamres.2006.09.002

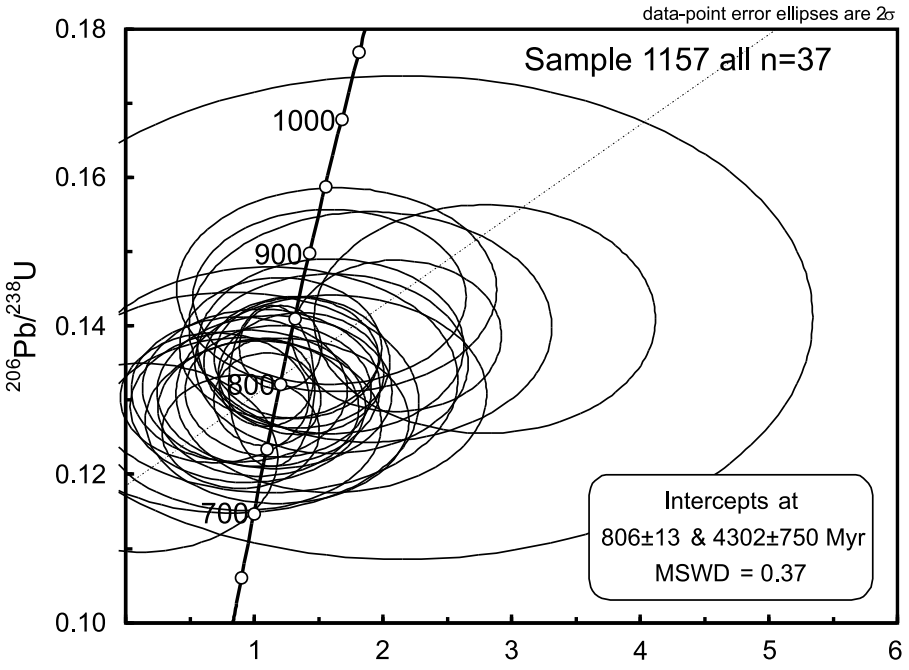
Zhao, P., Xu, B., Zhang, Ch., 2017. A rift system in southeastern Central Asian Orogenic Belt: Constraint from sedimentological, geochronological and geochemical investigations of the Late Carboniferous-Early Permian strata in northern Inner Mongolia (China). Gondwana Research, **47:** 342–357; https://doi.org/10.1016/j.gr.2016.06.013

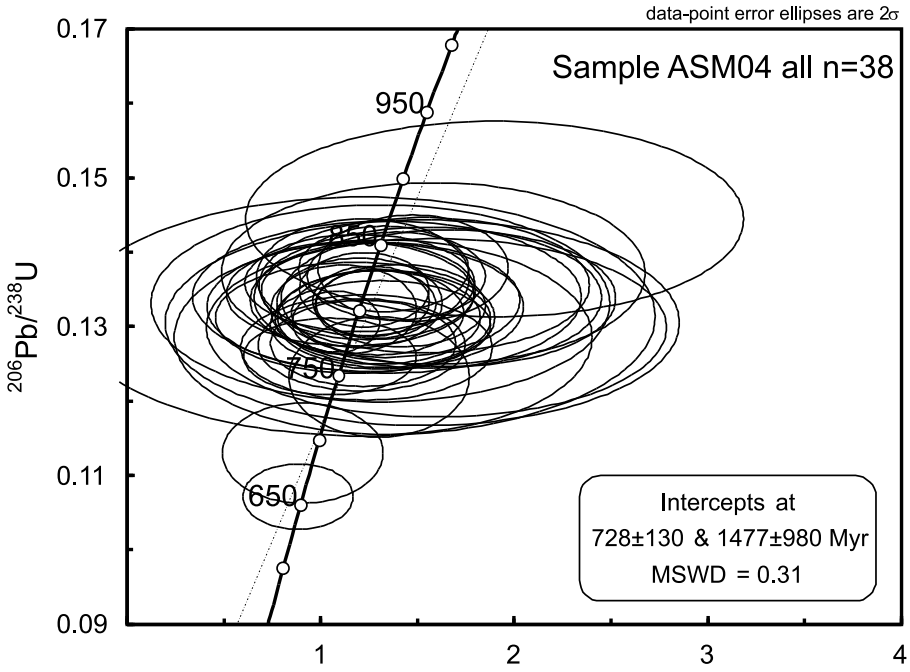
Zhao, P., Appel, E., Xu, B., Sukhbaatar, T., 2020. First paleomagnetic result from the Early Permian volcanic rocks in northeastern Mongolia: Evolutional implication for the Paleo-Asian Ocean and the Mongol-Okhotsk Ocean. Journal of Geophysical Research: Solid Earth, **125,** e2019JB017338; https://doi.org/ 10.1029/2019JB017338

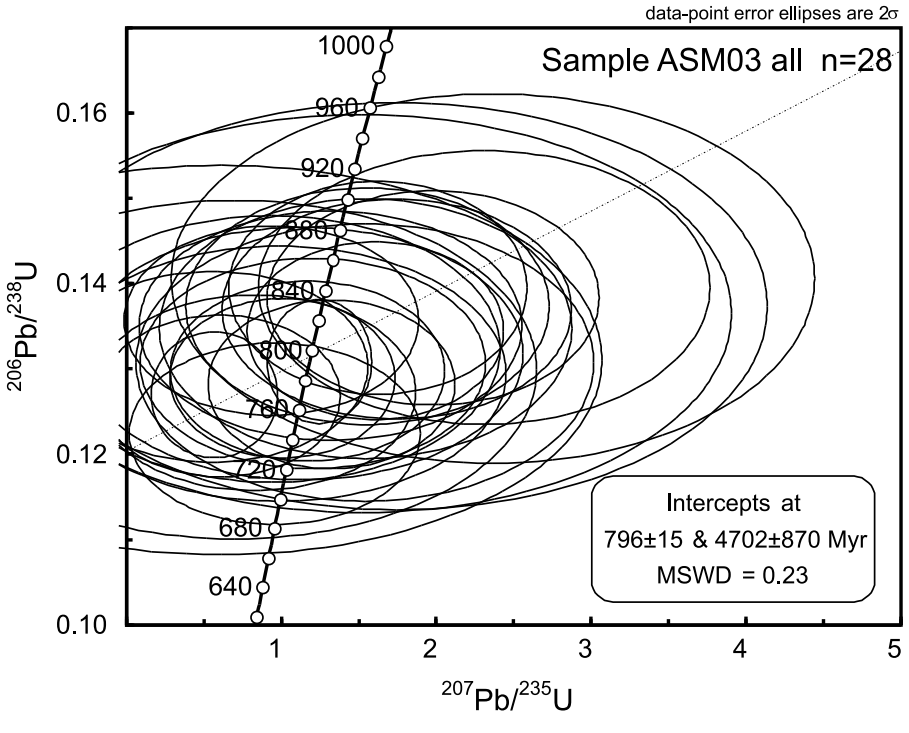
Zhao, Y., Song, B., Zhang, S.H., 2006. The central Mongolian microcontinent: its Yangtze affinity and tectonic implications. In: Proceedings of symposium on continental growth and orogeny in Asia: 135–136, Taipei.

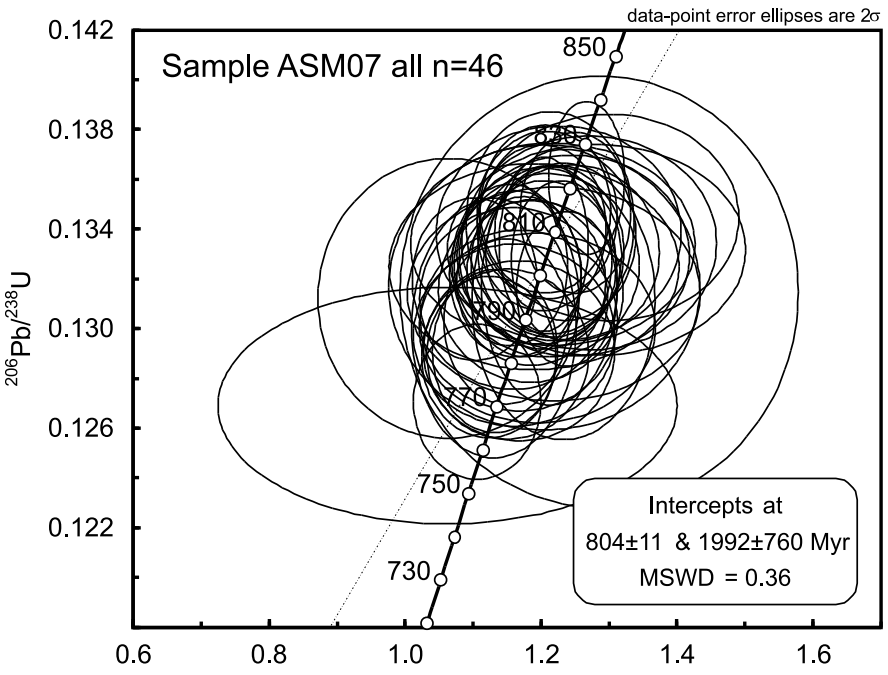
Zhou, H., Zhao, G., Han, Y., Zhang, D., Wang, M., Zhao, S., Pei, X., Zhao, Q., Tserendash, N. Geng, H., Zhang, Y., Enkh-Orshikh, O., 2023. The early Permian high-temperature felsic magmatism induced by slab break off in Southern Mongolia, Central Asian Orogenic Belt and its tectonic implications, Lithos, **442–443**; 107083. https://doi.org/10.1016/j.lithos.2023.107083

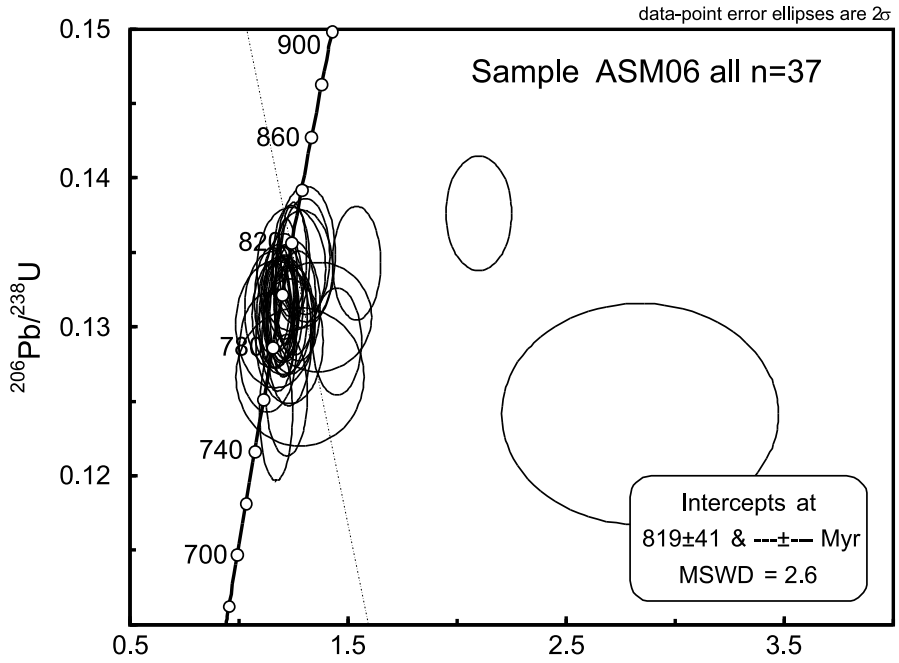
APPENDIX 1
The Concordia diagrams with all dataset

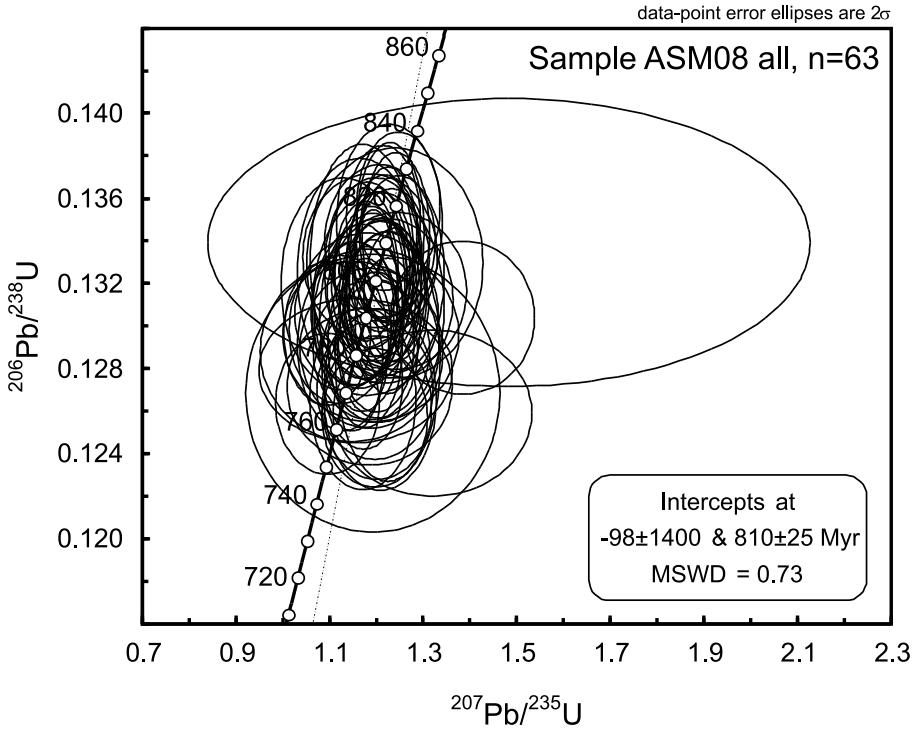


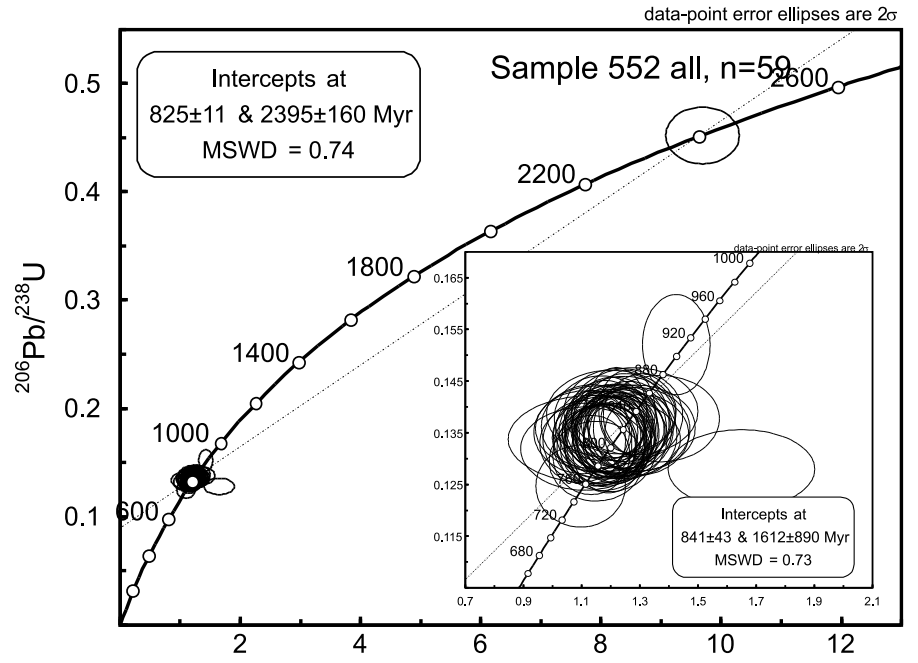


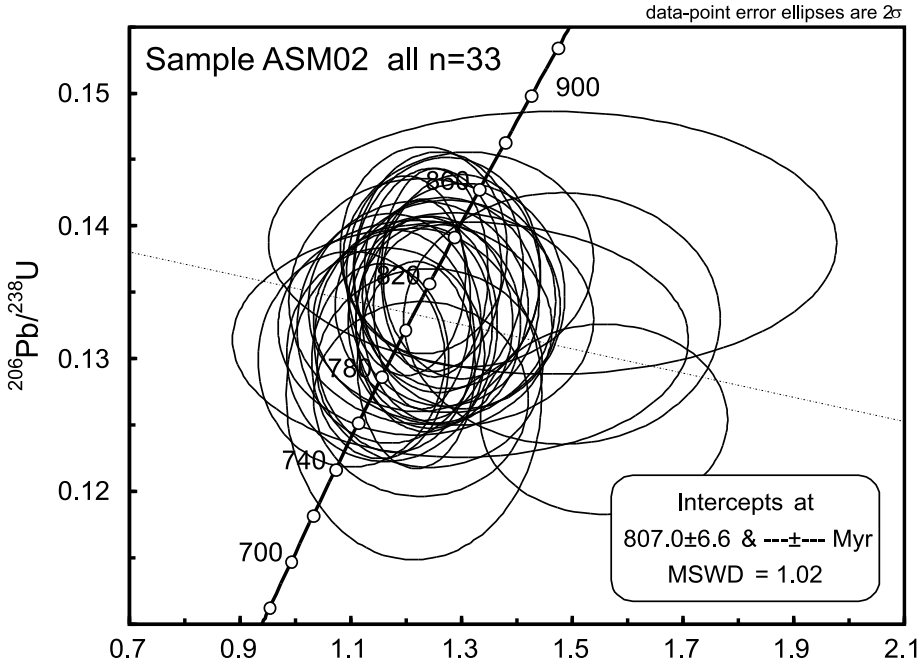


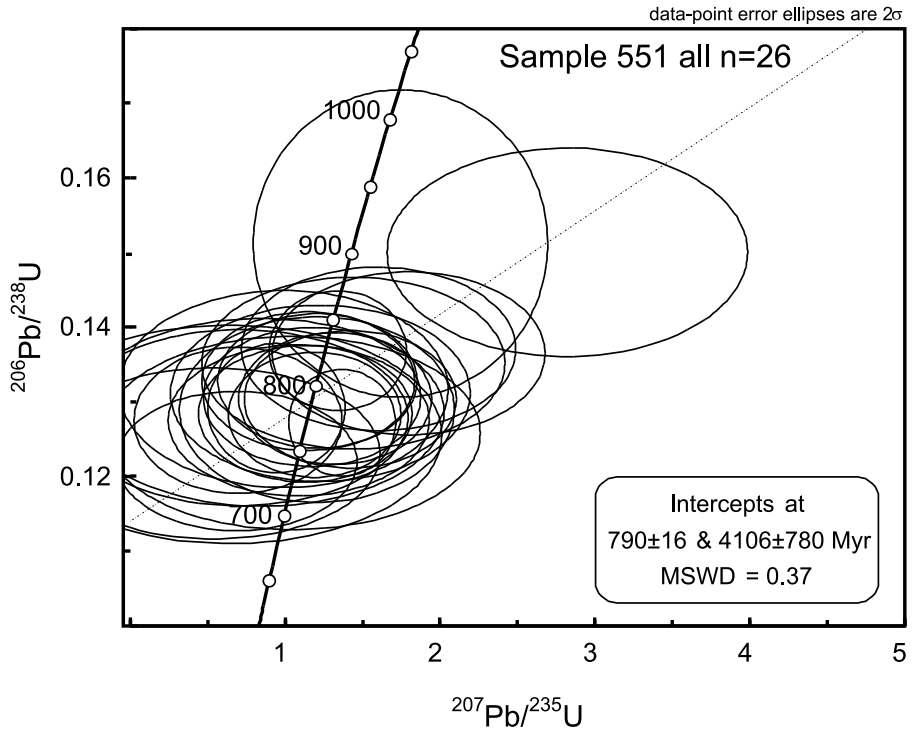

data-point error ellipses are 2σ
Sample ASM07 all n=46
850
810
790
770
750
730
Intercepts at
804±11 & 1992±760 Myr
MSWD = 0.36
0.142
0.138
0.134
0.130
0.126
0.122
0.6
0.8
1.0
1.2
1.4
1.6
206Pb/238U

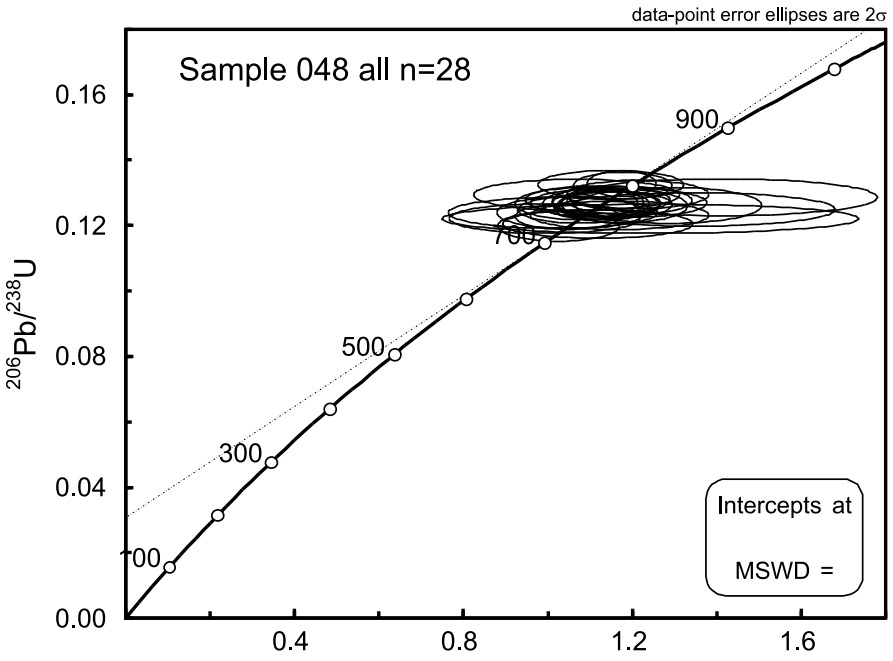

data-point error ellipses are 2σ
Sample ASM06 all n=37
900
860
820
780
740
700
Intercepts at
819±41 & ---±--- Myr
MSWD = 2.6
0.15
0.14
0.13
0.12
0.5
1.5
2.5
3.5
206Pb/238U

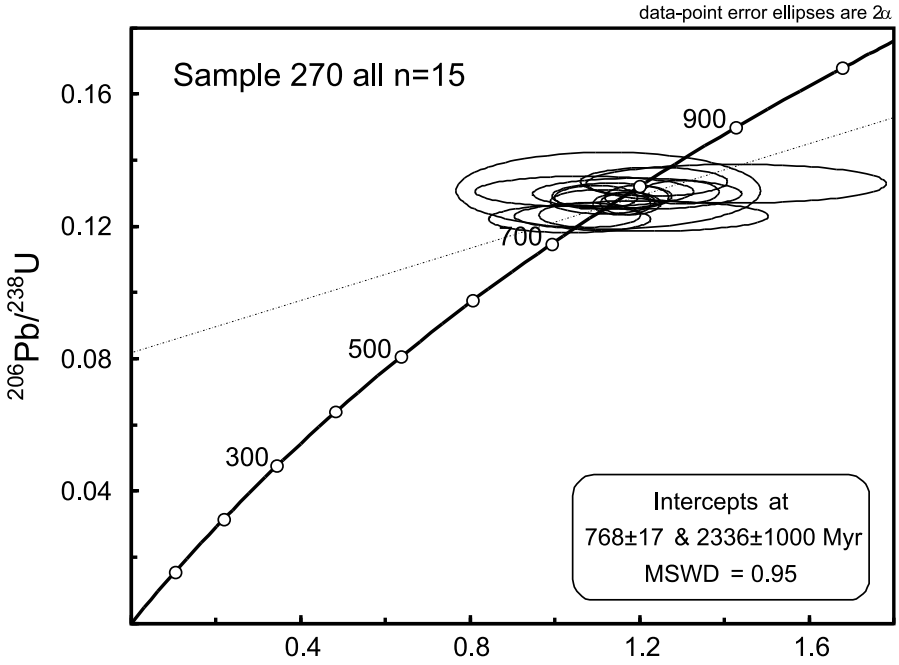

data-point error ellipses are 2σ
Sample ASM08 all, n=63
860
840
820
800
780
760
740
720
Intercepts at
-98±1400 & 810±25 Myr
MSWD = 0.73
0.140
0.136
0.132
0.128
0.124
0.120
0.7
0.9
1.1
1.3
1.5
1.7
1.9
2.1
2.3
206Pb/238U
207Pb/235U

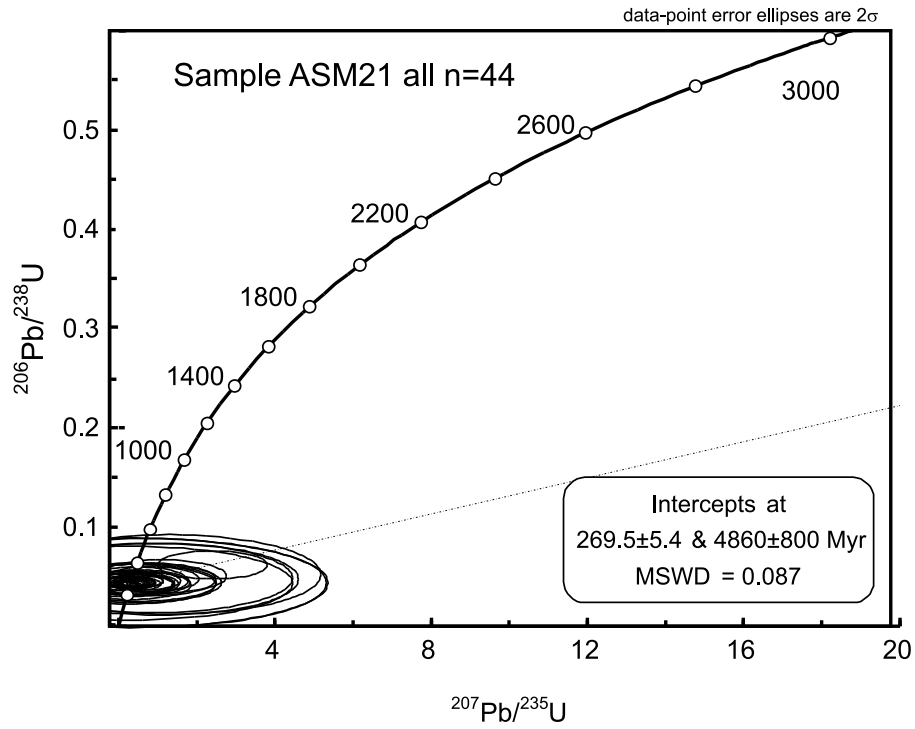

data-point error ellipses are 2σ
Sample 552 all, n=59
Intercepts at
825±11 & 2395±160 Myr
MSWD = 0.74
Intercepts at
841±43 & 1612±890 Myr
MSWD = 0.73
$^{206}Pb/^{238}U$

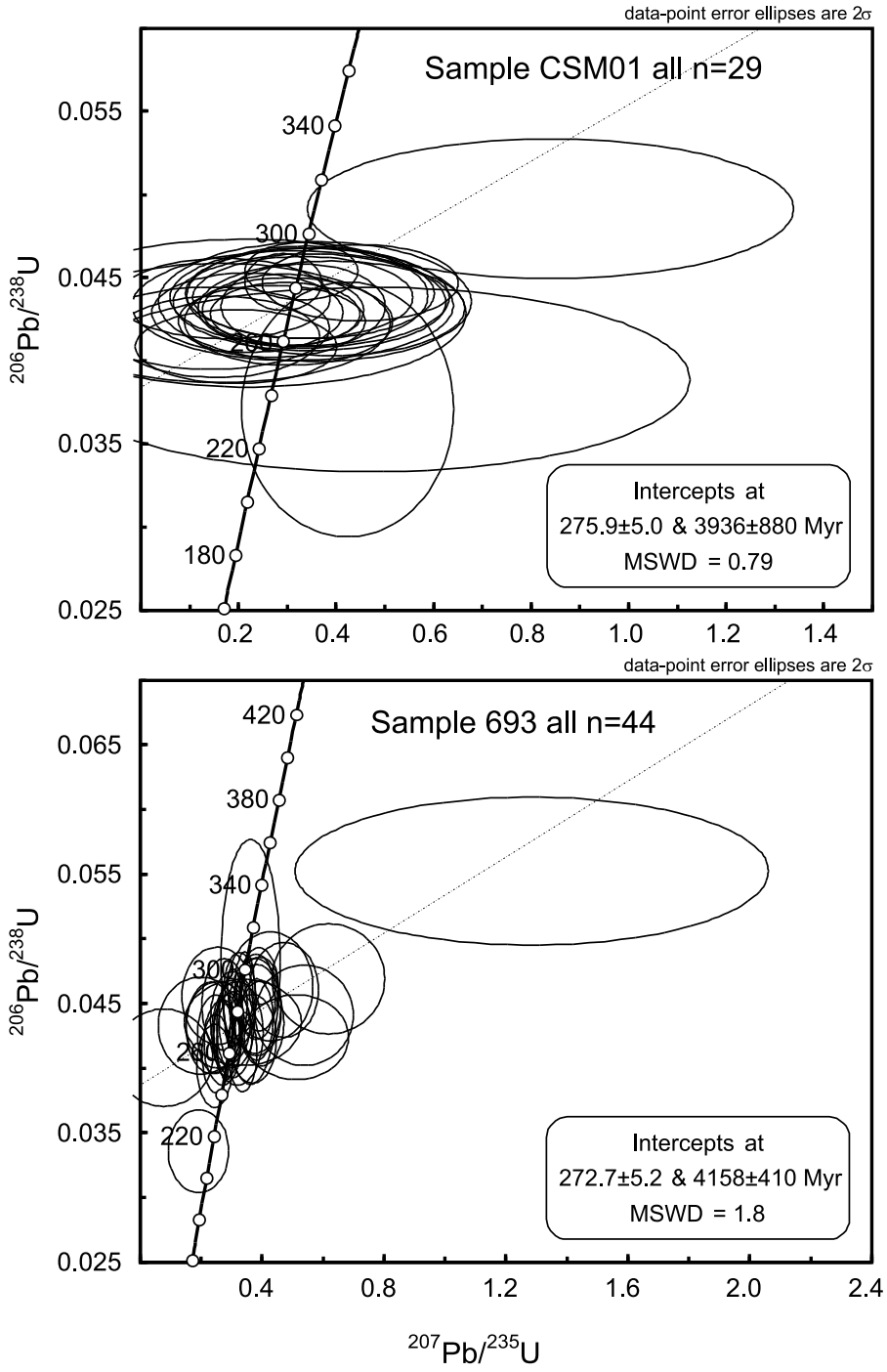

data-point error ellipses are 2σ
Sample ASM02 all n=33
Intercepts at
807.0±6.6 & ---±--- Myr
MSWD = 1.02
$^{206}Pb/^{238}U$


data-point error ellipses are 2σ
Sample 551 all n=26
Intercepts at
790±16 & 4106±780 Myr
MSWD = 0.37
$^{206}Pb/^{238}U$
$^{207}Pb/^{235}U$

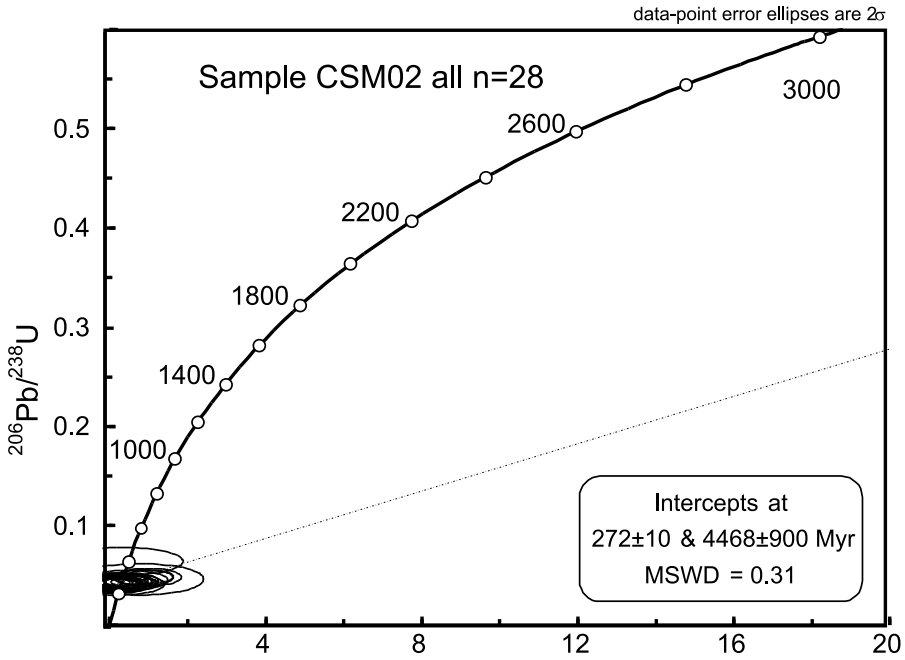

data-point error ellipses are 2σ
Sample 048 all n=28
900
700
500
300
100
Intercepts at
MSWD =
0.16
0.12
0.08
0.04
0.00
0.4
0.8
1.2
1.6
206Pb/238U

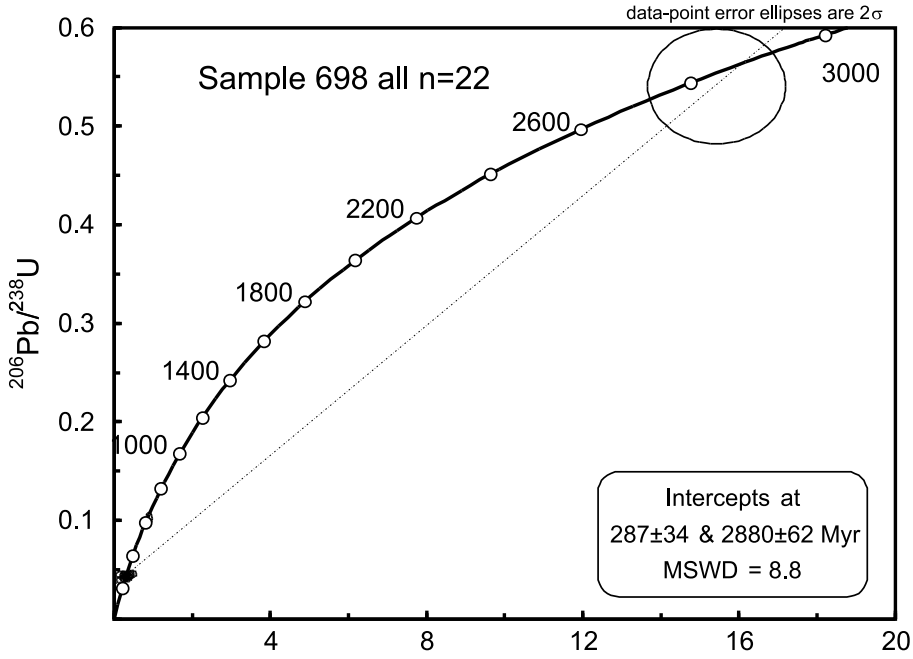

data-point error ellipses are 2α
Sample 270 all n=15
900
700
500
300
Intercepts at
768±17 & 2336±1000 Myr
MSWD = 0.95
0.16
0.12
0.08
0.04
0.4
0.8
1.2
1.6
206Pb/238U

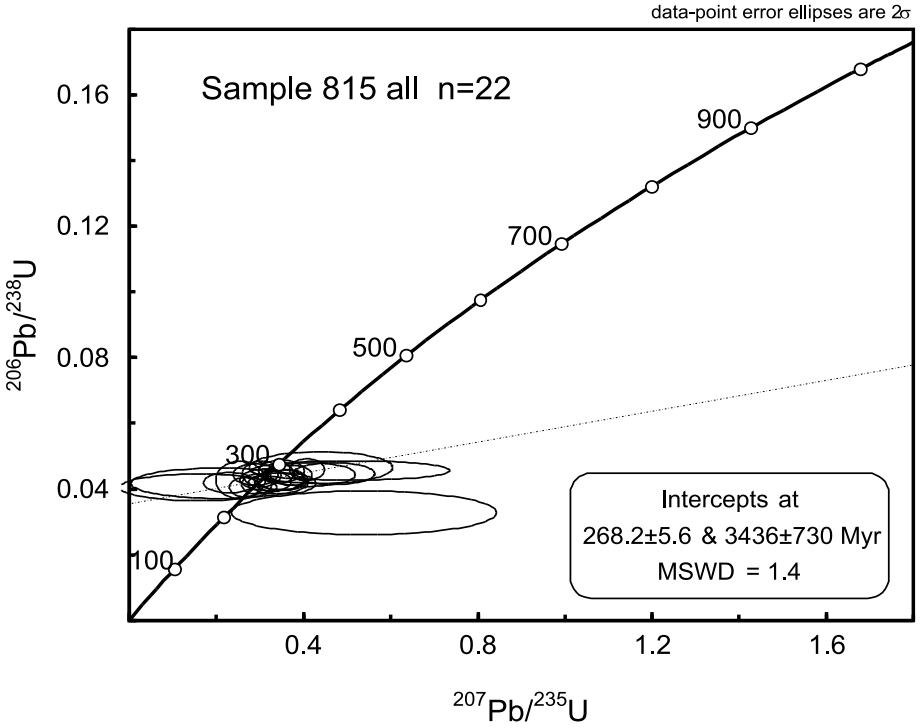

data-point error ellipses are 2σ
Sample ASM21 all n=44
3000
2600
2200
1800
1400
1000
Intercepts at
269.5±5.4 & 4860±800 Myr
MSWD = 0.087
0.5
0.4
0.3
0.2
0.1
4
8
12
16
20
206Pb/238U
207Pb/235U


data-point error ellipses are 2σ
Sample CSM01 all n=29
340
300
260
220
180
0.055
0.045
0.035
0.025
0.2
0.4
0.6
0.8
1.0
1.2
1.4
Intercepts at
275.9±5.0 & 3936±880 Myr
MSWD = 0.79
$^{206}Pb/^{238}U$

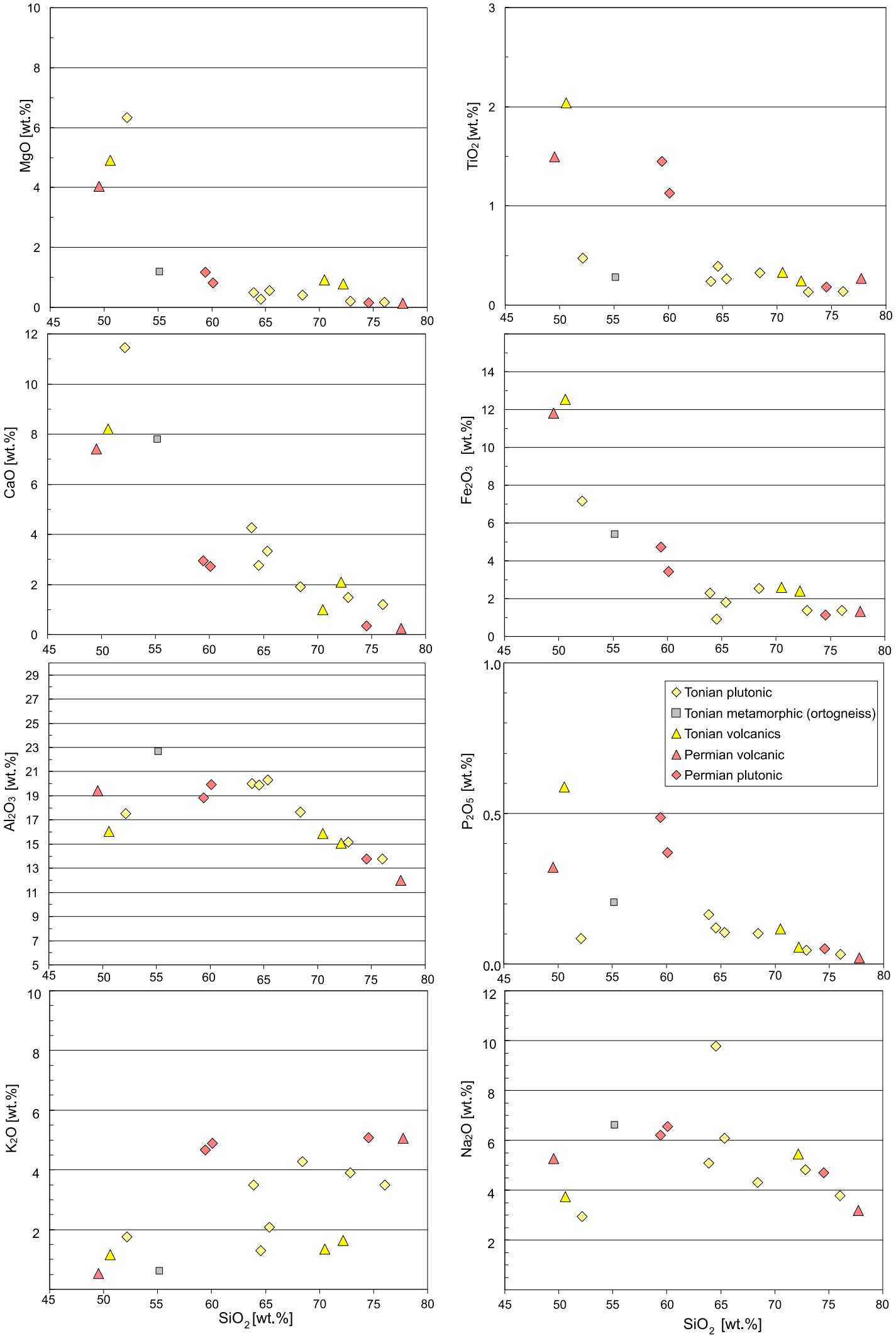
data-point error ellipses are 2σ
Sample 693 all n=44
420
380
340
300
260
220
0.065
0.055
0.045
0.035
0.025
0.4
0.8
1.2
1.6
2.0
2.4
Intercepts at
272.7±5.2 & 4158±410 Myr
MSWD = 1.8
$^{206}Pb/^{238}U$
$^{207}Pb/^{235}U$


data-point error ellipses are 2σ
Sample CSM02 all n=28
3000
2600
2200
1800
1400
1000
Intercepts at
272±10 & 4468±900 Myr
MSWD = 0.31
$^{206}Pb/^{238}U$
0.1
0.2
0.3
0.4
0.5
4
8
12
16
20


data-point error ellipses are 2σ
Sample 698 all n=22
3000
2600
2200
1800
1400
1000
Intercepts at
287±34 & 2880±62 Myr
MSWD = 8.8
$^{206}Pb/^{238}U$
0.1
0.2
0.3
0.4
0.5
0.6
4
8
12
16
20


data-point error ellipses are 2σ
Sample 815 all n=22
900
700
500
300
100
Intercepts at
268.2±5.6 & 3436±730 Myr
MSWD = 1.4
$^{206}Pb/^{238}U$
0.04
0.08
0.12
0.16
0.4
0.8
1.2
1.6
$^{207}Pb/^{235}U$

APPENDIX 2
Harker diagrams



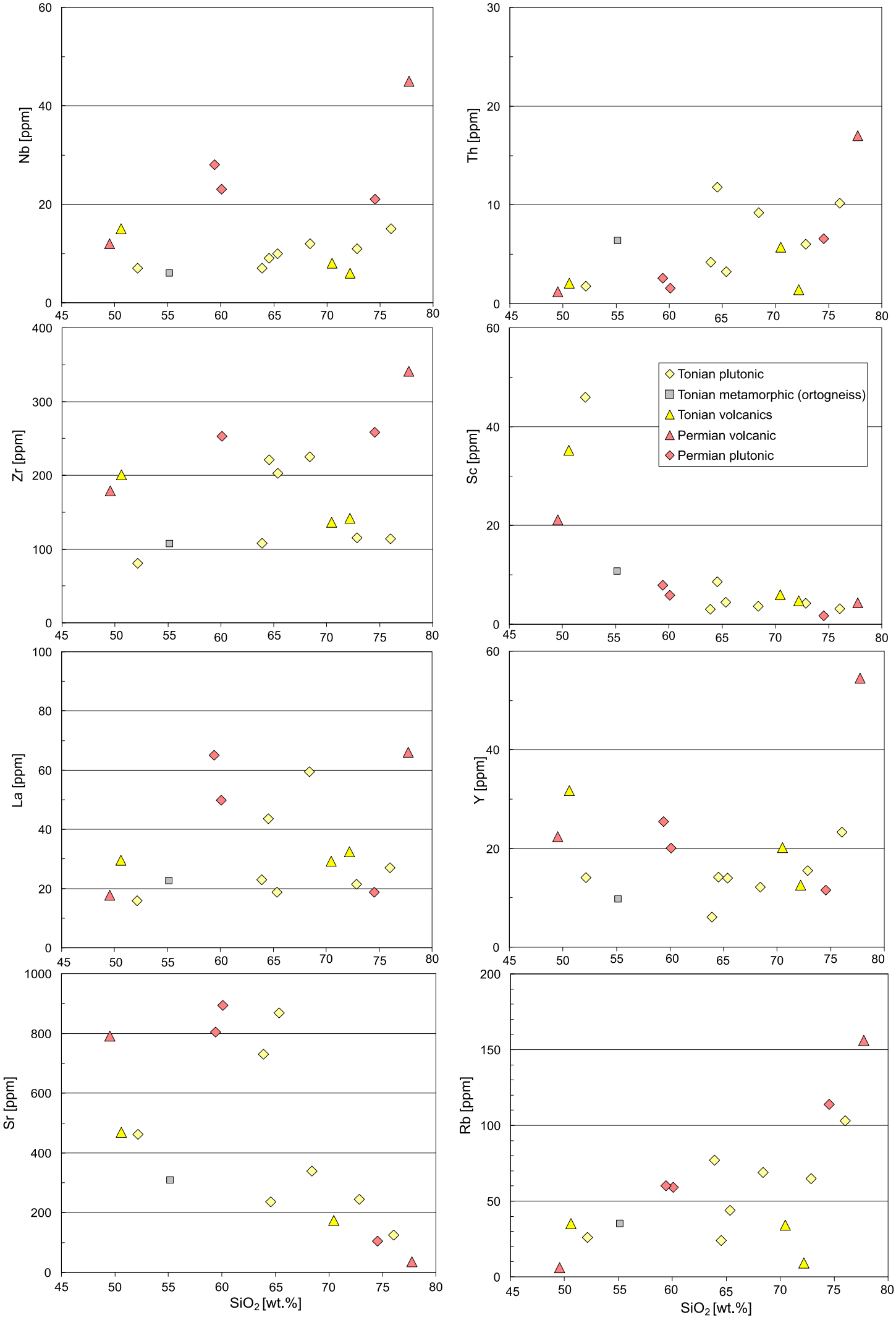

Nb [ppm]
Th [ppm]
Zr [ppm]
Sc [ppm]
La [ppm]
Y [ppm]
Sr [ppm]
Rb [ppm]
SiO2 [wt.%]
SiO2 [wt.%]
Tonian plutonic
Tonian metamorphic (ortogneiss)
Tonian volcanics
Permian volcanic
Permian plutonic

Table S1. U-Pb-Th isotopic ratios and age data

N=31

Spot	overct corr. 204Pb /206Pb	±%	207Pb /206Pb	±%	208Pb /206Pb	±%	206Pb /238U	±%	% 206Pb$_c$	ppm U	ppm Th	4-corr ppm 206Pb*	4-corr ppm 208Pb*	232Th /238U	±%	(1) 206Pb /238U Age	(2) 206Pb /238U Age	(3) 206Pb /238U Age	(1) 207Pb /206Pb Age	% Dis-cor-dant	(1) 238U /206Pb*	±%	(1) 207Pb* /206Pb*	±%	(1) 207Pb* /235U	±%	(1) 206Pb* /238U	±%	err corr
1157.22.1	4,7E-3	38	0,0674	4,3	0,47	2,4	0,359	1,6	8,68	32	27	2,8	0,7	1,25	1,17	743 ±30	809 ±18	770 ±22	#ЧИСЛО!	#ЧИСЛО!	8,18	4,2	0,0673	352,2	0,12	352,2	0,1222	4,2	0,0
1157.4.1	1,4E-3	70	0,0713	2,9	0,25	2,6	0,376	2,4	2,48	42	27	4,8	0,9	0,66	0,82	764 ±18	776 ±13	763 ±15	259 ±643	-207	7,95	2,5	0,0514	28,0	0,89	28,1	0,1257	2,5	0,1
1157.23.1	4,1E-3	49	0,0639	4,6	0,29	3,7	0,365	1,6	7,57	19	16	2,3	0,3	0,85	1,18	765 ±33	827 ±18	812 ±21	#ЧИСЛО!	#ЧИСЛО!	7,94	4,6	0,0008	4131,4	0,01	4131,4	0,1260	4,6	0,0
1157.37.1	8,6E-4	195	0,0643	4,9	0,44	2,8	0,341	2,1	1,58	28	28	2,9	1,2	1,12	1,06	769 ±27	782 ±16	739 ±20	287 ±1125	-200	7,89	3,7	0,0516	49,8	0,90	49,7	0,1268	3,7	0,1
1157.35.1	2,9E-4	546	0,0713	7,6	0,37	3,0	0,330	1,6	0,54	25	23	2,7	1,0	0,97	1,05	772 ±26	770 ±16	746 ±19	839 ±739	+8	7,86	3,6	0,0670	35,5	1,18	35,7	0,1272	3,6	0,1
1157.7.1	5,7E-4	211	0,0663	3,4	0,37	2,5	0,375	3,7	1,05	28	28	3,1	1,1	1,02	0,93	781 ±21	788 ±15	763 ±17	529 ±676	-51	7,76	2,9	0,0580	30,8	1,03	31,0	0,1289	2,9	0,1
1157.21.1	9,3E-4	148	0,0668	3,7	0,36	2,8	0,360	2,3	1,71	28	27	3,3	1,0	1,00	1,00	783 ±24	795 ±16	774 ±18	335 ±892	-142	7,74	3,2	0,0532	39,4	0,95	39,5	0,1292	3,2	0,1
1157.15.1	1,5E-3	149	0,0681	4,9	0,44	7,2	0,351	2,9	2,74	19	20	2,1	0,8	1,13	1,25	786 ±35	805 ±19	766 ±26	~4 ±1743	+238	7,71	4,7	0,0460	72,3	0,82	72,4	0,1296	4,7	0,1
1157.2.1	3,3E-4	195	0,0659	2,5	0,16	2,7	0,366	0,9	0,60	52	24	5,9	0,9	0,47	0,69	788 ±15	793 ±12	785 ±13	647 ±331	-23	7,69	2,0	0,0612	15,4	1,10	15,5	0,1301	2,0	0,1
1157.33.1	2,1E-3	53	0,0695	3,4	0,46	2,6	0,353	3,6	3,63	38	46	3,8	1,2	1,16	0,96	790 ±21	816 ±15	779 ±19	~457 ±1143	+290	7,67	2,7	0,0384	43,8	0,69	43,8	0,1303	2,7	0,1
1157.29.1	-1,6E-3	125	0,0663	4,6	0,42	3,1	0,364	1,6	--	20	22	2,3	1,1	1,15	1,19	793 ±31	770 ±17	742 ±21	1395 ±588	+46	7,64	4,1	0,0886	30,6	1,60	30,9	0,1308	4,1	0,1
1157.28.1	4,4E-4	317	0,0703	3,5	0,36	5,2	0,353	1,3	0,81	27	22	3,0	1,1	0,86	0,96	794 ±24	796 ±15	762 ±19	739 ±680	-8	7,63	3,2	0,0639	32,2	1,16	32,3	0,1311	3,2	0,1
1157.19.1	1,3E-5	8406	0,0656	3,5	0,42	2,4	0,352	2,3	0,02	32	34	3,6	1,5	1,11	0,92	795 ±21	795 ±15	762 ±18	786 ±521	-1	7,62	2,8	0,0654	24,8	1,18	25,0	0,1312	2,8	0,1
1157.10.1	1,3E-3	94	0,0679	3,6	0,40	2,8	0,378	2,9	2,40	25	26	2,8	1,5	1,06	1,00	796 ±23	813 ±16	780 ±19	127 ±915	-560	7,61	3,0	0,0496	38,9	0,88	39,0	0,1314	3,0	0,1
1157.36.1	8,1E-4	172	0,0697	3,5	0,48	2,7	0,355	1,6	1,48	27	33	3,1	1,4	1,25	1,05	797 ±25	805 ±16	767 ±21	528 ±783	-54	7,60	3,3	0,0580	35,7	1,05	35,8	0,1316	3,3	0,1
1157.16.1	4,2E-4	115	0,0684	2,2	0,25	2,0	0,360	2,8	0,77	70	44	7,9	1,9	0,66	0,60	799 ±25	802 ±25	784 ±27	684 ±246	-18	7,58	3,4	0,0623	11,5	1,13	12,0	0,1319	3,4	0,3
1157.30.1	3,7E-4	149	0,0650	2,3	0,19	2,3	0,351	1,7	0,67	75	37	8,6	1,5	0,51	0,62	801 ±14	807 ±12	793 ±13	592 ±295	-38	7,55	1,8	0,0597	13,6	1,09	13,7	0,1324	1,8	0,1
1157.32.1	3,9E-4	577	0,0666	4,9	0,25	4,2	0,358	1,7	0,70	22	13	2,5	0,6	0,62	1,25	803 ±36	808 ±19	787 ±20	640 ±1149	-27	7,53	4,7	0,0610	53,4	1,12	53,6	0,1327	4,7	0,1
1157.20.1	-6,7E-4	146	0,0644	5,5	0,37	2,4	0,362	1,1	--	35	33	4,0	1,6	0,98	0,86	808 ±19	800 ±14	768 ±17	1039 ±387	+24	7,49	2,5	0,0739	19,2	1,36	19,3	0,1336	2,5	0,1
1157.17.1	-1,2E-3	141	0,0693	4,2	0,37	3,1	0,370	1,7	--	20	19	2,4	1,0	0,98	1,14	816 ±28	796 ±17	768 ±20	1336 ±520	+41	7,41	3,7	0,0859	26,9	1,60	27,1	0,1349	3,7	0,1
1157.27.1	1,1E-5	9908	0,0715	3,1	0,46	2,1	0,370	1,1	0,02	38	46	4,4	2,1	1,25	0,86	817 ±21	812 ±14	781 ±18	967 ±450	+17	7,40	2,7	0,0713	22,1	1,33	22,2	0,1351	2,7	0,1
1157.18.1	-2,8E-4	346	0,0668	3,0	0,57	3,1	0,359	1,0	--	44	64	5,2	3,0	1,49	0,79	820 ±19	816 ±14	763 ±19	951 ±401	+15	7,37	2,4	0,0708	19,6	1,32	19,7	0,1357	2,4	0,1
1157.6.1	4,2E-4	269	0,0697	5,7	0,56	2,1	0,376	1,3	0,77	28	39	3,3	1,8	1,45	0,96	828 ±22	831 ±16	776 ±21	730 ±563	-14	7,30	2,8	0,0636	26,6	1,20	26,7	0,1370	2,8	0,1
1157.8.1	2,2E-4	211	0,0667	2,0	0,34	1,6	0,368	2,1	0,40	92	79	10,9	3,6	0,89	0,57	828 ±13	831 ±12	804 ±13	725 ±228	-15	7,30	1,7	0,0635	10,8	1,20	10,9	0,1371	1,7	0,2
1157.5.1	-1,2E-3	128	0,0665	4,0	0,57	2,4	0,362	2,3	--	22	32	2,6	1,6	1,49	1,06	829 ±27	811 ±16	758 ±22	1294 ±513	+38	7,29	3,5	0,0841	26,4	1,59	26,6	0,1373	3,5	0,1
1157.12.1	-2,2E-3	58	0,0797	3,4	0,45	2,5	0,363	1,5	--	25	26	3,0	1,6	1,07	1,01	837 ±24	793 ±16	754 ±19	1801 ±282	+57	7,21	3,0	0,1101	15,5	2,11	15,8	0,1387	3,0	0,2
1157.34.1	-2,6E-3	86	0,0629	5,1	0,48	3,1	0,364	1,7	--	18	21	2,2	1,2	1,21	1,28	844 ±36	811 ±19	760 ±24	1597 ±560	+50	7,15	4,5	0,0985	30,0	1,90	30,3	0,1398	4,5	0,1
1157.31.1	-5,9E-3	39	0,0674	4,9	0,49	3,0	0,347	1,6	--	22	28	2,7	1,7	1,31	1,21	850 ±36	770 ±18	734 ±23	2271 ±326	+67	7,10	4,5	0,1436	18,9	2,79	19,4	0,1409	4,5	0,2
1157.25.1	-3,8E-3	137	0,0589	9,1	0,22	7,4	0,321	4,9	--	10	6	1,3	0,4	0,62	1,96	851 ±76	806 ±28	788 ±29	1807 ±1089	+56	7,09	9,4	0,1105	59,8	2,15	60,7	0,1411	9,4	0,2
1157.26.1	-1,2E-3	128	0,0631	9,8	0,53	2,4	0,347	1,5	--	30	41	3,7	2,1	1,42	1,02	867 ±27	854 ±18	801 ±22	1191 ±537	+29	6,95	3,3	0,0797	27,2	1,58	27,4	0,1439	3,3	0,1
1157.11.1	-1,1E-3	158	0,0658	4,3	0,45	2,8	0,341	2,4	--	24	28	3,0	1,5	1,22	1,11	872 ±32	857 ±18	819 ±22	1246 ±603	+32	6,90	3,9	0,0820	30,8	1,64	31,0	0,1449	3,9	0,1

Errors are 1-sigma; Pb$_c$ and Pb* indicate the common and radiogenic portions, respectively.

Error in Standard calibration was 0.28% (not included in above errors but required when comparing data from different mounts).

(1) Common Pb corrected using measured 204Pb.

(2) Common Pb corrected by assuming 206Pb/238U-207Pb/235U age-concordance

n=23

Concordia age 810.6 ±9. Ma

1157

n=33

Spot	overct corr. 204Pb /206Pb	±%	207Pb /206Pb	±%	208Pb /206Pb	±%	206Pb /238U	±%	% 206Pb$_c$	ppm U	ppm Th	4-corr ppm 206Pb*	4-corr ppm 208Pb*	232Th /238U	±%	(1) 206Pb /238U Age	(2) 206Pb /238U Age	(3) 206Pb /238U Age	(1) 207Pb /206Pb Age	% Dis-cor-dant	(1) 238U /206Pb*	±%	(1) 207Pb* /206Pb*	±%	(1) 207Pb* /235U	±%	(1) 206Pb* /238U	±%	err corr
ASM02.16.1	-1,9E-4	126	0,0674	4,1	0,428	1,2	0,313	3,3	--	179	184	19,2	8,4	1,06	0,43	762 ±17	738 ±17	718 ±20	1427 ±103	+49	7,97	2,3	0,0901	5,4	1,56	5,9	0,1254	2,3	0,4
ASM02.6.1	-2,4E-4	103	0,0661	1,8	0,325	1,4	0,299	2,8	--	121	103	13,2	4,4	0,89	0,46	770 ±17	766 ±17	746 ±19	930 ±123	+18	7,88	2,4	0,0701	6,0	1,23	6,5	0,1270	2,4	0,4
ASM02.38.1	1,7E-4	183	0,0716	1,7	0,379	1,3	0,376	3,9	0,31	95	86	10,4	3,9	0,94	0,96	773 ±29	769 ±30	738 ±34	904 ±137	+15	7,85	4,0	0,0692	6,7	1,21	7,8	0,1273	4,0	0,5
ASM02.21.1	1,6E-4	183	0,0720	1,7	0,246	3,5	0,308	4,1	0,29	115	73	12,8	3,1	0,66	0,99	784 ±17	780 ±17	769 ±19	920 ±129	+16	7,73	2,4	0,0697	6,3	1,24	6,7	0,1293	2,4	0,4
ASM02.7.1	-1,3E-4	68	0,0663	1,8	0,414	1,5	0,360	2,9	--	272	297	30,3	12,8	1,13	0,27	785 ±18	782 ±19	754 ±22	875 ±54	+11	7,72	2,5	0,0682	2,6	1,22	3,6	0,1295	2,5	0,7
ASM02.27.1	1,5E-4	104	0,0666	1,4	0,348	1,1	0,356	2,3	0,27	145	132	16,2	5,6	0,94	0,40	787 ±17	788 ±18	763 ±20	757 ±79	-4	7,70	2,3	0,0645	3,7	1,15	4,4	0,1298	2,3	0,5
ASM02.12.1	4,2E-4	55	0,0675	1,6	0,262	2,5	0,376	1,6	0,76	109	65	12,1	2,6	0,61	1,08	788 ±19	779 ±21	751 ±24	656 ±122	-21	7,70	2,6	0,0615	5,7	1,10	6,3	0,1299	2,6	0,4
ASM02.13.1	1,3E-4	183	0,0667	1,6	0,304	2,5	0,345	1,8	0,25	131	107	14,7	4,4	0,84	0,43	790 ±19	790 ±19	773 ±21	765 ±121	-3	7,67	2,5	0,0647	5,8	1,16	6,3	0,1303	2,5	0,4
ASM02.10.1	9,7E-5	189	0,0665	1,4	0,305	3,6	0,351	3,7	0,18	168	134	18,9	5,8	0,82	0,63	795 ±19	796 ±20	775 ±23	779 ±90	-2	7,62	2,6	0,0651	4,3	1,18	5,0	0,1313	2,6	0,5
ASM02.20.1	-1,4E-4	451	0,0697	2,8	0,185	3,0	0,340	1,0	--	43	20	4,8	0,9	0,49	0,76	796 ±21	790 ±19	780 ±20	976 ±258	+20	7,61	2,8	0,0716	12,7	1,30	13,0	0,1314	2,8	0,2
ASM02.34.1	2,0E-4	110	0,0670	1,7	0,208	1,7	0,365	2,1	0,36	132	70	15,0	3,0	0,55	0,47	801 ±20	802 ±21	788 ±22	746 ±110	-8	7,56	2,7	0,0641	5,2	1,17	5,8	0,1323	2,7	0,5
ASM02.24.1	2,2E-4	164	0,0698	2,0	0,237	6,4	0,341	1,8	0,39	78	48	8,9	2,1	0,64	0,55	801 ±19	800 ±19	787 ±21	828 ±166	+3	7,56	2,5	0,0667	7,9	1,22	8,3	0,1323	2,5	0,3
ASM02.4.1	-3,1E-5	473	0,0672	1,4	0,228	1,4	0,350	2,4	--	233	132	26,5	6,1	0,59	0,36	802 ±19	801 ±19	783 ±21	858 ±71	+7	7,54	2,5	0,0677	3,4	1,24	4,2	0,1326	2,5	0,6
ASM02.32.1	-1,2E-4	142	0,0674	1,5	0,291	1,3	0,335	1,9	--	166	128	18,9	5,6	0,80	0,41	803 ±17	799 ±18	782 ±20	904 ±82	+12	7,54	2,3	0,0692	4,0	1,26	4,6	0,1326	2,3	0,5
ASM02.5.1	1,7E-4	86	0,0699	1,2	0,197	1,2	0,354	1,9	0,32	188	95	21,5	4,1	0,52	0,62	803 ±17	802 ±17	790 ±18	850 ±71	+6	7,54	2,3	0,0674	3,4	1,23	4,1	0,1327	2,3	0,6
ASM02.31.1	1,1E-4	177	0,0695	1,4	0,187	1,5	0,348	2,4	0,19	140	65	16,0	3,0	0,48	0,84	803 ±19	801 ±19	790 ±20	868 ±88	+8	7,53	2,5	0,0680	4,2	1,24	4,9	0,1327	2,5	0,5
ASM02.9.2	1,6E-4	230	0,0724	2,0	0,290	1,8	0,328	3,4	0,29	78	45	8,9	2,6	0,59	0,56	805 ±19	801 ±18	784 ±20	932 ±157	+15	7,52	2,5	0,0701	7,7	1,29	8,0	0,1330	2,5	0,3
ASM02.17.1	-2,9E-4	110	0,0766	5,0	0,299	1,7	0,339	2,6	--	73	54	8,3	2,6	0,76	0,55	805 ±22	790 ±22	774 ±24	1216 ±144	+36	7,52	2,9	0,0808	7,3	1,48	7,9	0,1330	2,9	0,4
ASM02.26.1	-1,3E-4	220	0,0673	1,9	0,240	1,8	0,352	2,8	--	86	51	9,9	2,4	0,61	0,52	810 ±19	807 ±19	787 ±20	901 ±124	+11	7,47	2,4	0,0691	6,0	1,28	6,5	0,1339	2,4	0,4
ASM02.23.1	-6,0E-5	451	0,0653	1,9	0,238	1,7	0,328	2,5	--	96	62	11,1	2,7	0,67	0,49	810 ±18	810 ±19	796 ±20	811 ±130	+0	7,47	2,4	0,0662	6,2	1,22	6,7	0,1339	2,4	0,4
ASM02.3.1	-2,5E-5	261	0,0661	0,9	0,502	0,6	0,368	1,9	--	610	776	70,2	35,6	1,31	0,60	811 ±18	811 ±19	766 ±23	821 ±34	+1	7,46	2,4	0,0665	1,6	1,23	2,9	0,1341	2,4	0,8
ASM02.8.1	-2,5E-4	90	0,0649	1,7	0,315	3,1	0,363	1,5	--	121	96	13,9	4,5	0,83	1,07	812 ±18	810 ±18	783 ±21	884 ±104	+9	7,45	2,4	0,0685	5,0	1,27	5,6	0,1343	2,4	0,4
ASM02.25.1	-6,8E-5	494	0,0654	2,0	0,232	1,8	0,349	0,7	--	73	45	8,4	2,0	0,64	0,54	812 ±21	812 ±22	797 ±23	818 ±157	+1	7,45	2,8	0,0664	7,5	1,23	8,0	0,1343	2,8	0,4
ASM02.9.1	-3,0E-4	80	0,0659	1,7	0,233	1,6	0,344	2,6	--	106	64	12,2	3,0	0,63	0,46	815 ±20	811 ±20	794 ±21	934 ±105	+14	7,42	2,6	0,0702	5,1	1,30	5,7	0,1347	2,6	0,4
ASM02.19.1	-1,1E-4	150	0,0676	1,5	0,204	1,5	0,362	2,5	--	163	88	19,1	4,0	0,56	0,41	823 ±18	820 ±18	808 ±19	907 ±79	+10	7,34	2,3	0,0693	3,8	1,30	4,5	0,1362	2,3	0,5
ASM02.33.1	-1,2E-4	98	0,0656	1,2	0,414	0,8	0,351	2,0	0,21	247	267	28,9	12,0	1,12	0,36	823 ±17	826 ±18	793 ±21	738 ±61	-12	7,34	2,3	0,0639	2,9	1,20	3,7	0,1362	2,3	0,6
ASM02.35.1	-7,8E-5	271	0,0666	1,5	0,228	1,4	0,351	0,5	--	122	73	14,4	3,4	0,61	0,70	825 ±20	823 ±21	807 ±22	861 ±98	+4	7,33	2,6	0,0677	4,7	1,27	5,4	0,1364	2,6	0,5
ASM02.2.1	-1,6E-5	533	0,0663	1,0	0,235	0,9	0,359	0,4	--	275	167	32,2	7,7	0,63	0,27	825 ±18	825 ±19	807 ±20	822 ±44	-0	7,33	2,4	0,0665	2,1	1,25	3,2	0,1364	2,4	0,7
ASM02.36.1	-4,0E-5	451	0,0663	1,5	0,183	1,6	0,356	1,3	--	117	59	13,8	2,6	0,52	0,79	825 ±21	825 ±22	814 ±23	833 ±87	+1	7,33	2,7	0,0669	4,2	1,26	5,0	0,1365	2,7	0,5
ASM02.18.1	7,8E-5	150	0,0674	2,1	0,266	2,0	0,391	1,5	0,14	160	111	18,8	5,0	0,71	0,35	826 ±18	826 ±18	807 ±20	815 ±70	-1	7,32	2,3	0,0663	3,3	1,25	4,0	0,1367	2,3	0,6
ASM02.11.1	-2,3E-4	135	0,0660	1,8	0,376	1,4	0,378	1,7	--	90	82	10,6	4,1	0,94	0,58	830 ±19	828 ±19	789 ±21	906 ±136	+9	7,27	2,4	0,0692	6,6	1,31	7,0	0,1375	2,4	0,3
ASM02.22.1	7,2E-5	261	0,0657	1,4	0,217	1,4	0,364	1,9	0,13	147	81	17,4	3,8	0,57	0,40	834 ±18	837 ±18	818 ±20	764 ±94	-10	7,24	2,3	0,0647	4,4	1,23	5,0	0,1382	2,3	0,5
ASM02.14.1	-5,7E-4	126	0,0685	5,4	0,183	3,0	0,338	1,1	--	39	20	4,6	0,9	0,53	0,78	837 ±23	827 ±21	821 ±22	1110 ±280	+26	7,21	2,9	0,0766	14,0	1,46	14,3	0,1387	2,9	0,2

ASM02

Errors are 1-sigma; Pb$_c$ and Pb* indicate the common and radiogenic portions, respectively.

Error in Standard calibration was 0.71% (not included in above errors but required when comparing data from different mounts).

(1) Common Pb corrected using measured 204Pb.

(2) Common Pb corrected by assuming 206Pb/238U-207Pb/235U age-concordance

(3) Common Pb corrected by assuming 206Pb/238U-208Pb/232Th age-concordance

n=29

Concordia age 808.2 ±5.5 Ma

Titanite

N=7

Spot	overct corr. 204Pb /206Pb	±%	207Pb /206Pb	±%	208Pb /206Pb	±%	206Pb /238U	±%	206Pb /254	±%	?-corr 204Pb /206Pb	% 206Pb$_c$	ppm U	ppm Th	?-corr ppm 206Pb*	?-corr ppm 208Pb*	232Th /238U	±%	(1) 206Pb /238U Age	(2) 206Pb /238U Age	(3) 206Pb /238U Age	(1) 207Pb /206Pb Age	% Dis-cor-dant	(1) 238U /206Pb*	±%	(1) 207Pb* /206Pb*	±%	(1) 207Pb* /235U	±%	(1) 206Pb* /238U	±%	err corr
ASM02.1.1	1,4E-3	28	0,092	1,2	0,38	0,8	4,1	3,9	0,25	1,3	0,0018	3,26	59	81	6,8	2,17	1,42	1,05	817 ±18	812 ±17	864 ±22	969 ±172	623 ±33	+17	7,4	2,3	0,071	8,4	1,3	8,7	0,135	2,3	0,3
ASM02.2.1	4,6E-3	10	0,146	1,0	0,39	2,1	4,0	4,4	0,25	2,4	0,0056	10,30	53	41	5,6	1,08	0,80	1,29	764 ±17	750 ±16	770 ±21	1196 ±177	720 ±63	+38	7,9	2,4	0,080	9,0	1,4	9,3	0,126	2,4	0,3
ASM02.3.1	8,5E-3	9	0,208	9,2	0,65	5,8	4,5	6,1	0,27	3,4	0,0100	18,27	27	40	2,8	0,90	1,53	1,28	755 ±23	731 ±29	793 ±37	1421 ±552	616 ±68	+50	8,0	3,3	0,090	28,9	1,5	29,1	0,124	3,3	0,1
ASM02.4.1	1,8E-3	10	0,100	1,4	0,50	0,9	4,0	5,1	0,24	2,2	0,0024	4,48	122	224	13,1	5,65	1,90	1,45	769 ±13	760 ±13	832 ±19	1043 ±83	594 ±17	+28	7,9	1,8	0,074	4,1	1,3	4,5	0,127	1,8	0,4
ASM02.6.1	1,4E-3	12	0,088	3,3	0,25	2,8	4,2	2,8	0,25	1,4	0,0016	2,91	124	103	13,9	2,69	0,86	0,84	795 ±13	792 ±14	821 ±16	890 ±117	607 ±29	+11	7,6	1,8	0,069	5,7	1,2	5,9	0,131	1,8	0,3
ASM02.9.1	1,0E-3	13	0,082	1,4	0,13	1,2	4,1	4,2	0,24	2,3	0,0012	2,12	159	63	17,4	1,54	0,41	1,62	775 ±15	773 ±16	787 ±16	828 ±74	571 ±37	+7	7,8	2,1	0,067	3,5	1,2	4,1	0,128	2,1	0,5
ASM02.10.1	9,3E-4	15	0,080	5,6	0,18	7,4	4,4	5,5	0,25	2,5	0,0010	1,91	136	90	14,8	2,18	0,69	0,91	772 ±13	771 ±14	795 ±15	823 ±157	555 ±46	+7	7,9	1,7	0,067	7,5	1,2	7,7	0,127	1,7	0,2

ASM02

Errors are 1-sigma; Pb$_c$ and Pb* indicate the common and radiogenic portions, respectively.

Error in Standard calibration was 0.55% (not included in above errors but required when comparing data from different mounts).

(1) Common Pb corrected using measured 204Pb.

(2) Common Pb corrected by assuming 206Pb/238U-207Pb/235U age-concordance

(3) Common Pb corrected by assuming 206Pb/238U-208Pb/232Th age-concordance

n=6

Concordia age 785 ±11 Ma

N=28

Spot	overct corr. 204Pb /206Pb	±%	207Pb /206Pb	±%	208Pb /206Pb	±%	206Pb /238U	±%	% 206Pb$_c$	ppm U	ppm Th	4-corr ppm 206Pb*	4-corr ppm 208Pb*	232Th /238U	±%	(1) 206Pb /238U Age	(2) 206Pb /238U Age	(3) 206Pb /238U Age	(1) 207Pb /206Pb Age	% Dis-cor-dant	(1) 238U /206Pb*	±%	(1) 207Pb* /206Pb*	±%	(1) 207Pb* /235U	±%	(1) 206Pb* /238U	±%	err corr
ASM03.21.1	4,6E-4	337	0,0634	2,4	0,356	1,6	0,352	3,4	0,83	95	88	10,0	3,5	0,95	1,57	744 ±25	751 ±16	725 ±18	480 ±883	-58	8,17	3,6

ASM04.39.1	1,3E-3	56	0,0910	7,3	0,152	10	0,362	3,0	2,31	117	68	13,0	1,28	0,587	0,40	789 ±14	782 ±12	817 ±12	1012 ±358	+23	7,68	1,9	0,0729	17,6	1,31	17,7	0,1302	1,8	0,10		
ASM04.18.1	-1,8E-3	120	0,0593	8,7	0,214	15	0,314	4,2	--	66	61	7,4	2,04	0,964	1,48	791 ±32	772 ±16	799 ±21	1310 ±685	+42	7,66	4,3	0,0848	35,3	1,53	35,6	0,1305	4,3	0,12		
ASM04.35.1	-1,1E-4	300	0,0584	3,4	0,053	18	0,366	3,1	--	231	99	25,9	1,48	0,444	0,27	791 ±10	797 ±9	821 ±10	601 ±183	-34	7,65	1,3	0,0599	8,4	1,08	8,5	0,1306	1,3	0,15		
ASM04.14.1	-7,2E-4	123	0,0629	1,7	0,219	2	0,365	2,4	--	108	79	12,2	2,99	0,751	0,45	794 ±15	788 ±11	1018 ±346	+23	7,63	2,0	0,0732	17,1	1,32	17,2	0,1310	2,0	0,12		
ASM04.10.1	-6,1E-4	174	0,0563	10,5	0,127	3	0,352	3,3	--	79	34	8,9	1,33	0,445	0,49	795 ±17	795 ±12	790 ±11	779 ±524	-2	7,62	2,3	0,0651	24,9	1,18	25,1	0,1312	2,3	0,09		
ASM04.42.1	-7,7E-4	108	0,0609	1,6	0,141	18	0,367	2,1	--	112	96	12,7	2,15	0,880	0,43	795 ±15	789 ±10	836 ±15	983 ±332	+20	7,62	2,0	0,0719	16,3	1,30	16,4	0,1312	2,0	0,12		
ASM04.32.1	-3,0E-4	793	0,0632	5,1	0,176	7	0,335	2,6	--	51	32	5,8	1,08	0,639	0,70	796 ±38	794 ±21	799 ±22	853 ±1041	+7	7,61	5,0	0,0675	50,1	1,22	50,4	0,1313	5,0	0,10		
ASM04.41.1	-6,4E-4	108	0,0620	1,5	0,142	6	0,361	1,9	--	123	78	13,9	2,32	0,653	0,39	798 ±13	793 ±10	812 ±11	964 ±284	+18	7,58	1,8	0,0712	13,9	1,29	14,0	0,1319	1,8	0,13		
ASM04.34.1	5,0E-3	11	0,0587	2,2	0,183	21	0,375	3,0	0,92	182	268	20,9	3,45	1,511	0,58	805 ±12	594 ±22	805 ±12	652 ±292	-24	7,56	1,8	0,0614	13,8	1,12	13,9	0,1323	1,8	0,13		
ASM04.29.1	-2,8E-4	451	0,0632	2,0	0,166	12	0,390	1,4	--	73	44	8,4	1,48	0,618	1,43	803 ±20	802 ±11	808 ±14	846 ±562	+5	7,54	2,7	0,0673	27,0	1,23	27,2	0,1327	2,7	0,10		
ASM04.7.1	-8,5E-4	78	0,0650	5,0	0,159	23	0,336	3,9	--	169	114	19,3	3,68	0,699	0,37	804 ±13	793 ±10	814 ±17	1123 ±252	+30	7,53	1,7	0,0771	12,6	1,41	12,8	0,1328	1,7	0,13		
ASM04.45.1	-3,6E-5	1256	0,0697	3,3	0,082	12	0,354	2,9	--	163	81	18,6	1,57	0,512	0,31	805 ±11	801 ±9	833 ±10	933 ±199	+15	7,52	1,4	0,0702	9,7	1,29	9,8	0,1330	1,4	0,15		
ASM04.2.1	-3,4E-4	544	0,0665	2,4	0,154	9	0,353	1,4	--	61	30	7,0	1,17	0,509	0,63	806 ±31	800 ±18	801 ±20	966 ±751	+18	7,51	4,1	0,0713	36,8	1,31	37,0	0,1331	4,1	0,11		
ASM04.6.1	-4,8E-4	131	0,0585	4,9	0,143	31	0,353	2,4	--	159	137	18,2	2,94	0,888	0,72	806 ±14	807 ±12	852 ±22	789 ±302	-2	7,51	1,8	0,0654	14,4	1,20	14,5	0,1332	1,8	0,13		
ASM04.24.1	1,9E-4	245	0,0712	1,1	0,126	16	0,393	2,3	0,34	176	107	20,2	2,44	0,629	0,32	807 ±11	805 ±9	836 ±13	885 ±199	+9	7,50	1,4	0,0686	9,6	1,26	9,7	0,1334	1,4	0,15		
ASM04.43.1	-7,7E-4	142	0,0614	1,9	0,228	2	0,346	2,2	--	85	71	9,8	2,51	0,862	0,49	808 ±18	802 ±10	812 ±12	997 ±432	+20	7,49	2,4	0,0724	21,3	1,33	21,4	0,1335	2,4	0,11		
ASM04.44.1	-2,0E-3	71	0,0626	4,0	0,166	5	0,348	1,3	--	71	41	8,2	1,92	0,592	0,55	809 ±22	786 ±11	789 ±12	1425 ±403	+46	7,47	2,8	0,0900	21,1	1,66	21,3	0,1338	2,8	0,13		
ASM04.1.1	-1,4E-3	105	0,0649	2,1	0,160	14	0,350	2,1	--	72	53	8,3	1,74	0,759	0,50	810 ±22	820 ±15	797 ±11	1297 ±455	+40	7,47	2,9	0,0842	23,4	1,55	23,6	0,1339	2,9	0,12		
ASM04.21.1	-8,7E-4	178	0,0603	6,1	0,124	20	0,376	2,4	--	72	41	8,3	1,29	0,594	0,60	810 ±24	804 ±12	821 ±15	1006 ±617	+21	7,47	3,1	0,0727	30,4	1,34	30,6	0,1340	3,1	0,10		
ASM04.3.1	-4,2E-4	223	0,0561	6,8	0,167	23	0,336	2,8	--	126	90	14,5	2,67	0,739	0,44	813 ±16	817 ±11	831 ±19	681 ±482	-21	7,44	2,1	0,0622	22,6	1,15	22,7	0,1344	2,1	0,09		
ASM04.20.1	-7,4E-4	115	0,0565	1,9	0,112	21	0,367	2,4	--	106	52	12,3	1,72	0,501	0,44	815 ±15	814 ±10	821 ±14	840 ±375	+3	7,42	2,0	0,0671	18,0	1,25	18,1	0,1348	2,0	0,11		
ASM04.8.1	-3,5E-4	145	0,0608	1,4	0,087	32	0,370	0,5	--	202	185	23,4	2,36	0,945	0,34	816 ±12	816 ±10	895 ±16	801 ±231	-2	7,41	1,5	0,0658	11,0	1,22	11,1	0,1349	1,5	0,13		
ASM04.23.1	-1,4E-3	96	0,0623	2,1	0,178	2	0,346	2,1	--	84	48	9,8	2,24	0,594	0,54	819 ±21	804 ±11	801 ±12	1249 ±442	+37	7,38	2,7	0,0821	22,6	1,54	22,7	0,1355	2,7	0,12		
ASM04.25.1	-7,8E-4	108	0,0530	9,4	0,151	14	0,349	2,8	--	116	68	13,5	2,43	0,607	0,43	821 ±15	823 ±11	824 ±14	749 ±424	-10	7,36	2,0	0,0642	20,1	1,20	20,2	0,1358	2,0	0,10		
ASM04.36.1	6,4E-4	128	0,0740	1,3	0,170	9	0,372	2,2	1,17	128	68	14,1	2,06	0,598	0,43	825 ±18	827 ±15	840 ±16	765 ±385	-8	7,32	2,3	0,0647	16,1	1,22	16,4	0,1366	2,3	0,13		
ASM04.46.1	-3,7E-4	189	0,0685	1,4	0,137	16	0,388	1,3	--	126	109	14,8	2,24	0,895	0,40	826 ±14	819 ±10	878 ±14	1036 ±271	+22	7,31	1,8	0,0738	13,4	1,39	13,5	0,1368	1,8	0,13		
ASM04.11.1	-1,4E-3	124	0,0643	2,4	0,178	2	0,367	0,9	--	64	36	7,6	1,71	0,573	0,63	828 ±28	811 ±16	808 ±17	1285 ±547	+38	7,29	3,6	0,0837	28,1	1,58	28,3	0,1371	3,6	0,13	ASM04	
ASM04.16.1	-5,5E-4	120	0,0620	1,4	0,116	24	0,367	2,7	--	159	157	18,8	2,57	1,021	0,39	832 ±13	829 ±10	908 ±16	923 ±276	+11	7,26	1,7	0,0698	13,4	1,33	13,5	0,1377	1,7	0,13		
ASM04.17.1	-1,3E-3	58	0,0599	4,2	0,095	17	0,359	2,3	--	104	49	12,3	1,74	0,484	0,40	832 ±17	821 ±14	836 ±15	1140 ±267	+29	7,26	2,1	0,0777	13,4	1,48	13,6	0,1378	2,1	0,16	n=14	
ASM04.13.1	2,4E-3	82	0,0622	5,0	0,142	17	0,370	2,1	--	51	29	6,4	1,44	0,588	0,67	870 ±31	840 ±13	851 ±14	1535 ±516	+46	6,92	3,7	0,0954	27,6	1,90	27,7	0,1444	3,7	0,13	Concordia age 816.2 ±3.9 Ma	

Errors are 1-sigma; Pb_c and Pb^* indicate the common and radiogenic portions, respectively.

Error in Standard calibration was 0.37% (not included in above errors but required when comparing data from different mounts).

(1) Common Pb corrected using measured 204Pb.

(2) Common Pb corrected by assuming 206Pb/238U-207Pb/235U age-concordance

(3) Common Pb corrected by assuming 206Pb/238U-208Pb/232Th age-concordance

N=37	Spot	overct corr. 204Pb /206Pb	±%	207Pb /206Pb	±%	208Pb /206Pb	±%	206Pb /238U	±%	% 206Pb	ppm U	ppm Th	4-corr ppm 206Pb	4-corr ppm 208Pb	232Th /238U	±%	(1) 206Pb /238U Age	(2) 206Pb /238U Age	(3) 206Pb /238U Age	(1) 207Pb /206Pb Age	% Dis-cor-dant	(1) 238U /206Pb*	±%	(1) 207Pb* /206Pb*	±%	(1) 207Pb* /235U	±%	(1) 206Pb* /238U	±%	err corr		
	ASM06.5.1	1,9E-5	491	0,0686	0,9	0,405	1,9	0,418	1,7	0,03	218	211	23,3	9,5	1,00	1,38	755 ±11	751 ±11	716 ±13	878 ±45	+15	8,05	1,5	0,0683	2,2	1,170	2,6	0,1242	1,5	0,6		
	ASM06.42.1	2,7E-3	9	0,2000	6,8	0,477	8,0	0,367	2,2	4,96	141	67	15,6	6,6	0,49	0,63	754 ±17	660 ±20	665 ±25	2517 ±748	+74	8,05	2,4	0,1659	8,8	2,840	9,1	0,1241	2,4	0,3		
	ASM06.18.1	5,2E-4	25	0,0780	1,0	0,199	1,0	0,352	2,3	0,95	147	73	15,8	2,9	0,51	0,57	762 ±10	756 ±10	753 ±10	943 ±60	+20	7,97	1,3	0,0705	2,9	1,219	3,2	0,1254	1,3	0,4		
	ASM06.25.1	3,2E-3	14	0,1187	1,2	0,353	1,3	0,388	1,9	5,82	67	37	7,3	1,8	0,58	0,46	769 ±11	761 ±9	743 ±11	1022 ±187	+26	7,90	1,5	0,0733	9,3	1,280	9,4	0,1266	1,5	0,2		
	ASM06.27.1	1,8E-4	106	0,0665	1,5	0,375	1,1	0,415	2,0	0,33	81	76	8,9	3,3	0,97	0,45	778 ±9	779 ±9	748 ±11	740 ±96	-5	7,80	1,3	0,0640	4,6	1,131	4,7	0,1283	1,3	0,3		
	ASM06.39.1	3,2E-4	39	0,0860	1,9	0,234	1,0	0,415	1,5	0,58	106	50	11,7	2,6	0,49	0,32	782 ±8	767 ±8	754 ±9	1234 ±58	+39	7,75	1,1	0,0815	3,0	1,450	3,2	0,1290	1,1	0,4		
	ASM06.4.1	3,8E-4	59	0,0747	1,4	0,280	1,3	0,369	3,9	0,70	74	48	8,2	2,2	0,67	0,42	782 ±10	779 ±10	758 ±11	905 ±102	+14	7,75	1,3	0,0692	4,9	1,232	5,1	0,1290	1,3	0,3		
	ASM06.31.1	5,2E-5	152	0,0669	1,5	0,236	0,9	0,403	1,9	0,09	182	107	20,2	4,8	0,61	0,27	783 ±8	782 ±8	764 ±9	811 ±48	+4	7,75	1,1	0,0662	2,3	1,178	2,5	0,1291	1,1	0,4		
	ASM06.15.1	3,7E-4	37	0,0743	1,0	0,491	0,7	0,418	2,1	0,68	182	211	20,3	9,8	1,19	0,30	784 ±11	780 ±11	735 ±13	897 ±63	+13	7,73	1,5	0,0689	3,1	1,229	3,4	0,1293	1,5	0,4		
	ASM06.10.1	2,9E-4	93	0,0692	1,6	0,317	1,3	0,397	2,0	0,53	80	63	9,0	2,8	0,82	0,46	789 ±10	789 ±10	765 ±11	776 ±131	-2	7,68	1,3	0,0651	6,2	1,168	6,4	0,1302	1,3	0,2		
	ASM06.8.1	2,0E-4	68	0,0716	2,0	0,262	1,7	0,436	1,9	0,36	124	77	13,9	3,6	0,64	0,33	791 ±9	788 ±9	767 ±9	891 ±72	+12	7,66	1,1	0,0688	3,5	1,237	3,7	0,1305	1,1	0,3		
	ASM06.37.1	1,9E-4	50	0,0678	1,0	0,311	0,8	0,400	1,9	0,36	151	116	17,0	5,2	0,79	0,29	792 ±8	793 ±8	767 ±9	772 ±51	-3	7,65	1,1	0,0649	2,4	1,170	2,7	0,1307	1,1	0,4		
	ASM06.17.1	2,6E-3	8	0,1131	3,9	0,331	3,0	0,408	2,2	4,83	160	106	18,0	4,4	0,69	0,47	792 ±9	782 ±9	779 ±10	1083 ±147	+29	7,65	1,1	0,0756	7,3	1,361	7,4	0,1307	1,1	0,2		
	ASM06.1.1	-5,3E-5	369	0,0657	1,5	0,243	1,3	0,413	2,0	--	95	57	10,7	2,6	0,62	0,41	792 ±9	791 ±9	771 ±10	821 ±94	+4	7,65	1,2	0,0665	4,5	1,199	4,7	0,1308	1,2	0,3		
	ASM06.36.1	2,2E-4	47	0,0674	1,0	0,372	0,8	0,387	2,0	0,40	170	157	19,1	7,0	0,95	0,30	793 ±8	794 ±8	762 ±10	752 ±54	-6	7,64	1,1	0,0643	2,5	1,160	2,8	0,1308	1,1	0,4		
	ASM06.23.1	1,4E-5	449	0,0668	0,8	0,348	0,6	0,404	2,1	0,03	277	243	31,2	10,9	0,90	0,22	794 ±10	793 ±11	765 ±12	827 ±33	+4	7,63	1,4	0,0666	1,6	1,204	2,1	0,1310	1,4	0,7		
	ASM06.14.1	-1,3E-5	1025	0,0669	1,1	0,316	0,9	0,396	2,5	--	136	108	15,3	4,9	0,82	0,34	794 ±10	792 ±10	767 ±11	840 ±66	+6	7,63	1,3	0,0671	3,2	1,212	3,5	0,1310	1,3	0,4		
	ASM06.26.1	-2,7E-5	380	0,0656	1,0	0,250	0,9	0,397	1,1	--	156	96	17,6	4,5	0,64	0,29	794 ±8	794 ±8	773 ±9	806 ±52	+1	7,62	1,1	0,0660	2,5	1,193	2,7	0,1311	1,1	0,4		
	ASM06.2.1	3,0E-4	59	0,0680	1,3	0,293	1,1	0,395	0,6	0,55	114	81	12,8	3,7	0,74	0,39	794 ±9	796 ±9	772 ±10	731 ±91	-9	7,63	1,2	0,0637	4,3	1,151	4,4	0,1311	1,2	0,3		
	ASM06.33.1	-7,9E-6	933	0,0659	0,9	0,232	0,8	0,405	1,9	--	167	95	18,8	4,4	0,59	0,26	795 ±8	794 ±8	774 ±9	808 ±38	+2	7,62	1,1	0,0660	1,8	1,194	2,1	0,1312	1,1	0,5		
	ASM06.43.1	-2,6E-5	201	0,0668	0,8	0,436	0,6	0,378	2,2	--	262	292	29,6	13,0	1,15	0,23	795 ±8	793 ±8	758 ±10	844 ±31	+6	7,62	1,1	0,0672	1,5	1,216	1,8	0,1312	1,1	0,6		
	ASM06.30.1	4,8E-5	233	0,0674	1,1	0,316	0,9	0,409	1,4	0,09	126	97	14,2	4,5	0,80	0,31	795 ±8	794 ±9	766 ±10	830 ±55	+4	7,62	1,1	0,0667	2,6	1,208	2,9	0,1312	1,1	0,4		
	ASM06.13.1	-2,7E-4	52	0,0665	1,1	0,452	0,8	0,372	2,7	--	174	195	19,6	9,1	1,16	0,32	796 ±9	791 ±9	750 ±10	936 ±61	+16	7,61	1,1	0,0703	3,0	1,273	3,2	0,1314	1,1	0,4		
	ASM06.41.1	2,1E-4	52	0,0664	1,0	0,292	0,9	0,417	1,8	0,38	144	105	16,2	4,7	0,76	0,30	798 ±8	800 ±9	776 ±9	724 ±56	-11	7,59	1,1	0,0635	2,7	1,153	2,9	0,1318	1,1	0,4		
	ASM06.9.1	2,1E-4	44	0,0678	1,0	0,199	1,0	0,429	1,9	0,39	146	72	16,6	3,2	0,51	0,61	799 ±8	800 ±9	785 ±9	764 ±49	-5	7,58	1,1	0,0647	2,3	1,176	2,6	0,1319	1,1	0,4		
	ASM06.6.1	-1,7E-5	754	0,0688	1,3	0,230	1,2	0,409	2,4	--	99	56	11,2	2,6	0,57	0,38	799 ±9	796 ±9	777 ±10	900 ±59	+12	7,58	1,2	0,0690	2,9	1,256	3,1	0,1319	1,2	0,4		
	ASM06.12.1	1,0E-5	471	0,0666	0,6	0,223	1,1	0,423	1,9	0,02	347	195	39,4	8,9	0,58	0,33	800 ±8	800 ±8	783 ±9	819 ±25	+2	7,56	1,0	0,0664	1,2	1,210	1,6	0,1322	1,0	0,6		
	ASM06.11.1	3,8E-5	233	0,0665	2,0	0,316	0,8	0,401	3,0	0,07	194	155	22,1	7,0	0,83	0,28	803 ±8	803 ±9	778 ±9	805 ±58	+0	7,53	1,1	0,0659	2,8	1,207	3,0	0,1327	1,1	0,4		
	ASM06.44.1	2,8E-6	1333	0,0664	0,6	0,387	0,5	0,407	2,0	0,01	376	364	42,9	16,8	1,00	0,31	805 ±10	805 ±10	771 ±12	818 ±22	+2	7,52	1,3	0,0664	1,0	1,218	1,7	0,1330	1,3	0,8		
	ASM06.34.1	4,6E-4	48	0,0738	1,4	0,270	1,3	0,395	2,0	0,84	75	45	8,7	2,2	0,62	0,42	810 ±10	809 ±9	784 ±10	842 ±105	+4	7,47	1,3	0,0671	5,0	1,240	5,2	0,1339	1,3	0,2		
	ASM06.39.2	7,1E-4	28	0,0800	1,2	0,299	1,0	0,385	2,4	1,29	109	73	12,6	3,5	0,69	0,36	810 ±9	806 ±9	784 ±10	924 ±88	+13	7,47	1,2	0,0699	4,3	1,290	4,4	0,1339	1,2	0,3		
	ASM06.3.1	7,8E-4	19	0,0941	0,8	0,241	0,9	0,439	1,9	1,42	136	63	15,6	3,4	0,48	0,30	812 ±9	795 ±9	786 ±9	1273 ±52	+38	7,45	1,2	0,0832	2,7	1,540	2,9	0,1343	1,2	0,4		
	ASM06.40.1	2,6E-5	403	0,0673	1,0	0,298	0,9	0,382	2,3	0,05	171	128	19,7	5,9	0,77	0,29	813 ±9	812 ±9	788 ±10	835 ±52	+3	7,44	1,1	0,0669	2,5	1,240	2,8	0,1344	1,1	0,4		
	ASM06.7.1	1,6E-4	93	0,0726	1,2	0,284	1,0	0,429	2,2	0,30	106	71	12,2	3,4	0,70	0,41	815 ±9	811 ±9	788 ±10	936 ±68	+14	7,42	1,2	0,0703	3,3	1,305	3,5	0,1347	1,2	0,3		
	ASM06.32.1	-9,8E-5	65	0,0659	0,8	0,273	0,7	0,395	2,6	--	239	161	27,6	7,7	0,70	0,23	815 ±8	814 ±8	789 ±9	847 ±33	+4	7,42	1,1	0,0673	1,6	1,251	1,9	0,1348	1,1	0,6		
	ASM06.38.1	3,4E-4	51	0,0747	2,2	0,316	0,9	0,394	1,6	0,55	134	101	15,5	4,8	0,78	0,34	816 ±11	812 ±11	787 ±12	940 ±80	+14	7,41	1,4	0,0704	3,9	1,309	4,2	0,1349	1,4	0,3		
	ASM06.35.1	2,2E-3	9	0,1404	0,7	0,405	1,8	0,414	2,0	4,01	163	110	19,3	6,5	0,69	0,66	831 ±9	786 ±8	780 ±11	1811 ±49	+58	7,27	1,1	0,1107	2,7	2,100	2,8	0,1376	1,4	0,4	ASM06	

Errors are 1-sigma; Pb_c and Pb^* indicate the common and radiogenic portions, respectively. n=22

Error in Standard calibration was 0.26% (not included in above errors but required when comparing data from different mounts). Concordia age 799.9 ±2.9 Ma

(1) Common Pb corrected using measured 204Pb.

(2) Common Pb corrected by assuming 206Pb/238U-207Pb/235U age-concordance

(3) Common Pb corrected by assuming 206Pb/238U-208Pb/232Th age-concordance

N=46	Spot	overct corr. 204Pb /206Pb	±%	207Pb /206Pb	±%	208Pb /206Pb	±%	206Pb /238U	±%	% 206Pb	ppm U	ppm Th	4-corr ppm 206Pb	4-corr ppm 208Pb	232Th /238U	±%	(1) 206Pb /238U Age	(2) 206Pb /238U Age	(3) 206Pb /238U Age	(1) 207Pb /206Pb Age	% Dis-cor-dant	(1) 238U /206Pb*	±%	(1) 207Pb* /206Pb*	±%	(1) 207Pb* /235U	±%	(1) 206Pb* /238U	±%	err corr		
	ASM07.23.1	1,8E-4	73	0,06580	1,1	0,342	0,9	0,333	1,4	0,34	196	166	21,4	7,3	0,87	0,30	771 ±7	773 ±7	744 ±8	713 ±70	-9	7,870	1,0	0,0631	3,3	1,106	3,5	0,1271	1,0	0,29		
	ASM07.35.1	1,8E-4	70	0,06625	1,2	0,569	1,3	0,406	2,5	0,33	131	183	14,6	8,3	1,44	0,35	783 ±8	784 ±8	728 ±10	729 ±67	-8	7,746	1,0	0,0636	3,2	1,132	3,3	0,1291	1,0	0,31		
	ASM07.7.1	2,3E-4	88	0,06897	1,4	0,237	1,3	0,392	2,8	0,43	90	53	10,0	2,3	0,61	0,92	783 ±8	782 ±8	766 ±9	793 ±100	+1	7,746	1,1	0,0656	4,8	1,168	4,9	0,1291	1,1	0,23		
	ASM07.18.1	1,3E-4	162	0,06681	1,5	0,166	1,6	0,356	2,5	0,25	96	40	10,7	1,7	0,43	0,41	788 ±9	787 ±8	776 ±9	770 ±107	-2	7,708	1,2	0,0649	5,1	1,160	5,2	0,1297	1,2	0,22		
	ASM07.2.1	5,8E-5	445	0,06746	1,5	0,287	1,3	0,390	3,3	0,11	82	57	9,1	2,6	0,72	0,44	788 ±9	787 ±8	762 ±9	826 ±121	+5	7,691	1,2	0,0666	5,8	1,194	5,9	0,1300	1,2	0,20		
	ASM07.5.1	1,9E-4	86	0,06587	1,2	0,225	1,2	0,401	2,4	0,35	112	64	12,5	2,8	0,59	0,35	788 ±12	790 ±12	773 ±13	711 ±86	-12	7,691	1,6	0,0631	4,0	1,131	4,4	0,1300	1,6	0,38		
	ASM07.15.1	-8,0E-5	230	0,06707	1,3	0,381	1,0	0,409	2,0	--	113	104	12,7	4,9	0,95	0,39	794 ±13	792 ±13	756 ±15	875 ±85	+10	7,629	1,7	0,0682	4,1	1,233	4,5	0,1311	1,7	0,39		
	ASM07.26.1	4,2E-4	61	0,06497	2,8	0,268	1,4	0,435	2,4	0,78	69	45	7,7	2,0	0,68	0,48	795 ±13	801 ±13	776 ±14	559 ±156	+45	7,621	1,8	0,0588	7,2	1,064	7,4	0,1312	1,8	0,24		
	ASM07.12.1	3,2E-4	99	0,07188	1,9	0,288	1,6	0,383	3,1	0,58	67	49	7,6	2,1	0,75	0,52	796 ±10	794 ±9	777 ±10	847 ±148	+6	7,611	1,3	0,0673	7,1	1,219	7,2	0,1314	1,3	0,18		
	ASM07.29.1	4,8E-5	411	0,06604	1,4	0,313	1,1	0,431	2,6	0,09	100	79	11,3

ASM08.15.1	3,7E-4	78	0,0700	1,7	0,136	4,10	0,409	2,3	0,68	53	17	5,9	0,7	0,34	1,77	781 ±10	782 ±9	774 ±10	761 ±144	-3	7,76	1,3	0,0646	6,8	1,147	7,0	0,1288	1,3	0,2	
ASM08.48.1	-1,0E-4	118	0,0662	1,0	0,200	0,99	0,361	3,2	--	204	105	22,6	4,6	0,53	0,27	782 ±8	779 ±8	766 ±8	858 ±56	+9	7,76	1,0	0,0677	2,7	1,203	2,9	0,1289	1,0	0,4	
ASM08m.67.1	2,2E-3	8	0,0990	0,7	0,379	0,61	0,396	2,0	4,08	246	236	27,2	8,4	0,99	0,24	781 ±8	780 ±7	780 ±9	836 ±87	+7	7,76	1,0	0,0669	4,2	1,189	4,3	0,1289	1,0	0,2	
ASM08.39.1	1,8E-4	125	0,0692	1,4	0,466	0,96	0,394	2,5	0,32	107	125	11,9	5,5	1,21	0,66	782 ±9	781 ±9	743 ±11	828 ±104	+6	7,75	1,2	0,0667	5,0	1,186	5,1	0,1290	1,2	0,2	
ASM08.23.1	1,9E-4	60	0,0662	1,9	0,268	0,79	0,421	2,1	0,35	206	137	22,9	6,1	0,68	0,27	782 ±9	784 ±9	762 ±10	724 ±70	-9	7,75	1,3	0,0635	3,3	1,129	3,5	0,1290	1,3	0,4	
ASM08.12.1	4,3E-5	245	0,0667	0,9	0,359	0,69	0,430	2,6	0,08	272	242	30,1	10,9	0,92	0,27	783 ±9	783 ±9	752 ±11	808 ±51	+3	7,74	1,3	0,0660	2,5	1,177	2,8	0,1292	1,3	0,5	
ASM08.41.1	1,4E-4	80	0,0693	1,0	0,341	1,61	0,417	2,0	0,25	245	205	27,2	9,3	0,86	0,29	784 ±8	782 ±8	754 ±9	849 ±53	+8	7,74	1,0	0,0673	2,6	1,200	2,8	0,1292	1,0	0,4	
ASM08.42.1	-4,5E-5	584	0,0659	2,9	0,505	1,09	0,400	2,3	--	73	87	8,1	4,2	1,23	0,48	785 ±10	784 ±9	730 ±11	823 ±132	+5	7,72	1,3	0,0665	6,3	1,188	6,5	0,1296	1,3	0,2	
ASM08.13.1	3,2E-4	41	0,0658	1,1	0,328	0,87	0,403	1,9	0,58	187	152	20,8	6,7	0,84	0,53	786 ±8	790 ±8	762 ±9	648 ±71	-23	7,71	1,1	0,0613	3,3	1,095	3,5	0,1297	1,1	0,3	
ASM08.56.1	3,3E-4	47	0,0674	1,2	0,231	1,12	0,385	2,7	0,60	144	84	16,0	3,6	0,61	0,34	787 ±8	790 ±8	774 ±9	698 ±81	-13	7,70	1,1	0,0627	3,8	1,123	4,0	0,1298	1,1	0,3	
ASM08m.61.1	4,8E-5	183	0,0690	0,9	0,217	0,82	0,408	2,1	0,09	250	135	27,9	6,1	0,56	0,85	788 ±7	785 ±8	771 ±8	878 ±43	+11	7,69	1,0	0,0683	2,1	1,224	2,3	0,1300	1,0	0,4	
ASM08.52.1	1,0E-4	116	0,0665	1,0	0,269	0,86	0,382	3,9	0,19	220	144	24,7	6,6	0,67	0,28	790 ±10	791 ±10	767 ±11	775 ±59	-2	7,67	1,4	0,0650	2,8	1,169	3,1	0,1304	1,4	0,4	
ASM08m.63.1	1,2E-3	19	0,0936	1,0	0,250	2,97	0,321	3,1	2,14	142	67	15,9	3,4	0,49	0,32	790 ±8	779 ±8	767 ±9	1121 ±88	+31	7,67	1,1	0,0770	4,4	1,384	4,5	0,1304	1,1	0,2	
ASM08.38.1	8,2E-4	27	0,0774	1,2	0,288	2,60	0,357	2,3	1,50	166	116	18,6	4,9	0,72	0,36	791 ±9	791 ±9	775 ±10	791 ±108	-0	7,66	1,2	0,0655	5,2	1,179	5,3	0,1306	1,2	0,2	
ASM08.31.1	1,6E-4	82	0,0663	1,1	0,173	1,13	0,400	3,0	0,29	139	59	15,6	2,6	0,44	0,31	791 ±8	793 ±8	779 ±8	742 ±66	-7	7,66	1,1	0,0640	3,1	1,153	3,3	0,1306	1,1	0,3	
ASM08.54.1	2,6E-4	46	0,0680	1,0	0,159	1,15	0,392	1,8	0,48	174	66	19,5	3,0	0,39	0,30	791 ±8	793 ±8	780 ±8	748 ±62	-6	7,66	1,0	0,0642	2,9	1,156	3,1	0,1306	1,0	0,3	
ASM08.49.1	5,6E-5	127	0,0663	0,7	0,247	0,66	0,427	2,8	0,10	287	177	32,2	8,0	0,64	0,22	791 ±7	791 ±7	772 ±8	790 ±37	-0	7,66	1,0	0,0655	1,7	1,180	2,0	0,1306	1,0	0,5	
ASM08.50.1	--	11243	0,0661	0,8	0,369	0,63	0,435	2,6	0,00	308	285	34,7	12,9	0,95	0,25	793 ±7	792 ±8	781 ±9	810 ±40	+2	7,64	1,0	0,0661	1,9	1,193	2,1	0,1309	1,0	0,5	
ASM08.36.1	6,1E-5	327	0,0676	1,3	0,323	1,05	0,426	2,0	0,11	131	109	14,7	4,8	0,86	0,39	793 ±13	792 ±13	769 ±14	829 ±93	+5	7,64	1,7	0,0667	4,5	1,204	4,8	0,1309	1,7	0,4	
ASM08.32.1	5,5E-5	223	0,0684	1,0	0,422	0,72	0,407	2,9	0,10	225	236	25,4	10,8	1,08	0,30	794 ±8	792 ±8	756 ±9	858 ±58	+8	7,63	1,0	0,0676	2,8	1,222	3,0	0,1311	1,0	0,4	
ASM08.16.1	-3,1E-5	639	0,0667	2,3	0,198	1,39	0,372	2,0	--	115	56	13,0	2,6	0,50	0,39	795 ±9	793 ±9	777 ±9	843 ±101	+6	7,62	1,2	0,0672	4,9	1,215	5,0	0,1312	1,2	0,2	
ASM08.14.1	9,4E-5	53	0,0672	0,6	0,296	1,88	0,441	2,2	0,17	479	349	54,0	16,0	0,75	1,71	796 ±9	796 ±10	771 ±11	803 ±26	+1	7,61	1,3	0,0659	1,3	1,194	1,8	0,1314	1,3	0,7	
ASM08.28.1	-4,3E-5	269	0,0660	1,1	0,185	1,17	0,415	2,0	--	115	53	13,0	2,6	0,48	0,33	796 ±8	795 ±8	781 ±9	826 ±57	+4	7,61	1,1	0,0666	2,7	1,208	2,9	0,1315	1,1	0,4	
ASM08m.66.1	5,9E-4	15	0,0770	0,6	0,240	0,64	0,419	1,8	1,09	317	171	35,8	7,9	0,56	0,23	796 ±7	794 ±7	777 ±8	881 ±41	+10	7,61	1,0	0,0684	2,0	1,240	2,2	0,1315	1,0	0,4	
ASM08.33.1	1,0E-6	11775	0,0670	1,0	0,300	0,84	0,400	2,0	0,00	223	167	25,2	7,6	0,77	0,74	797 ±8	796 ±8	771 ±9	837 ±58	+5	7,60	1,0	0,0670	2,8	1,216	3,0	0,1316	1,0	0,4	
ASM08.58.1	5,4E-4	40	0,0763	1,1	0,319	0,99	0,409	2,4	0,99	141	105	16,0	4,9	0,77	0,98	797 ±9	794 ±8	771 ±9	885 ±98	+11	7,60	1,1	0,0685	4,7	1,244	4,9	0,1316	1,1	0,2	
ASM08.59.1	--	12773	0,0667	0,9	0,307	0,73	0,388	2,2	0,00	285	216	32,3	10,0	0,78	0,82	798 ±8	797 ±8	771 ±9	828 ±49	+4	7,59	1,0	0,0667	2,3	1,212	2,5	0,1318	1,0	0,4	
ASM08.57.1	9,3E-5	109	0,0669	1,7	0,185	1,07	0,410	2,3	0,17	146	67	16,5	3,0	0,47	0,30	799 ±8	799 ±8	791 ±9	826 ±57	-1	7,58	1,0	0,0655	2,8	1,192	3,0	0,1319	1,0	0,3	
ASM08m.62.1	3,4E-4	54	0,0669	1,3	0,276	3,72	0,416	2,7	0,62	122	86	13,9	3,7	0,72	0,40	799 ±12	803 ±12	782 ±13	675 ±97	-20	7,58	1,5	0,0620	4,5	1,129	4,8	0,1320	1,5	0,3	
ASM08.7.1	8,3E-5	122	0,0664	1,0	0,331	0,77	0,404	3,0	0,15	203	166	23,0	7,6	0,84	0,28	801 ±8	802 ±8	772 ±9	780 ±51	-3	7,56	1,0	0,0652	2,4	1,189	2,7	0,1323	1,0	0,4	
ASM08.19.1	5,5E-5	137	0,0665	0,8	0,283	0,67	0,433	3,0	0,10	299	211	34,0	9,7	0,73	0,79	801 ±9	801 ±9	778 ±10	798 ±39	-0	7,56	1,2	0,0657	1,8	1,199	2,2	0,1323	1,2	0,6	
ASM08.43.1	6,7E-5	190	0,0693	1,0	0,208	0,96	0,432	2,3	0,12	164	82	18,7	3,9	0,52	0,29	802 ±11	799 ±11	783 ±12	878 ±59	+9	7,55	1,4	0,0683	2,9	1,247	3,2	0,1325	1,4	0,4	
ASM08.22.1	2,6E-4	70	0,0674	1,4	0,152	1,64	0,378	2,9	0,47	74	28	8,5	1,2	0,39	1,08	802 ±13	804 ±13	794 ±13	733 ±92	-10	7,55	1,7	0,0637	4,4	1,164	4,7	0,1325	1,7	0,7	
ASM08.29.1	2,3E-4	51	0,0680	1,0	0,187	1,04	0,394	2,3	0,43	155	71	17,6	3,2	0,47	0,29	802 ±10	804 ±10	789 ±10	761 ±61	-6	7,54	1,3	0,0646	2,9	1,181	3,2	0,1326	1,3	0,4	
ASM08.47.1	1,4E-4	62	0,0665	0,9	0,247	0,81	0,419	1,7	0,26	226	136	25,7	6,3	0,62	0,26	803 ±8	804 ±8	782 ±8	756 ±46	-7	7,54	1,0	0,0644	2,2	1,178	2,4	0,1326	1,0	0,4	
ASM08.46.1	-4,1E-5	656	0,0670	1,6	0,430	1,12	0,396	3,0	--	99	106	11,3	4,9	1,11	0,46	805 ±13	803 ±12	765 ±15	857 ±124	+7	7,52	1,7	0,0676	6,0	1,240	6,2	0,1330	1,7	0,3	
ASM08.24.1	4,3E-5	208	0,0664	0,9	0,196	1,01	0,397	2,2	0,08	223	106	25,4	5,0	0,49	0,78	805 ±8	805 ±8	788 ±8	800 ±45	-1	7,52	1,0	0,0658	2,2	1,207	2,4	0,1330	1,0	0,4	
ASM08.26.1	2,2E-4	54	0,0670	2,1	0,207	2,35	0,406	2,7	0,41	137	68	15,7	3,2	0,51	0,33	805 ±13	807 ±13	789 ±14	734 ±74	-10	7,52	1,7	0,0638	3,5	1,170	3,9	0,1330	1,7	0,4	
ASM08.30.1	-6,2E-5	171	0,0663	0,9	0,209	0,93	0,406	2,7	--	167	86	19,1	4,1	0,53	0,45	806 ±8	804 ±8	787 ±8	844 ±51	+5	7,51	1,0	0,0672	2,4	1,233	2,6	0,1331	1,0	0,4	
ASM08.55.1	2,5E-4	81	0,0682	1,4	0,162	1,58	0,402	2,1	0,46	78	31	9,0	1,4	0,41	0,78	806 ±9	808 ±9	796 ±9	761 ±101	-6	7,50	1,2	0,0646	4,8	1,187	5,0	0,1333	1,2	0,2	
ASM08.11.1	2,4E-5	554	0,0655	1,2	0,165	1,26	0,392	1,2	0,04	120	48	13,8	2,3	0,41	0,33	807 ±8	808 ±8	793 ±9	778 ±67	-4	7,49	1,1	0,0651	3,2	1,198	3,4	0,1334	1,1	0,3	
ASM08.9.1	--	9469	0,0661	1,0	0,194	1,00	0,411	1,9	0,00	152	74	17,5	3,4	0,50	0,29	809 ±8	809 ±8	793 ±8	808 ±47	-0	7,48	1,0	0,0661	2,2	1,218	2,5	0,1337	1,0	0,4	
ASM08.3.1	2,8E-5	600	0,0658	1,2	0,168	1,33	0,327	1,9	0,05	134	56	15,4	2,6	0,43	0,33	811 ±8	811 ±8	797 ±9	787 ±81	-3	7,46	1,1	0,0654	3,8	1,208	4,0	0,1340	1,1	0,3	
ASM08.8.1	2,5E-3	8	0,1155	11,5	0,434	6,73	0,428	1,1	4,55	287	224	33,0	11,8	0,80	0,46	810 ±16	796 ±21	765 ±23	1205 ±347	+35	7,47	2,1	0,0803	17,6	1,483	17,7	0,1339	2,1	0,1	
ASM08.35.1	1,2E-5	585	0,0664	0,8	0,257	0,73	0,416	2,3	0,02	262	165	30,2	7,8	0,65	0,42	812 ±8	812 ±8	789 ±8	813 ±37	+0	7,45	1,0	0,0662	1,8	1,226	2,0	0,1342	1,0	0,5	
ASM08.53.1	-2,8E-5	314	0,0666	0,9	0,166	0,99	0,421	1,5	--	187	78	21,5	3,6	0,43	0,27	813 ±9	812 ±9	799 ±9	839 ±43	+3	7,44	1,2	0,0670	2,1	1,242	2,4	0,1343	1,2	0,5	
ASM08.44.1	3,0E-5	245	0,0668	1,3	0,258	0,66	0,394	2,8	0,05	342	236	39,5	10,3	0,71	0,21	813 ±10	813 ±10	797 ±11	818 ±42	+1	7,44	1,3	0,0664	2,0	1,229	2,4	0,1344	1,3	0,5	
ASM08.21.1	1,5E-6	10095	0,0661	1,2	0,196	1,24	0,396	2,1	0,00	125	61	14,5	2,9	0,50	0,35	816 ±11	816 ±11	799 ±11	808 ±73	-1	7,42	1,4	0,0660	3,5	1,228	3,8	0,1349	1,4	0,4	
ASM08.8.2	-1,6E-5	639	0,0650	1,0	0,225	0,93	0,404	2,5	--	184	103	21,4	4,9	0,58	0,29	817 ±8	818 ±8	797 ±9	782 ±52	-5	7,40	1,0	0,0652	2,5	1,215	2,7	0,1351	1,0	0,4	ASM08
ASM08.40.1	1,2E-4	98	0,0684	1,0	0,281	0,90	0,416	1,6	0,22	167	114	19,4	5,4	0,70	0,31	820 ±8	820 ±8	794 ±9	828 ±57	+1	7,37	1,1	0,0667	2,7	1,247	2,9	0,1356	1,1	0,4	

Errors are 1-sigma; Pb$_c$ and Pb* indicate the common and radiogenic portions, respectively.

Error in Standard calibration was 0,24% (not included in above errors but required when comparing data from different mounts).

(1) Common Pb corrected using measured 204Pb.

(2) Common Pb corrected by assuming 206Pb/238U-207Pb/235U age-concordance

(3) Common Pb corrected by assuming 206Pb/238U-208Pb/232Th age-concordance

n=43

Concordia age 799.9 ±2.4 Ma

n=60

Spot	overcl corr. 204Pb /206Pb	±%	207Pb /206Pb	±%	208Pb /206Pb	±%	206Pb /238U	±%	% 206Pb$_c$	ppm U	ppm Th	4-corr ppm 206Pb	4-corr ppm 208Pb	232Th /238U	±%	(1) 206Pb /238U Age	(2) 206Pb /238U Age	(3) 206Pb /238U Age	(1) 207Pb /206Pb Age	% Dis-cor-dant	(1) 238U /206Pb*	±%	(1) 207Pb* /206Pb*	±%	(1) 207Pb* /235U	±%	(1) 206Pb* /238U	±%	err corr
552.20.2	1,1E-3	21	0,07959	1,3	0,433	0,8	1,83	2,1	1,81	166	68	15,5	4,0	0,54	0,38	793 ±19	758 ±19	713 ±22	735 ±108	-3	8,020	2,6	0,0638	5,1	1,097	5,8	0,1247	2,6	0,45
552.14.1	1,0E-3	28	0,10744	3,3	0,432	2,8	1,84	2,2	1,80	118	83	3,57	1,54	1,11	776 ±18	749 ±18	807 ±24	1497 ±109	+51	7,814	2,4	0,0935	5,8	1,649	6,2	0,1280	2,4	0,39	
552.22.1	3,3E-4	66	0,06919	1,6	0,198	1,6	0,401	4,4	0,61	56	26	6,3	1,18	0,47	0,47	785 ±18	786 ±18	769 ±19	755 ±110	-4	7,721	2,4	0,0644	5,2	1,150	5,7	0,1295	2,4	0,42
552.15.1	2,9E-4	57	0,06709	1,4	0,289	1,2	0,441	2,6	0,54	70	52	7,8	2,21	0,77	0,43	792 ±18	795 ±18	774 ±20	703 ±88	-13	7,650	2,4	0,0629	4,1	1,133	4,8	0,1307	2,4	0,50
552.52.1	5,1E-4	98	0,06944	1,9	0,238	1,7	0,390	2,9	0,94	91	79	9,3	1,83	0,58	0,56	799 ±19	804 ±19	783 ±20	839 ±165	-27	7,579	2,5	0,0610	7,1	1,109	8,3	0,1319	2,5	0,31
552.48.1	2,5E-4	54	0,06908	1,2	0,431	0,9	0,400	1,9	0,47	99	106	11,3	4,83	1,10	0,36	800 ±21	768 ±17	753 ±19	609 ±1028	-27	7,95	4,2	0,060	47,5	1,04	47,7	0,1258	4,2	0,09
552.9.1	2,3E-4	90	0,06776	1,4	0,293	1,2	0,394	2,4	0,42	85	63	9,7	2,80	0,76	0,42	800 ±19	801 ±20	778 ±22	757 ±103	-6	7,568	2,6	0,0645	4,9	1,174	5,5	0,1321	2,6	0,46
552.53.1	1,8E-4	110	0,06840	1,5	0,219	1,5	0,442	2,0	0,33	58	31	6,6	1,42	0,55	0,47	800 ±20	800 ±20	783 ±22	800 ±98	-0	7,566	2,6	0,0658	4,7	1,199	5,4	0,1322	2,6	0,49
552.6.1	3,5E-4	38	0,06894	1,3	0,372	2,1	0,412	2,7	0,64	83	77	9,5	3,44	0,95	0,39	802 ±18	804 ±18	773 ±21	738 ±72	-9	7,548	2,4	0,0639	3,4	1,167	4,1	0,1325	2,4	0,57
552.3.1	2,7E-4	59	0,06721	1,4	0,255	1,2	0,414	2,0	0,50	80	51	9,1	2,25	0,66	0,40	802 ±18	805 ±18	785 ±20	718 ±84	-12	7,547	2,4	0,0633	3,9	1,156	4,6	0,1325	2,4	0,52
552.44.1	3,5E-4	63	0,06932	1,6	0,314	1,4	0,374	2,5	0,65	62	48	7,1	2,17	0,79	0,47	802 ±18	804 ±19	778 ±21	804 ±119	-8	7,546	2,4	0,0641	5,3	1,172	5,9	0,1325	2,4	0,42
552.16.1	2,3E-4	75	0,06773	1,4	0,290	1,2	0,426	2,1	0,42	76	54	8,7	2,46	0,74	0,43	804 ±18	805 ±19	781 ±20	756 ±87	-7	7,531	2,4	0,0644	4,1	1,180	4,8	0,1328	2,4	0,50
552.4.1	2,7E-4	56	0,06747	1,3	0,322	1,0	0,389	2,4	0,49	95	76	10,9	3,44	0,83	0,37	805 ±18	807 ±18	780 ±21	727 ±79	-11	7,523	2,4	0,0636	3,7	1,165	4,4	0,1329	2,4	0,54
552.37.2	5,6E-4	39	0,06895	1,3	0,255	1,3	0,356	3,3	1,03	79	47	8,3	2,01	0,65	0,41	805 ±18	810 ±19	790 ±20	633 ±114	-29	7,523	2,4	0,0608	5,3	1,115	5,9	0,1329	2,4	0,41
552.14.2	1,2E-4	104	0,06843	1,4	0,284	1,1	0,436	1,7	0,22	94	66	10,7	3,03	0,72	0,39	805 ±18	804 ±18	781 ±20	828 ±65	+3	7,521	2,4	0,0667	3,1	1,222	3,9	0,1330	2,4	0,61
552.25.1	4,2E-4	43	0,06640	1,4	0,251	1,3	0,407	2,4	0,77	84	53	9,6	2,31	0,65	0,41	807 ±18	813 ±19	792 ±20	615 ±100	-33	7,495	2,4	0,0603	4,6	1,109	5,2	0,1334	2,4	0,46
552.2.1	1,5E-4	87	0,06749	1,3	0,302	1,8	0,429	2,3	0,27	87	67	10,0	3,00	0,79	0,38	809 ±19	809 ±20	786 ±22	785 ±66	-3	7,482	2,5	0,0653	3,2	1,204	4,1	0,1337	2,5	0,63
552.46.1	4,7E-4	90	0,06883	2,1	0,198	2,1	0,393	1,7	0,86	37	18	4,3	0,77	0,51	0,59	809 ±20	813 ±20	799 ±21	675 ±219	-21	7,477	2,6	0,0620	10,2	1,144	10,6	0,1338	2,6	0,25
552.40.1	2,9E-4	74	0,06779	2,4	0,349	1,1	0,419	2,9	0,53	72	62	8,3	2,85	0,89	0,42	811 ±19	813 ±19	782 ±21	727 ±119	-12	7,461	2,4	0,0636	5,6	1,175	6,1	0,1340	2,4	0,40
552.23.1	-6,6E-5	267	0,06665	1,5	0,270	1,3	0,418	2,1	--	82	54	9,5	2,60	0,68	0,96	811 ±19	810 ±19	785 ±21	856 ±84	+6	7,455	2,4	0,0676	4,0	1,250	4,7	0,1341	2,4	0,52
552.5.1	2,1E-4	66	0,06790	1,3	0,315	1,1	0,410	3,2	0,38	90	71	10,4	3,23	0,81	0,38	811 ±18	813 ±19	786 ±21	771 ±70	-6	7,456	2,4	0,0649	3,3	1,200	4,1	0,1341	2,4	0,58
552.43.1	-1,4E-5	611	0,06594	1,1	0,188	0,8	0,382	2,5	--	151	148	17,5	4,85	1,01	0,30	812 ±19	812 ±19	778 ±22	811 ±46	-0	7,451	2,5	0,0662	2,2	1,224	3,3	0,1342	2,5	0,75
552.29.1	9,3E-5	140	0,06549	1,3	0,333	1,0	0,407	2,1	0,17	96	78	11,1	3,71	0,84	0,37	812 ±18	814 ±19	782 ±21	746 ±68	-9	7,448	2,4	0,0641	3,2	1,187	4,0	0,1343	2,4	0,59
552.45.1	2,8E-4	58	0,06905	1,3	0,360	1,0	0,420	1,5	0,51	89	80	10,3	3,66	0,92	0,39	812 ±18	813 ±19	783 ±21	774 ±82	-5	7,448	2,4	0,0650	3,9	1,203	4,6	0,1343	2,4	0,52
552.54.1	1,5E-4	93	0,06851	1,4	0,354	1,1	0,406	2,2	0,27	85	74	9,8	3,47	0,90	0,41	812 ±18	812 ±19	781 ±21	819 ±68	+1	7,445	2,4	0,0664	3,3	1,230	4,0	0,1343	2,4	0,59
552.26.1	3,3E-4	60	0,06742	1,6	0,263	1,4	0,397	2,1	0,61	65	42	7,5	1,91	0,67	0,47	812 ±19	816 ±19	793 ±21	694 ±106	-18	7,446	2,4	0,0626	5,0	1,159	5,5	0,1343	2,4	0,44
552.44.2	4,4E-4	34	0,07012	1,6	0,390	1,6	0,331	2,6	0,73	114	104	9,6	5,16	0,96	0,54	814 ±18	819 ±18	779 ±21	934 ±64	+14	7,429	2,4	0,0702	3,1	1,304	3,9	0,1347	2,4	0,60
552.12.1	1,9E-4	132	0,07163	1,6	0,310	1,3	0,395	2,8	0,35	70	54	8,1	2,50	0,79	0,46	815 ±19	812 ±19	789 ±21	896 ±113	+10	7,424	2,4	0,0689	5,5	1,280	6,0	0,1347	2,4	0,41
552.49.1	1,7E-4	91	0,06739	1,4	0,354	1,0	0,406	1,5	0,31	88	75	10,1	3,57	0,89	0,40	816 ±18	817 ±19	783 ±21	772 ±79	-6	7,415	2,4	0,0649	3,7	1,207	4,4	0,1349	2,4	0,54
552.11.1	1,3E-4	140	0,06756	1,5	0,280	1,3	0,413	3,1	0,23	76	53	8,9	2,47	0,71	0,44	816 ±18	816 ±19	792 ±21	799 ±87	-2	7,413	2,4	0,0658	4,1	1,223	4,8	0,1349	2,4	0,50
552.34.1	1,9E-4	106	0,06713	1,4	0,298	1,2

551.29.1	-1,3E-3	101	0,0656	2,2	0,255	1,8	0,348	4,1	--	111	77	14,4	4,3	0,72	3,54	908 ±47		891 ±44		872 ±47		1286 ±420		+32	6,61	5,6	0,084	21,6	1,75	22,3	0,1512	5,6	0,25	

Errors are 1-sigma; Pb$_c$ and Pb* indicate the common and radiogenic portions, respectively.
Error in Standard calibration was 0.53% (not included in above errors but required when comparing data from different mounts).
(1) Common Pb corrected using measured 204Pb.
(2) Common Pb corrected by assuming 206Pb/238U-207Pb/235U age-concordance
(3) Common Pb corrected by assuming 206Pb/238U-208Pb/232Th age-concordance

n=19
Concordia age 787.4 ±9.4Ma

N=15

Spot	overct corr. 204Pb /206Pb	±%	207Pb /206Pb	±%	208Pb /206Pb	±%	206Pb /238U	±%	% 206Pb$_c$	ppm U	ppm Th	4-corr ppm 206Pb	4-corr ppm 208Pb	232Th /238U	±%	(1) 206Pb /238U Age	(2) 206Pb /238U Age	(3) 206Pb /238U Age	(1) 207Pb /206Pb Age	Dis-cor-dant	(1) 238U /206Pb*	±%	(1) 207Pb* /206Pb*	±%	(1) 207Pb* /235U	±%	(1) 206Pb* /238U	±%	err corr	
270.5.2	1,3E-3	107	0,0677	3,0	0,274	2,5	0,291	3,1	0,71	98	94	7,0	1,9	0,69	0,53	743 ±23		746 ±23		728 ±117		928 ±160		+23	8,19	1,5	0,0616	6,1	1,028	6,8	0,1210	1,9	0,1	
270.5.1	3,9E-4	112	0,0765	4,8	0,278	2,9	0,295	2,2	0,71	98	94	7,0	1,9	0,69	0,53	748 ±11		742 ±10		728 ±11		955 ±206		+23	8,12	1,5	0,0709	10,1	1,204	10,7	0,1231	1,9	0,1	
270.4.1	2,0E-4	93	0,0664	1,3	0,354	1,0	0,403	2,4	0,36	99	88	10,5	3,7	0,92	0,38	750 ±9		751 ±9		724 ±10		728 ±93		-3	8,10	1,2	0,0636	4,4	1,082	4,5	0,1234	1,2	0,3	
270.3.1	-2,9E-5	297	0,0658	1,0	0,196	1,0	0,324	0,4	--	205	99	22,4	4,5	0,50	0,27	769 ±8		768 ±8		752 ±9		814 ±45		+6	7,89	1,1	0,0662	2,1	1,157	2,4	0,1267	1,1	0,5	
270.5.2	-8,4E-5	113	0,0661	0,9	0,456	0,6	0,341	2,8	--	257	291	28,1	13,0	1,17	0,25	770 ±8		768 ±8		728 ±10		847 ±46		+10	7,88	1,1	0,0673	2,2	1,178	2,5	0,1269	1,1	0,4	
270.11.1	2,2E-4	62	0,0675	1,3	0,217	3,2	0,324	3,0	0,53	160	86	17,5	3,7	0,55	0,34	773 ±9		775 ±9		759 ±9		719 ±93		-8	7,84	1,2	0,0633	4,4	1,113	4,5	0,1275	1,2	0,3	
270.9.1	2,4E-4	57	0,0653	1,1	0,317	1,7	0,394	2,2	0,44	158	125	17,4	5,4	0,82	0,32	781 ±8		784 ±8		758 ±10		667 ±74		-18	7,77	1,1	0,0618	3,5	1,097	3,7	0,1288	1,1	0,3	
270.8.1	6,9E-6	1453	0,0672	1,0	0,310	0,8	0,362	2,4	0,01	209	165	23,1	7,2	0,81	0,27	781 ±8		780 ±8		757 ±9		842 ±49		+8	7,76	1,1	0,0672	2,4	1,193	2,6	0,1289	1,1	0,4	
270.7.1	2,6E-4	80	0,0675	1,4	0,299	1,2	0,340	2,9	0,47	122	89	13,5	4,0	0,75	0,38	783 ±9		785 ±9		759 ±10		732 ±105		-7	7,74	1,2	0,0637	4,9	1,134	5,1	0,1292	1,2	0,2	
270.6.2	3,4E-4	78	0,0716	5,5	0,167	2,3	0,382	1,9	0,62	43	16	4,8	0,8	0,38	0,60	787 ±11		786 ±11		773 ±11		828 ±174		+5	7,70	1,5	0,0667	8,3	1,194	8,4	0,1299	1,5	0,2	
270.6.1	3,4E-4	34	0,0771	1,0	0,160	1,2	0,375	1,6	0,62	134	44	15,0	2,2	0,34	0,31	790 ±8		783 ±8		773 ±9		992 ±52		+22	7,67	1,1	0,0722	2,6	1,298	2,8	0,1303	1,1	0,4	
270.2.1	6,1E-4	64	0,0682	1,8	0,938	1,6	0,317	2,2	1,11	76	165	7,9	7,4	2,42	0,48	791 ±11		797 ±10		690 ±18		583 ±212		-38	7,66	1,4	0,0594	9,8	1,070	9,9	0,1305	1,4	0,1	
270.1.2	4,3E-4	120	0,0687	2,7	0,337	2,1	0,375	1,6	0,79	27	23	3,0	1,0	0,87	0,76	792 ±27		795 ±27		769 ±30		689 ±267		-16	7,65	3,6	0,0624	12,5	1,126	13,0	0,1308	3,6	0,3	
270.1.1	-4,1E-4	131	0,0721	2,5	0,455	1,8	0,346	2,4	--	30	34	3,5	1,6	1,16	0,70	804 ±14		793 ±12		755 ±15		1144 ±198		+32	7,52	1,8	0,0779	10,0	1,427	10,1	0,1329	1,8	0,2	270
270.10.1	1,2E-4	202	0,0688	1,7	0,193	3,6	0,340	1,7	0,22	77	38	8,8	1,7	0,51	0,46	808 ±10		807 ±10		795 ±11		838 ±116		+4	7,49	1,3	0,0670	5,6	1,234	5,7	0,1335	1,3	0,2	

Errors are 1-sigma; Pb$_c$ and Pb* indicate the common and radiogenic portions, respectively.
Error in Standard calibration was 0.26% (not included in above errors but required when comparing data from different mounts).
(1) Common Pb corrected using measured 204Pb.
(2) Common Pb corrected by assuming 206Pb/238U-207Pb/235U age-concordance
(3) Common Pb corrected by assuming 206Pb/238U-208Pb/232Th age-concordance

n=12
Concordia age 784.1 ±6.9 Ma

n=28

Spot	overct corr. 204Pb /206Pb	±%	207Pb /206Pb	±%	208Pb /206Pb	±%	206Pb /238U	±%	% 206Pb$_c$	ppm U	ppm Th	4-corr ppm 206Pb	4-corr ppm 208Pb	232Th /238U	±%	(1) 206Pb /238U Age	(2) 206Pb /238U Age	(3) 206Pb /238U Age	(1) 207Pb /206Pb Age	Dis-cor-dant	(1) 238U /206Pb*	±%	(1) 207Pb* /206Pb*	±%	(1) 207Pb* /235U	±%	(1) 206Pb* /238U	±%	err corr	
048.1.1	5,3E-4	42	0,0698	1,3	0,26	1,1	0,352	3,2	0,98	126	104	10,4	4,1	0,70	0,38	729 ±11		730 ±11		719 ±12		677 ±118		-8	8,35	1,6	0,0621	5,1	1,03	5,7	0,1197	1,6	0,3	
048.41.1	5,4E-5	688	0,0681	1,7	0,25	1,1	0,290	2,3	0,16	151	96	15,5	7,9	0,66	0,82	733 ±10		730 ±9		717 ±10		847 ±168		+14	8,30	1,5	0,0673	9,1	1,12	9,2	0,1205	1,4	0,2	
048.20.1	4,3E-4	93	0,0652	1,5	0,15	2,1	0,322	3,4	0,79	58	58	7,0	2,1	0,38	1,22	743 ±11		747 ±10		738 ±10		564 ±202		-33	8,19	1,5	0,0589	9,0	0,99	9,1	0,1221	1,4	0,2	
048.8.1	7,1E-3	6	0,1748	5,0	0,55	2,9	0,372	2,9	12,94	234	197	24,6	8,3	0,87	0,34	742 ±10		733 ±13		720 ±14		1037 ±326		+30	8,19	1,5	0,0738	16,1	1,24	16,2	0,1221	1,5	0,1	
048.26.1	3,1E-4	61	0,0663	1,3	0,21	1,3	0,327	2,8	0,56	184	100	19,3	3,9	0,56	0,34	746 ±9		748 ±9		736 ±10		668 ±100		-12	8,15	1,3	0,0618	4,6	1,05	4,8	0,1227	1,3	0,3	
048.40.2	4,7E-5	688	0,0696	2,7	0,17	3,2	0,310	3,0	0,09	130	54	13,7	2,3	0,43	0,41	748 ±10		744 ±10		736 ±10		896 ±149		+17	8,12	1,4	0,0689	7,2	1,17	7,4	0,1231	1,4	0,2	
048.6.1	5,1E-4	76	0,0667	1,7	0,20	3,3	0,368	2,2	0,94	90	42	9,5	1,7	0,48	0,48	753 ±11		757 ±10		742 ±11		576 ±215		-32	8,07	1,5	0,0592	9,9	1,01	10,0	0,1238	1,5	0,2	
048.39.1	2,6E-4	106	0,0654	1,5	0,23	1,3	0,313	2,7	0,47	162	95	17,2	3,9	0,61	0,38	753 ±12		755 ±11		739 ±12		663 ±141		-14	8,07	1,6	0,0617	6,6	1,05	6,8	0,1239	1,6	0,2	
048.23.1	1,4E-4	152	0,0643	1,3	0,20	1,3	0,345	2,6	0,26	173	92	18,5	3,7	0,55	0,36	758 ±10		760 ±9		747 ±10		681 ±112		-12	8,01	1,3	0,0622	5,3	1,07	5,4	0,1248	1,3	0,2	
048.2.1	3,8E-3	13	0,1317	1,3	0,36	1,4	0,349	4,4	6,89	125	65	13,4	3,1	0,54	0,74	759 ±12		746 ±10		735 ±12		1153 ±197		+36	8,01	1,7	0,0783	9,9	1,35	10,1	0,1249	1,7	0,2	
048.37.1	7,0E-4	32	0,0780	1,2	0,19	1,4	0,338	2,2	1,29	165	71	17,8	3,0	0,45	0,36	765 ±12		762 ±12		754 ±13		864 ±104		+12	7,94	1,7	0,0678	5,0	1,18	5,2	0,1259	1,7	0,3	
048.5.1	1,4E-3	21	0,0938	2,3	0,24	1,3	0,349	2,4	2,55	183	99	19,0	3,9	0,56	0,83	766 ±13		757 ±13		757 ±14		1040 ±137		+28	7,93	1,8	0,0740	6,8	1,29	7,0	0,1261	1,8	0,3	
048.35.1	-1,3E-4	155	0,0646	1,2	0,25	1,1	0,349	2,7	--	194	122	21,0	5,4	0,65	0,33	767 ±9		765 ±9		745 ±10		822 ±96		+7	7,92	1,3	0,0665	4,6	1,16	4,8	0,1263	1,3	0,3	
048.3.1	-1,4E-4	125	0,0638	1,3	0,26	1,1	0,342	1,3	--	178	116	19,3	5,1	0,67	0,34	767 ±9		767 ±9		747 ±10		799 ±83		+4	7,91	1,3	0,0658	4,0	1,15	4,2	0,1264	1,3	0,3	
048.16.1	-7,4E-5	281	0,0635	1,2	0,29	18,0	0,335	2,3	--	232	203	25,2	7,4	0,90	1,06	768 ±11		768 ±11		762 ±24		761 ±102		-1	7,91	1,5	0,0646	4,8	1,13	5,1	0,1265	1,5	0,3	
048.25.1	1,9E-4	122	0,0647	1,4	0,30	1,2	0,341	2,2	0,36	174	131	19,0	5,6	0,77	0,43	769 ±11		771 ±11		748 ±13		671 ±124		-15	7,90	1,6	0,0619	5,8	1,08	6,0	0,1266	1,6	0,3	
048.13.1	9,3E-5	139	0,0660	1,0	0,25	0,9	0,365	1,9	0,17	256	160	27,9	6,9	0,65	0,48	769 ±12		769 ±12		751 ±13		762 ±65		-1	7,89	1,6	0,0646	3,1	1,13	3,5	0,1267	1,6	0,5	
048.12.1	1,3E-4	172	0,0655	1,4	0,20	3,1	0,349	1,8	0,25	152	81	16,6	3,3	0,55	0,38	770 ±10		771 ±10		759 ±10		728 ±116		-6	7,88	1,3	0,0636	5,5	1,11	5,6	0,1269	1,3	0,2	
048.33.1	-2,7E-4	104	0,0643	1,5	0,30	1,2	0,337	2,4	--	128	100	14,0	4,4	0,81	0,40	770 ±10		767 ±10		744 ±11		875 ±126		+13	7,88	1,4	0,0682	6,1	1,19	6,2	0,1269	1,4	0,2	
048.29.1	2,0E-4	72	0,0663	1,0	0,29	0,9	0,342	2,3	0,36	300	222	32,8	9,4	0,76	0,31	771 ±11		772 ±11		751 ±12		722 ±73		-7	7,87	1,5	0,0634	3,4	1,11	3,7	0,1270	1,5	0,4	
048.38.1	-1,9E-4	118	0,0652	1,5	0,21	1,4	0,325	1,4	--	153	83	16,8	3,7	0,56	0,39	774 ±10		771 ±10		755 ±10		864 ±101		+11	7,84	1,4	0,0679	4,9	1,19	5,1	0,1275	1,4	0,3	
048.28.1	2,3E-4	111	0,0668	1,4	0,21	1,4	0,339	2,3	0,43	158	80	17,3	3,5	0,52	0,37	775 ±10		777 ±10		761 ±10		722 ±130		-8	7,82	1,4	0,0634	6,1	1,12	6,3	0,1278	1,4	0,2	
048.32.1	-9,3E-4	64	0,0666	2,1	0,46	1,4	0,344	2,3	--	89	103	9,8	4,8	1,20	0,55	780 ±13		766 ±11		730 ±13		1191 ±206		+37	7,78	1,8	0,0797	10,4	1,41	10,6	0,1286	1,8	0,2	
048.34.1	4,3E-4	85	0,0662	1,7	0,38	1,2	0,358	2,8	0,79	95	96	10,6	4,0	1,04	0,84	784 ±11		789 ±10		762 ±12		599 ±199		-33	7,73	1,5	0,0599	9,2	1,07	9,3	0,1293	1,5	0,2	
048.30.1	-2,1E-4	122	0,0650	1,4	0,15	2,8	0,345	2,0	--	151	59	16,8	2,7	0,40	0,38	785 ±10		782 ±10		770 ±10		866 ±114		+10	7,73	1,4	0,0679	5,5	1,21	5,7	0,1294	1,4	0,2	48
048.14.1	-2,1E-5	786	0,0643	1,2	0,33	0,9	0,370	1,5	--	223	184	25,3	8,4	0,85	0,32	800 ±10		801 ±10		772 ±11		761 ±81		-5	7,57	1,3	0,0646	3,9	1,18	4,1	0,1321	1,3	0,3	
048.27.1	2,0E-4	113	0,0657	3,0	0,25	1,1	0,342	1,9	0,36	195	120	22,1	5,4	0,64	0,34	802 ±10		805 ±10		784 ±11		705 ±128		-15	7,55	1,4	0,0629	6,0	1,15	6,2	0,1324	1,4	0,2	n=19
048.24.1	9,3E-5	116	0,0655	0,8	0,29	0,7	0,368	1,6	0,17	391	281	44,5	12,7	0,74	0,24	803 ±9		805 ±9		781 ±10		747 ±55		-8	7,53	1,2	0,0642	2,6	1,17	2,9	0,1327	1,2	0,4	Concordia age 768.7 ±4.5 Ma

Errors are 1-sigma; Pb$_c$ and Pb* indicate the common and radiogenic portions, respectively.
Error in Standard calibration was 0.28% (not included in above errors but required when comparing data from different mounts).
(1) Common Pb corrected using measured 204Pb.
(2) Common Pb corrected by assuming 206Pb/238U-207Pb/235U age-concordance
(3) Common Pb corrected by assuming 206Pb/238U-208Pb/232Th age-concordance

n=44

Spot	overct corr. 204Pb /206Pb	±%	207Pb /206Pb	±%	208Pb /206Pb	±%	206Pb /238U	±%	% 206Pb$_c$	ppm U	ppm Th	4-corr ppm 206Pb	4-corr ppm 208Pb	232Th /238U	±%	(1) 206Pb /238U Age	(2) 206Pb /238U Age	(3) 206Pb /238U Age	(1) 207Pb /206Pb Age	Dis-cor-dant	(1) 238U /206Pb*	±%	(1) 207Pb* /206Pb*	±%	(1) 207Pb* /235U	±%	(1) 206Pb* /238U	±%	err corr	
ASM21.5.2	1,1E-3	108	0,0705	4,0	0,34	1,4	0,265	3,1	1,42	264	569	9,51	8,11	2,23	0,34	265 ±7		265 ±7		249 ±13		331 ±1263		+33	23,8	2,5	0,0705	4,0	0,36	4,8	0,0419	3,1	0,6	
ASM21.5.1	4,8E-5	2723	0,0527	2,4	0,85	1,1	0,1262	3,3	0,09	264	569	9,51	8,11	2,23	0,34	265 ±7		265 ±2		238 ±4		283 848		+7	23,8	2,5	0,052	37	0,30	37	0,0420	2,5	0,07	
ASM21.16.1	9,9E-4	1048	0,0512	7,3	0,28	5,2	0,1215	4,2	1,82	28	18	1,01	0,25	0,66	0,95	267 ±51		272 ±5		262 ±5		-606 11893		+147	23,6	19,2	0,036	437	0,21	437	0,0423	19,2	0,04	
ASM21.15.1	-6,8E-4	322	0,0546	3,0	0,60	1,6	0,1234	3,1	--	166	250	6,04	3,79	1,56	0,43	268 ±11		264 ±2		247 ±4		756 1025		+66	23,5	4,0	0,064	49	0,38	49	0,0425	4,0	0,08	
ASM21.10.1	7,5E-4	474	0,0651	6,9	0,53	2,2	0,1224	4,0	1,36	98	123	3,57	1,85	1,30	0,55	269 ±18		268 ±6		253 ±8		378 2186		+29	23,4	6,8	0,054	97	0,32	97	0,0427	6,8	0,07	
ASM21.3.1	-1,9E-3	130	0,0511	3,5	0,55	1,8	0,1202	3,9	--	144	201	5,28	2,22	1,44	1,33	270 ±12		261 ±2		244 ±4		148 882		+78	23,4	4,4	0,078	43	0,46	44	0,0428	4,4	0,10	
ASM21.6.1	2,0E-4	9527	0,0489	11,7	0,23	7,9	0,1176	2,4	0,37	15	8	0,56	0,12	0,53	1,26	273 ±95		275 ±6		266 ±7		-8 15034		+3593	23,1	35,0	0,046	623	0,27	624	0,0433	35,0	0,06	
ASM21.8.1	-3,4E-3	711	0,0642	10,7	0,22	8,9	0,1158	2,7	--	12	5	0,45	0,15	0,47	1,41	275 ±114		255 ±6		250 ±7		1814 5120		+87	22,9	41,6	0,111	282	0,67	285	0,0436	41,6	0,15	
ASM21.11.1	-6,4E-5	4584	0,0493	3,8	0,46	2,2	0,1220	3,2	--	115	138	4,33	2,02	1,24	0,50	275 ±16		276 ±6		264 ±8		207 2003		-34	22,9	5,8	0,050	86	0,30	87	0,0436	5,8	0,07	
ASM21.17.1	-1,4E-3	711	0,0590	6,7	0,25	5,3	0,1178	2,9	--	29	18	1,10	0,33	0,65	0,91	276 ±48		267 ±4		262 ±5		1166 3452		+78	22,9	17,5	0,079	174	0,47	175	0,0437	17,5	0,10	
ASM21.12.1	8,5E-4	2694	0,0620	10,2	0,18	9,7	0,1312	2,6	1,56	13	6	0,51	0,08	0,46	1,37	276 ±115		275 ±12		173 1614		-61	22,9	42,2	0,050	692	0,30	693	0,0437	42,2	0,06	
ASM21.18.1	-1,5E-3	714	0,0534	7,3	0,24	5,8	0,1230	1,8	--	25	16	0,95	0,27	0,64	0,96	276 ±52		268 ±7		264 ±8		1058 3972		+75	22,9	18,8	0,075	197	0,45	198	0,0437	18,8	0,10	
ASM21.4.1	-1,2E-3	185	0,0557	3,1	0,58	1,7	0,1241	2,8	--	154	221	5,80	3,59	1,48	0,44	276 ±11		269 ±4		251 ±5		1015 875		+74	22,9	4,2	0,073	43	0,44	43	0,0437	4,2	0,10	
ASM21.9.1	-1,4E-3	229	0,0507	3,9	0,46	4,3	0,1176	1,1	--	100	112	3,91	1,97	1,16	0,53	286 ±17		279 ±3		264 ±5		965 1314		+72	22,1	5,9	0,071	64	0,45	65	0,0453	5,9	0,09	
ASM21.20.1	-4,8E-3	179	0,0578	6,2	0,20	5,6	0,1202	1,8	--	31	16	1,26	0,44	0,53	0,86	297 ±42		271 ±4		269 ±5		1980 1541		+97	21,2	14,3	0,122	87	0,79	88	0,0471	14,3	0,16	
ASM21.2.1	-7,5E-3	259	0,0600	9,6	0,20	8,5	0,1165	4,5	--	13	6	0,54	0,24	0,49	1,49	260 ±6		256 ±7		241 ±6		2416 2384		+90	21,1	31,2	0,156	140	1,02	144	0,0473	31,2	0,22	
ASM21.19.1	-5,8E-3	313	0,0516	10,2	0,19	8,4	0,1222	2,3	--	15	8	0,61	0,23	0,54	1,27	305 ±89		277 ±6		273 ±7		2073 2976		+87	20,6	29,6	0,128	169	0,86	172	0,0485	29,6	0,17	
ASM21.7.1	-8,9E-3	98	0,0475	7,5	0,37	4,2	0,1226	1,6	--	30	26	1,30	0,81	0,89	2,54	315 ±43		273 ±5		258 ±6		2461 1001		+89	20,0	13,7	0,161	59	1,11	61	0,0501	13,7	0,22	
ASM21.13.1	-1,2E-2	182	0,0418	13,9	0,18	9,5	0,1241	2,5	--	13	6	0,56	0,29	0,51	1,34	327 ±101		275 ±7		269 ±7		2681 1918		+90	19,2	31,4	0,183	116	1,31	120	0,0520	31,4	0,26	
ASM21.26.1	2,4E-3	86	0,0502	5,4	0,460	5,6	0,131	2,9	4,39	70	81	2,4	0,9	1,18	0,72	253 ±12		265 ±7		251 ±9		#LICZBA!	#LICZBA!	#LICZBA!	24,97	4,6	0,0133	249,9	0,07	250,0	0,0401	4,6	0,0	
ASM21.28.1	-9,5E-4	551	0,0578	9,3	0,320	1,1	0,315	4,8	--	22	18	0,8	0,3	0,81	1,17	260 ±25		253 ±7		247 ±9		969 ±2115		+75	24,32	9,8	0,0714	103,6	0,40	104,1	0,0411	9,8	0,1	
ASM21.29.1	-7,5E-4	271	0,0543	5,5	0,416	3,4	0,117	1,4	--	71	75	2,6	1,1	1,08	0,72	265 ±13		260 ±9		250 ±11		775 ±935		+67	23,85	5,0	0,0650	44,5	0,38	44,7	0,0419	5,0	0,1	
ASM21.27.2	1,2E-6	185914	0,0559	6,0	0,199	5,3	0,115	2,6	0,00	44	21	1,6	0,3	0,51	0,81	265 ±14		263 ±9		260 ±10		446 ±1277		+41	23,84	5,2	0,0558	57,5	0,32	57,7	0,0419	5,2	0,1	
ASM21.37.1	9,3E-4	112	0,0610	3,2	0,531	1,9	0,119	1,8	1,70	149	190	5,4	2,8	1,32	0,47	266 ±8		268 ±6		252 ±8		67,0 ±790		-304	23,71	3,0	0,0474	33,2	0,28	33,3	0,0422	3,0	0,1	
ASM21.43.2	1,3E-3	270	0,0583	10,2	0,230	7,9	0,118	2,4	4,18	15	7	0,5	0,1	0,53	1,28	267 ±33		276 ±12		269 ±14		#LICZBA!	#LICZBA!	#LICZBA!	23,64	12,4	0,0236	413,9	0,14	414,0	0,0423	12,4	0,0	
ASM21.45.1	1,1E-3	491	0,0593	9,3	0,207	8,1	0,112	2,3	1,98	17	9	0,6	0,1	0,54	1,22	267 ±28		270 ±12		268 ±13		-156 ±4629		+278	23,61	10,7	0,0432	186,4	0,25	186,7	0,0424	10,7	0,1	
ASM21.23.1	2,0E-4	548	0,0513	4,0	0,594	2,1	0,127	2,3	0,37	139	199	5,1	3,0	1,48	0,55	268 ±9		269 ±8		248 ±11		115 ±800		-137	23,58	3,6	0,0483	33,9	0,28	34,1	0,0424	3,6	0,1	
ASM21.43.1	---	239488	0,0576	2,6	0,640	1,4	0,119	2,4	0,00	220	362	8,0	5,2	1,70	0,38	268 ±7		266 ±6		250 ±8		514 ±332		+49	23,56	2,5	0,0576	15,1	0,34	15,3	0,0424	2,5	0,2	
ASM21.32.1	1,0E-3	530	0,0603	9,5	0,300	6,5	0,131	2,3	1,86	17	12	0,6	0,2	0,77	1,27	269 ±29		271 ±11		266 ±13		-40 ±4371		+787	23,49	10,8	0,0453	180,0	0,27	180,3	0,0426	10,8	0,1	
ASM21.47.1	7,3E-4	241	0,0522	5,4

CSM01.16.1	-4,5E-4	259	0,0504	3,6	0,71	1,7	0,123	0,9	--	121	203	4,6	3,3	1,72	0,48	278 ±7	276 ±4	246 ±6	493 ±662	+45	22,70	2,5	0,0570	30,0	0,35	30,1	0,0441	2,5	0,1		
CSM01.21.1	-9,4E-5	828	0,0717	10,2	0,83	2,6	0,129	3,5	--	195	402	7,5	6,3	2,13	0,82	282 ±6	274 ±5	250 ±8	1014 ±368	+74	22,38	2,1	0,0730	18,1	0,45	18,3	0,0447	2,1	0,1		
CSM01.23.2	3,0E-4	113	0,0518	1,9	1,21	0,8	0,127	2,2	0,55	392	1179	15,1	18,4	3,10	0,27	282 ±4	284 ±4	225 ±9	65,6 ±260	-337	22,35	1,6	0,0473	10,9	0,29	11,0	0,0447	1,6	0,1		
CSM01.33.1	5,0E-4	100	0,0599	2,1	1,00	1,6	0,120	2,6	0,91	329	833	12,8	12,8	2,62	0,31	286 ±4	286 ±4	249 ±7	311 ±325	+8	22,03	1,6	0,0526	14,3	0,33	14,4	0,0454	1,6	0,1	CSM01	
CSM01.5.3	4,0E-3	-41	0,1769	5,8	0,80	1,6	0,131	2,9	7,25	101	157	3,57	0,54	309 ±11		282 ±8	371 ±7	2014 ±426		+87	20,35	3,5	0,1249	34,2	0,84	34,4	0,0491	3,5	0,1		

Errors are 1-sigma; Pb_c and Pb^* indicate the common and radiogenic portions, respectively. n=17

Error in Standard calibration was 0.28% (not included in above errors but required when comparing data from different mounts). Concordia age 276.2 ±3.0 Ma

(1) Common Pb corrected using measured 204Pb.

(2) Common Pb corrected by assuming 206Pb/238U-207Pb/235U age-concordance

(3) Common Pb corrected by assuming 206Pb/238U-208Pb/232Th age-concordance

Spot	204Pb /206Pb	±%	207Pb /206Pb	±%	208Pb /206Pb	±%	206Pb /238U	±%	% 206Pb	ppm U	ppm Th	7-corr ppm 206Pb*	7-corr ppm 208Pb*	232Th /238U	±%	(1) 206Pb /238U Age	(2) 206Pb /238U Age	(3) 206Pb /238U Age	(1) 207Pb /206Pb Age	% Dis-cor-dant	(1) 238U /206Pb*	±%	(1) 207Pb* /206Pb*	±%	207Pb* /235U	±%	(1) 206Pb* /238U	±%	err corr	
693.29.1	9,6E-4	48	0,0556	5,8	0,23	9,7	0,0921	2,3	0,64	33	31	0,67	0,16	0,53	1,2	213 ±8	215 ±8	210 ±9	-270 ±528	+182	29,78	3,9	0,0413	20,8	0,191	21,2	0,0336	3,9	0,2		
693.21.1	1,9E-3	32	0,1756	3,6	0,60	1,4	0,1071	0,8	15,51	29	19	2,65	0,76	0,64	1,5	258 ±8	256 ±7	261 ±10	1374 ±255	+42	25,68	3,1	0,0878	10,8	0,313	10,9	0,0408	3,1	0,3		
693.6.1	5,2E-4	47	0,0516	3,1	0,35	3,8	0,1057	1,8	0,04	51	43	1,79	0,63	0,87	1,7	254 ±8	256 ±8	246 ±10	-116 ±227	+325	24,89	3,3	0,0439	9,2	0,243	9,8	0,0402	3,3	0,3		
693.17.1	-5,4E-4	30	0,0511	3,3	0,91	0,9	0,1108	0,8	--	98	218	3,43	3,17	2,31	1,5	261 ±8	258 ±8	223 ±13	566 ±105	+55	24,23	3,0	0,0590	4,8	0,336	5,7	0,0413	3,0	0,5		
693.11.1	5,7E-4	32	0,0522	2,1	0,51	1,3	0,1155	1,4	0,09	73	95	2,60	1,34	1,35	1,5	260 ±8	262 ±8	249 ±10	-127 ±169	+311	24,31	3,0	0,0437	6,8	0,248	7,5	0,0411	3,0	0,4		
693.33.1	-8,9E-4	38	0,0504	3,3	0,43	2,0	0,1033	1,8	--	43	46	1,56	0,67	1,09	1,7	267 ±9	263 ±8	251 ±10	717 ±170	+64	23,66	3,3	0,0633	8,0	0,369	8,7	0,0423	3,3	0,4		
693.10.1	-2,4E-3	29	0,0546	8,7	0,39	2,6	0,1150	2,2	0,38	25	23	0,90	0,35	0,97	1,9	278 ±10	266 ±9	255 ±11	1392 ±225	+82	22,68	3,6	0,0884	11,7	0,538	12,3	0,0441	3,6	0,3		
693.5.1	2,0E-4	46	0,0515	1,8	0,80	0,9	0,1189	1,2	--	112	225	4,06	3,28	2,08	1,5	266 ±7	267 ±6	240 ±12	130 ±78	-107	23,78	2,8	0,0486	3,3	0,282	4,4	0,0420	2,8	0,6		
693.19.1	4,6E-4	53	0,0534	3,2	0,28	2,4	0,1043	0,9	0,23	36	28	1,30	0,37	0,80	1,7	265 ±8	267 ±8	263 ±10	30,1 ±207	-798	23,82	3,2	0,0466	8,6	0,270	9,2	0,0420	3,2	0,3		
693.36.1	4,2E-4	58	0,0580	3,1	0,35	3,9	0,0995	1,9	0,80	45	39	1,65	0,56	0,90	1,7	269 ±8	269 ±8	261 ±10	276 ±180	+3	23,48	3,2	0,0518	7,8	0,304	8,5	0,0426	3,2	0,4		
693.8.1	-3,2E-4	100	0,0494	5,6	0,27	6,9	0,1104	2,8	--	15	11	0,56	0,15	0,73	2,1	270 ±10	269 ±10	263 ±12	378 ±227	+29	23,41	3,8	0,0542	10,1	0,319	10,8	0,0427	3,8	0,4		
693.9.1	3,3E-4	49	0,0535	2,5	0,47	1,5	0,1270	1,6	0,23	48	58	1,76	0,83	1,24	1,6	268 ±8	269 ±8	257 ±10	128 ±135	-112	23,53	3,0	0,0486	5,7	0,285	6,5	0,0426	3,0	0,5		
693.32.1	-1,1E-3	29	0,0508	2,7	0,51	4,2	0,1032	1,6	--	62	79	2,27	1,18	1,32	1,6	274 ±8	254 ±11	268 ±12	815 ±144	+68	23,00	3,1	0,0663	6,9	0,397	7,6	0,0435	3,1	0,4		
693.17.2	2,5E-3	28	0,0527	4,1	0,45	2,6	0,1072	1,4	0,13	31	36	1,12	0,51	1,22	1,8	258 ±10	270 ±9	260 ±12	#LICZBA!	#LICZBA!	24,50	3,8	0,0136	85,4	0,077	85,5	0,0408	3,8	0,0		
693.20.1	-7,6E-4	28	0,0523	2,1	0,173	1,3	0,1068	0,8	77	110	2,85	1,86	1,48	1,7	276 ±8	272 ±8	242 ±11	717 ±106	+63	22,85	2,9	0,0633	5,0	0,382	5,8	0,0438	2,9	0,5		
693.42.1	6,7E-4	36	0,0518	2,6	0,61	1,4	0,1048	1,5	0,02	66	107	2,46	1,51	1,66	1,5	269 ±8	272 ±8	258 ±11	-231 ±231	+221	23,45	2,9	0,0419	9,2	0,246	9,6	0,0426	2,9	0,3		
693.14.1	7,6E-4	40	0,0672	17,9	0,88	4,6	0,1033	1,1	1,93	44	84	1,64	1,42	1,98	1,9	275 ±8	273 ±9	230 ±15	457 ±512	+41	22,96	3,1	0,0561	23,1	0,337	23,3	0,0435	3,1	0,1		
693.40.1	1,5E-4	77	0,0507	2,7	0,53	1,5	0,1168	1,6	--	55	74	2,05	1,10	1,39	1,6	273 ±8	275 ±8	259 ±11	123 ±106	-126	23,08	3,0	0,0485	4,5	0,290	5,4	0,0433	3,0	0,6		
693.12.1	7,5E-4	45	0,0502	3,6	0,41	2,2	0,1072	2,0	--	36	36	1,37	0,58	1,04	1,8	272 ±9	276 ±9	262 ±11	-418 ±362	+169	23,19	3,3	0,0390	13,8	0,232	14,2	0,0431	3,3	0,2		
693.39.1	1,9E-3	24	0,0709	2,4	0,56	1,6	0,1135	1,7	2,38	47	63	1,79	0,94	1,37	1,6	274 ±8	277 ±8	262 ±11	-178 ±413	+259	23,06	3,1	0,0428	16,5	0,256	16,8	0,0434	3,1	0,2		
693.28.1	2,4E-4	106	0,0538	4,8	0,20	7,6	0,1068	2,6	0,25	20	12	0,76	0,15	0,63	2,0	276 ±9	277 ±9	277 ±11	206 ±213	-35	22,86	3,5	0,0502	9,2	0,303	9,9	0,0437	3,5	0,4		
693.22.1	1,1E-4	100	0,0511	3,0	0,52	2,8	0,1053	1,8	--	49	63	1,86	0,98	1,32	1,7	276 ±8	277 ±8	260 ±11	172 ±104	-62	22,86	3,0	0,0495	4,5	0,299	5,4	0,0437	3,0	0,6		
693.43.1	-7,3E-4	45	0,0517	3,5	0,49	2,0	0,1043	2,0	--	39	48	1,46	0,72	1,27	1,7	281 ±9	277 ±9	263 ±11	683 ±171	+60	22,48	3,2	0,0623	8,0	0,382	8,6	0,0445	3,2	0,4		
693.25.1	1,3E-3	45	0,0528	4,7	0,23	3,8	0,0950	2,5	0,12	24	15	0,91	0,21	0,63	1,9	273 ±9	279 ±9	276 ±10	-870 ±820	+134	23,11	3,5	0,0331	28,5	0,197	28,7	0,0433	3,5	0,1		
693.23.1	-6,0E-4	56	0,0523	4,0	0,36	2,5	0,1017	2,2	0,05	33	30	1,27	0,46	0,92	1,7	283 ±9	280 ±9	269 ±11	638 ±184	+57	22,31	3,3	0,0610	8,6	0,377	9,2	0,0448	3,3	0,4		
693.18.1	-2,9E-3	29	0,0560	4,5	0,30	3,1	0,1113	2,4	0,51	21	17	0,79	0,23	0,84	1,9	296 ±11	280 ±9	275 ±11	1537 ±220	+83	21,32	3,7	0,0955	11,7	0,617	12,3	0,0469	3,7	0,3		
693.30.1	1,2E-4	58	0,0513	1,8	0,41	7,9	0,1059	1,2	--	127	147	4,88	2,04	1,19	1,4	281 ±8	282 ±8	276 ±11	171 ±65	-65	22,44	2,8	0,0495	2,8	0,304	4,0	0,0446	2,8	0,7		
693.15.1	-1,4E-3	34	0,0546	3,7	0,84	1,7	0,1136	2,0	0,34	39	82	1,51	1,27	2,16	1,7	290 ±9	282 ±9	253 ±14	1048 ±186	+74	21,71	3,3	0,0742	9,2	0,471	9,8	0,0461	3,3	0,3		
693.40.2	-4,8E-4	49	0,0536	3,0	0,45	1,8	0,1086	1,7	0,20	47	55	1,83	0,83	1,19	1,6	287 ±8	284 ±8	272 ±10	622 ±132	+55	21,97	3,0	0,0605	6,1	0,380	6,8	0,0455	3,0	0,4		
693.16.1	5,0E-4	58	0,0520	3,7	0,36	2,4	0,1117	2,0	--	32	28	1,26	0,46	0,89	1,8	283 ±9	286 ±9	273 ±11	-75 ±258	+488	22,26	3,2	0,0446	10,5	0,277	11,0	0,0449	3,2	0,3		
693.7.1	-9,7E-5	150	0,0505	4,4	0,32	2,9	0,1171	2,2	--	25	21	0,97	0,32	0,87	1,9	286 ±9	286 ±9	278 ±11	283 ±268	-1	22,04	3,2	0,0520	5,9	0,325	6,8	0,0454	3,2	0,5		
693.35.1	-9,9E-4	58	0,0526	5,6	0,39	3,3	0,1089	2,7	0,07	15	14	0,59	0,23	0,98	2,1	292 ±11	287 ±10	274 ±12	833 ±268	+66	21,59	3,7	0,0668	12,9	0,427	13,4	0,0463	3,7	0,3		
693.38.1	-7,7E-4	32	0,0502	2,5	0,59	2,8	0,1049	1,5	--	75	106	2,92	1,75	1,46	1,6	290 ±8	287 ±8	264 ±11	649 ±129	+56	21,70	2,9	0,0613	6,0	0,389	6,7	0,0461	2,9	0,4		
693.31.1	-2,0E-4	44	0,0513	1,7	0,19	1,6	0,1095	0,7	--	117	54	4,62	0,87	0,47	1,5	289 ±8	289 ±8	283 ±8	379 ±63	+24	21,78	2,7	0,0542	2,8	0,343	3,9	0,0459	2,7	0,7		
693.34.1	-6,3E-4	36	0,0515	2,6	0,56	1,4	0,1086	1,6	--	65	90	2,58	1,47	1,43	1,6	295 ±5	291 ±4	271 ±6	627 ±125	+54	21,39	1,6	0,0607	5,8	0,391	6,0	0,0467	1,6	0,3		
693.41.1	1,0E-3	45	0,0559	4,0	0,29	3,0	0,1052	2,3	0,47	27	20	1,09	0,31	0,75	1,8	287 ±9	292 ±9	284 ±11	-326 ±474	+192	21,93	3,4	0,0404	18,4	0,254	18,7	0,0456	3,4	0,2		
693.27.1	6,2E-4	73	0,0564	10	0,72	3,6	0,1167	0,9	24,11	7	5	0,28	0,07	0,76	1,7	307 ±14	297 ±17	282 ±23	2546 ±408	+88	19,10	4,1	0,1081	21,1	1,085	21,5	0,0728	4,1	0,2	693,0	
693.26.1	-2,2E-4	95	0,0512	5,3	0,59	26,9	0,0991	9,2	--	2	2	0,06	0,04	1,41	1,0	304 ±24	303 ±24	276 ±42	389 ±167	+23	20,74	8,0	0,0544	7,5	0,362	11,0	0,0482	8,0	0,7		

Errors are 1-sigma; Pb_c and Pb^* indicate the common and radiogenic portions, respectively. n=17

Error in Standard calibration was 0.50% (not included in above errors but required when comparing data from different mounts). Concordia age 273.0 ±4.4 Ma

(1) Common Pb corrected using measured 204Pb.

(2) Common Pb corrected by assuming 206Pb/238U-207Pb/235U age-concordance

(3) Common Pb corrected by assuming 206Pb/238U-208Pb/232Th age-concordance

Spot	204Pb /206Pb	±%	207Pb /206Pb	±%	208Pb /206Pb	±%	206Pb /238U	±%	% 206Pb	ppm U	ppm Th	7-corr ppm 206Pb*	7-corr ppm 208Pb*	232Th /238U	±%	(1) 206Pb /238U Age	(2) 206Pb /238U Age	(3) 206Pb /238U Age	(1) 207Pb /206Pb Age	% Dis-cor-dant	(1) 238U /206Pb*	±%	(1) 207Pb* /206Pb*	±%	207Pb* /235U	±%	(1) 206Pb* /238U	±%	err corr	
694.13.1	9,2E-5	108	0,0665	7,3	0,33	2,7	0,0925	3,4	1,90	33	36	1,26	0,28	0,66	1,7	256 ±7	251 ±7	240 ±8	780 ±71	+69	24,73	2,9	0,0652	3,4	0,363	4,4	0,0404	2,9	0,7		
694.15.1	1,9E-3	39	0,0534	4,1	0,28	4,0	0,1089	1,8	0,22	59	39	2,48	1,15	1,29	1,6	258 ±8	258 ±8	249 ±10	#LICZBA!	#LICZBA!	25,17	3,2	0,0287	10,1	0,157	10,3	0,0398	3,2	0,3		
698.25.1	-1,3E-4	100	0,0537	3,1	0,21	2,7	0,1070	1,8	0,27	34	17	1,19	0,24	0,54	1,7	263 ±8	262 ±8	257 ±9	433 ±100	+40	24,02	3,2	0,0555	4,5	0,319	5,5	0,0416	3,2	0,6		
698.6.1	6,1E-4	50	0,0512	3,5	0,29	2,5	0,1079	2,0	--	29	20	1,05	0,31	0,72	1,8	262 ±8	265 ±8	255 ±10	-219 ±295	+224	24,15	3,3	0,0421	11,7	0,241	12,2	0,0414	3,3	0,3		
698.20.1	-8,6E-4	41	0,0523	3,5	0,20	2,9	0,1038	1,1	0,09	27	13	0,97	0,20	0,51	1,7	271 ±9	266 ±8	261 ±9	764 ±172	+66	23,32	3,2	0,0647	8,2	0,382	8,8	0,0429	3,2	0,4		
698.18.1	4,5E-4	50	0,0603	2,8	0,19	2,7	0,1044	0,9	1,08	37	16	1,34	0,23	0,46	1,7	269 ±4	268 ±4	264 ±4	355 ±158	+25	23,50	1,5	0,0536	7,0	0,315	7,1	0,0426	1,5	0,2		
698.5.1	3,4E-4	87	0,0550	4,4	0,17	4,2	0,1110	2,5	0,42	14	6	0,52	0,09	0,40	2,0	268 ±10	269 ±10	264 ±10	192 ±235	+41	23,51	3,6	0,0499	10,1	0,293	10,7	0,0425	3,6	0,3		
698.12.1	-8,2E-4	33	0,0497	2,7	0,20	2,3	0,0995	1,9	--	53	27	1,95	0,41	0,52	1,5	273 ±8	269 ±8	263 ±8	658 ±143	+60	23,16	3,0	0,0615	6,7	0,366	7,3	0,0432	3,0	0,4		
698.22.1	4,7E-4	50	0,0536	3,0	0,21	2,6	0,1062	1,9	0,24	37	19	1,36	0,28	0,52	1,7	271 ±8	272 ±8	267 ±9	32,9 ±197	-739	23,31	3,1	0,0467	8,2	0,276	8,8	0,0429	3,1	0,4		
698.8.1	-1,0E-3	35	0,0520	3,6	0,60	1,7	0,1155	1,8	0,03	43	63	1,58	0,96	1,54	1,7	279 ±9	273 ±8	254 ±11	825 ±169	+68	22,65	3,1	0,0666	8,1	0,405	8,7	0,0442	3,1	0,4		
698.1.1	-3,9E-4	42	0,0503	2,4	0,70	1,2	0,1181	1,5	--	82	140	3,07	2,17	1,76	1,5	276 ±8	274 ±8	248 ±11	454 ±106	+40	22,89	2,9	0,0560	4,8	0,338	5,6	0,0437	2,9	0,5		
698.3.1	1,4E-4	83	0,0508	3,0	0,42	1,9	0,1199	1,8	--	37	38	1,37	0,58	1,07	1,7	274 ±8	275 ±8	262 ±10	118 ±124	-135	23,02	3,0	0,0484	5,3	0,290	6,1	0,0434	3,0	0,5		
698.14.1	2,8E-4	55	0,0498	2,6	0,29	1,9	0,1049	0,9	--	52	39	1,98	0,58	0,78	1,5	274 ±8	277 ±8	269 ±9	-22 ±139	+1390	22,99	2,9	0,0456	5,7	0,274	6,4	0,0435	2,9	0,4		
698.24.1	-8,8E-4	41	0,0557	3,3	0,21	3,0	0,1085	1,9	0,48	31	16	1,16	0,23	0,54	1,6	284 ±8	278 ±8	275 ±9	879 ±163	+69	22,18	3,1	0,0684	7,9	0,425	8,5	0,0451	3,1	0,4		
698.9.1	2,9E-4	60	0,0542	2,8	0,37	1,9	0,1110	1,6	0,29	45	40	1,73	0,63	0,92	1,6	279 ±8	280 ±8	268 ±10	196 ±137	-43	22,61	2,9	0,0500	5,9	0,305	6,6	0,0442	2,9	0,4		
698.16.1	-1,4E-3	35	0,0515	3,9	0,20	3,3	0,1117	2,1	--	23	12	0,88	0,18	0,52	1,7	287 ±9	280 ±9	276 ±9	983 ±207	+72	21,94	3,3	0,0719	10,2	0,452	10,7	0,0456	3,3	0,3		
698.20.2	-3,3E-4	58	0,0531	3,0	0,26	2,4	0,1030	1,8	0,14	50	29	1,91	0,49	0,60	1,8	284 ±8	281 ±8	272 ±9	522 ±120	+47	22,24	3,0	0,0578	5,5	0,358	6,2	0,0450	3,0	0,5		
698.4.2	5,8E-4	50	0,0526	3,4	0,26	2,6	0,1074	1,9	0,07	33	22	1,29	0,34	0,68	1,7	283 ±8	286 ±8	279 ±9	-113 ±265	+358	22,25	3,0	0,0440	10,7	0,272	11,2	0,0449	3,0	0,3		
698.10.1	9,9E-4	33	0,0539	2,8	0,16	2,8	0,1068	1,8	0,23	40	16	1,57	0,25	0,43	1,6	282 ±8	287 ±8	283 ±9	-405 ±348	+174	22,33	3,1	0,0392	13,3	0,242	13,7	0,0448	3,1	0,2		
698.15.1	1,4E-3	35	0,0506	6,8	0,27	2,8	0,1064	2,1	--	31	20	1,23	0,34	0,67	1,9	282 ±9	290 ±9	280 ±10	#LICZBA!	#LICZBA!	22,33	3,2	0,0293	28,7	0,181	28,8	0,0448	3,2	0,1		
698.7.1	1,6E-4	31	0,0665	1,6	0,06	1,7	0,2280	0,6	0,74	90	17	7,80	0,37	0,20	1,4	624 ±16	622 ±16	626 ±17	747 ±44	+17	9,83	2,7	0,0642	2,1	0,900	3,4	0,1017	2,7	0,8	698	
698.7.2	-7,8E-4	26	0,1978	1,1	0,59	2,5	1,3230	2,2	0,89	7	12	3,08	1,78	1,78	2,6	2785 ±100	2741 ±138	2646 ±128	2883 ±25	+4	1,85	4,4	0,2070	1,5	15,422	4,7	0,5403	4,4	0,9		

Errors are 1-sigma; Pb_c and Pb^* indicate the common and radiogenic portions, respectively. n=6

Error in Standard calibration was 0.53% (not included in above errors but required when comparing data from different mounts). Concordia age 267.9 ±5.2 Ma

(1) Common Pb corrected using measured 204Pb.

(2) Common Pb corrected by assuming 206Pb/238U-207Pb/235U age-concordance

(3) Common Pb corrected by assuming 206Pb/238U-208Pb/232Th age-concordance

Spot	overct corr. 204Pb /206Pb	±%	207Pb /206Pb	±%	208Pb /206Pb	±%	206Pb /238U	±%	% 206Pb	ppm U	ppm Th	4-corr ppm 206Pb*	4-corr ppm 208Pb*	232Th /238U	±%	(1) 206Pb /238U Age	(2) 206Pb /238U Age	(3) 206Pb /238U Age	(1) 207Pb /206Pb Age	% Dis-cor-dant	(1) 238U /206Pb*	±%	(1) 207Pb* /206Pb*	±%	207Pb* /235U	±%	(1) 206Pb* /238U	±%	err corr	
n=28																														
CSM02.5.1	1,1E-3	291	0,0600	2,6	0,358	3,6	0,1150	1,3	1,93	152	146	5,37	1,75	0,99	0,74	260 ±16	262 ±6	258 ±7	-86 ±2554	+412	24,31	6,0	0,044	104,3	0,25	104,4	0,0411	6,0	0,06		
CSM02.9.1	1,5E-3	322	0,0513	3,7	0,190	5,0	0,1161	2,3	2,69	85	41	3,05	0,42	0,49	0,45	264 ±23	272 ±3	267 ±4	#LICZBA!	#LICZBA!	23,89	8,9	0,029	252,8	0,17	253,0	0,0419	8,9	0,04		
CSM02.2.1	1,1E-3	426	0,0528	3,5	0,204	2,8	0,1098	2,3	1,93	95	47	3,44	0,58	0,51	0,43	266 ±22	271 ±3	265 ±4	-554 ±4976	+151	23,75	8,4	0,037	184,8	0,22	185,0	0,0421	8,4	0,05		
CSM02.6.1	1,2E-3	299	0,0517	3,1	0,376	1,9	0,1197	3,5	2,16	128	119	4,64	1,58	0,96	0,39	266 ±17	272 ±3	261 ±4	-786 ±4484	+137	23,72	6,6	0,034	158,5	0,20	158,7	0,0422	6,6	0,04		
CSM02.8.1	7,0E-5	6175	0,0570	5,5	0,276	2,4	0,1165	1,6	0,13	92	65	3,33	0,92	0,73	0,43	267 ±21	266 ±3	261 ±4	451 ±2503	+42	23,64	7,9	0,056	112,7	0,33	113,0	0,0423	7,9	0,07		
CSM02.7.1	-6,2E-4	656	0,0529	3,3	0,575	3,4	0,1184	1,7	--	147	215	5,64	3,37	1,51	0,42	281 ±20	277 ±3	261 ±5	669 ±2018	+59	22,45	7,4	0,062	94,3	0,38	94,5	0,0445	7,4	0,08		
CSM02.3.1	-5,4E-3	151	0,0464	6,1	0,400	2,9	0,1052	1,3	--	65	68	2,59	1,46	1,08	0,58	290 ±40	265 ±4	255 ±5	1985 ±1513	+87	21,70	14,1	0,122	85,0	0,77	86,2	0,0461	14,1	0,16		
CSM02.1.1	9,3E-4	508	0,0508	3,7	0,181	3,1	0,1748	0,9	1,70	67	33	3,66	0,55	0,51	0,55	400 ±36	409 ±10	402 ±11	-563 ±5253	+177	15,61	9,1	0,037	194,8	0,33	195,0	0,0640	9,1	0,05		
CSM02.17.2	2,1E-3	271	0,0570	10,6	0,63	2,5	0,1163	2,8	3,90	108	166	3,8	2,21	1,58	0,63	260 ±28	268 ±5	248 ±7	#LICZBA!	#LICZBA!	24,32	11,0	0,025	372,3	0,14	372,4	0,04112	11,0	0,03		
CSM02.21

Error in Standard calibration was 0.50% (not included in above errors but required when comparing data from different mounts).

(1) Common Pb corrected using measured 204Pb.

(2) Common Pb corrected by assuming 206Pb/238U-207Pb/235U age-concordance

(3) Common Pb corrected by assuming 206Pb/238U-208Pb/232Th age-concordance

Concordia age 268.7 ±4 Ma